DYNAMIC BEHAVIOR IN POLYHYDROGEN IRIDIUM COMPLEXES

A DISSERTATION SUBMITTED TO THE GRADUATE DIVISION OF THE UNIVERSITY OF HAWAIʻI AT MĀNOA IN PARTIAL SATISFACTION OF THE REQUIREMENTS FOR THE DEGREE OF

DOCTOR OF PHILOSOPHY

IN

CHEMISTRY

December 2019

By

Hope Tennyson Sartain

Dissertation Committee:

Craig M. Jensen, Chairperson
Kristin Kumashiro
Matthew F. Cain
Jakub Hyvl
Lloyd Hihara

COPYRIGHT PAGE

DEDICATION PAGE

Mom and Lar-ella;

"Nothing Stops Us"

In loving memory of Josephine Tennyson 11May22-15Oct13

Baby and Booger, Meow

ACKNOWLEDGEMENT PAGE

John Linzi, Wesley Yoshida, Dr. Walt Niemczura, Dr. John Head, Dr. Thomas Hemscheidt, and especially Dr. Craig M. Jensen for letting me find my own way

ABSTRACT

In 1984, Kubas and co-workers determined the molecular structure of $W(\eta^2\text{-}H_2)(L)_3(PR_3)_2$ by a single crystal neutron diffraction study. This seminal study established that molecular hydrogen could bind to a metal center in a "side-on" fashion without cleavage of the H-H bond forming the classical dihydride, $M\text{-}(H)_2$. The terms "Kubas compound" and "Kubas-interaction" are now familiar to all scientists working in the areas of metal hydrides and physi-sorbed hydrogen. The bonding in a Kubas complex is described as involving a donation of electrons from the H_2 σ orbital to a linear empty metal valence orbital and a back-bonding donation from a filled metal d_π orbital to the empty σ^* orbital of the H_2. In the Kubas interaction, the H_2 ligand is primarily considered a σ base and a σ^* acid. Alternatively, the bonding of an H_2 ligand to a metal center could involve an "end-on" interaction, a 3-center 4-electron bond rather than a non-classical 3-center 2-electron bond (Kubas interaction). In the end-on bonding model, the H_2 ligand is primarily considered a σ^* acid. We recently determined the molecular structure of $IrH_x\{2,6\text{-}C_6H_3\text{-}(OAs(t\text{Bu}_2))_2\}$ through a single crystal X-ray diffraction study. Surprisingly, upon refinement of both occupancy and position, the H_2 ligand was found to be oriented in an "end-on" rather than "side-on" coordination motif. This defense will discuss the details of the $M\text{-}(\eta^1\text{-}H_2)$ bonding mode and alternative characterization methods, most notably NMR spectroscopy. Through the studies of $IrH_x\{2,6\text{-}C_6H_3\text{-}(OAs(t\text{Bu}_2))_2\}$, and the possible discrete $M\text{-}(\eta^1\text{-}H_2)$ coordination, an earlier project of the Jensen lab was revisited. In order to gain insight into the dynamic polyhydrogen bonding of $M\text{-}(H)_2$ and $M\text{-}(\eta^2\text{-}H_2)$ in an alternate iridium system, neutron diffraction data of $IrBrH_x(i\text{Pr}_3\text{P})_2\cdot C_{10}H_8$ and $IrClH_x(i\text{Pr}_3\text{P})_2$ have been obtained and will be discussed. Surprisingly, upon

refinement of $IrClH_x(iPr_3P)_2$, the H_2 ligand was found in an unusual eclipsed conformation of one of the complexes in the crystal structure.

TABLE OF CONTENTS

LIST OF TABLES

LIST OF FIGURES, SCHEMES AND EQUATIONS BY CHAPTER

Chapter 1

Chapter 2

Figure 2.1 Representation of twisted η^2-H_2 unit found in $Fe(H)_2(\eta^2\text{-}H_2)PR_3$, where R = $EtPh_2$ and $R_3P'\text{-}H'\text{-}H'$ represent the expected plane for the η^2-H_2 conformation.

Figure 2.2 ORTEP diagram of the structure determined for $IrBrH_x(i\text{Pr}_3\text{P})_2\cdot C_{10}H_8$ **(1)** by neutron diffraction analysis. Atoms in the iridium coordination sphere have been labeled. Coordinatively saturated high occupancy and unsaturated low occupancy superimposed structural hydride ligand sets, H(A), H(B) and H(F), H(E), respectively, have been included. Coordinatively saturated high occupancy dihydrogen ligand, H(C)-H(D), has been included. Alkane hydrogens have been omitted for clarity. Thermal ellipsoids at 50 % probability.

Figure 2.3 ORTEP diagram of the structure determined for $IrClH_x(i\text{Pr}_3\text{P})_2$ **(2)** at 293(2) K by neutron diffraction analysis. Atoms in the iridium coordination sphere have been labeled. Coordinatively saturated structural hydrides, HY(1) and HY(2), have been included. Dynamically disordered dihydrogen ligand HY(11)-HY(12) has been included. Alkane hydrogens have been omitted for clarity. Thermal ellipsoids at 50 % probability.

Figure 2.4 ORTEP diagram of the structure determined for $IrClH_x(i\text{Pr}_3\text{P})_2$ **(3)** at 5(2) K by neutron diffraction analysis. Atoms in the iridium coordination sphere have been labeled. Coordinatively saturated and unsaturated superimposed structural hydride ligand sets, HY(1), HY(2) and HY(A), HY(B), respectively, have been included. Coordinatively saturated high and low occupancy dihydrogen ligands, H(11)-H(12) and H(21)-H(22), respectively, have been included. Alkane hydrogens have been omitted for clarity. Thermal ellipsoids at 50 % probability.

Figure 2.5 ORTEP diagram for iridium coordination sphere of **(1)**. $IrBr(H)_2(\eta^2\text{-}H_2)(i\text{Pr}_3\text{P})_2\cdot C_{10}H_8$ **(1a)** high occupancy coordinatively saturated hydrides, H(A) and H(B), η^2-H_2, H(C)-H(D), ligand. $IrBr(H)_2(i\text{Pr}_3\text{P})_2\cdot C_{10}H_8$ **(1b)** low occupancy coordinatively unsaturated hydrides, H(E) and H(F). Alkane carbons and hydrogens have been removed for clarity.

Figure 2.6 ORTEP diagram for iridium coordination sphere of $IrCl(H)_2(\eta^2\text{-}H_2)(i\text{Pr}_3\text{P})_2$ **(2)**. Coordinatively saturated hydrides, HY(1) and HY(2), and the dynamically disordered η^2-H_2, HY(11)-HY(12), ligand. Alkane carbons and hydrogens have been removed for clarity.

Figure 2.7 ORTEP diagram for iridium coordination sphere of **(3)**. $IrCl(H)_2(\eta^2\text{-}H_2)(i\text{Pr}_3\text{P})_2$ **(3a)** coordinatively saturated hydrides, HY(1) and HY(2), and the high occupancy $\eta^2\text{-}H_2$, HY(11)-HY(12), ligand. $IrCl(H)_2(\eta^2\text{-}H_2)(i\text{Pr}_3\text{P})_2$ **(3b)** coordinatively saturated hydrides, HY(1) and HY(2), and the low occupancy $\eta^2\text{-}H_2$, HY(21)-HY(22), ligand. $IrCl(H)_2(i\text{Pr}_3\text{P})_2$ **(3c)** coordinatively unsaturated hydrides, HY(A) and HY(B). Alkane carbons and hydrogens have been removed for clarity.

Figure 2.8 ORTEP diagram for iridium coordination sphere in **(1a)**. **(1aα)** equatorial plane, Br-Ir-H(B)-H(A) (blue). Tilted view down the Br-Ir-H(B) axis. **(1aβ)** equatorial plane, Br-Ir-H(B)-H(A) (blue). View down the H(A)-Ir-(H(C)-H(D)) axis. Alkane carbons and hydrogens have been removed for clarity.

Figure 2.9 ORTEP diagram for iridium coordination sphere in **(1a)**. Equatorial plane, Br-Ir-H(B)-H(A) (blue). Axial plane, H(A)-Ir-P(1)-P(2) (red). View down the H(A)-Ir-(H(C)-H(D)) axis. Alkane carbons and hydrogens have been removed for clarity.

Figure 2.10 ORTEP diagram for iridium coordination sphere in **(3a)**. **(3aα)** equatorial plane, Cl-Ir-HY(2)-HY(1) (blue). Tilted view down the Cl-Ir-HY(2) axis. **(3aβ)** equatorial plane, Cl-Ir-HY(2)-HY(1) (blue). View down the HY(1)-Ir-(HY(11)-HY(12)) axis. Alkane carbons and hydrogens have been removed for clarity.

Figure 2.11 ORTEP diagram for iridium coordination sphere in **(3b)**. **(3bα)** equatorial plane, Cl-Ir-HY(2)-HY(1) (blue). Tilted view down the Cl-Ir-HY(2) axis. **(3bβ)** equatorial plane, Cl-Ir-HY(2)-HY(1) (blue). View down the HY(1)-Ir-(HY(21)-HY(22)) axis. Alkane carbons and hydrogens have been removed for clarity.

Figure 2.12 ORTEP diagram for iridium coordination sphere in **(3a) and (3b)**. Equatorial plane, Cl-Ir-HY(2)-HY(1) (blue). Axial plane, HY(1)-Ir-P(1)-P(2) (red). View down the HY(1)-Ir-((HY(21)-HY(22)) axis. Alkane carbons and hydrogens have been removed for clarity.

Chapter 3

Figure 3.7 ^{1}H-^{1}H DQF-COSY NMR (500 MHz, 23 °C, tol-d_8), δ -14.28 and δ -17.23.

Figure 3.8 $^{1}H\{^{13}C$, δ -17.23} 1D-TOCSY @ δ -17.23 NMR (500 MHz, 23 °C, tol-d_8, H_2 (g)), inset δ -14.28, (br).

Figure 3.9 $^{1}H\{^{13}C$, δ -17.23} 1D-TOCSY @ δ -17.23 NMR (500 MHz, -80 °C, tol-d_8, H_2 (g)), δ -14.40, (m).

Figure 3.10 $^{1}H\{^{13}C$, δ -14.28} 1D-TOCSY @ δ -17.23 NMR (500 MHz, 23 °C, tol-d_8, H_2 (g)), inset δ -17.23, (br).

Figure 3.11 $^{1}H\{^{13}C$, δ -14.28} 1D-TOCSY @ δ -17.23 NMR (500 MHz, -80 °C, tol-d_8, H_2 (g)), inset δ -17.23, (br).

Figure 3.12 ^{1}H NMR assignments in the compound $IrH_x\{2,6\text{-}C_6H_3\text{-}(OAs(t\text{Bu}_2))_2\}$, including *t*Bu (4) and methylene protons (6). Top, partial $^{1}H\{^{13}C\}$ 1D-TOCSY @ δ -17.23 NMR spectrum (500 MHz, 23 °C, tol-d_8, H_2 (g)) δ 1.47 (m, CH_2, 6); bottom, partial $^{1}H\{^{13}C$, δ -14.28} 1D-TOCSY @ δ -17.23 NMR spectrum (500 MHz, 25 °C, tol-d_8, H_2 (g)) δ 1.47 (br, CH_2, 6).

Figure 3.13 $IrH_x\{2,6\text{-}C_6H_3\text{-}(OAs(t\text{Bu}_2))_2\}$.

Figure 3.14 Upfield partial spectra $^{13}C\{^{1}H\}$ NMR (125 MHz, 23 °C, tol-d_8): δ 42.07 (C_q), 31.04 (CH_3), 27.86 (CH_3), 27.44 (CH_3), 26.12 (CH_3).

Figure 3.15 Downfield partial spectrum $^{13}C\{^{1}H\}$ NMR (125 MHz, 23 °C, C_6D_6): δ 172.68 (aryl), 153.76 (aryl), 149.63 (aryl), 114.30 (aryl), 108.39 (aryl).

Figure 3.16 $^{1}H\{^{13}C\}$ NMR (500 MHz, 23 °C, tol-d_8, D_2 (g)): top inset δ 7.40 (d, $J_{H\text{-}H}$ = 5 Hz, CH, 1 and 3), 7.19 (t, $J_{H\text{-}H}$ = 5 Hz, CH, 2); bottom inset δ (br, 1.50, $2CH_3$, 4) and (br, 1.35, 3*t*Bu, 5).

Figure 4.4 $^{29}Si\{^{1}H\}$ NMR spectrum (79 MHz, 23 °C, C_6D_6), δ 16.80 (s), -110 silicate glass; inset δ 16.80, (s).

Scheme 4.1 Possible equilibrium in solution between hydrido-silyl product **(4)** and (M-η^2-$HSiR_3$) product **(5)**.

CHAPTER 1. Transition Metal Hydride Complexes

1.1 Introduction

Transition metal (TM) hydride complexes are ubiquitous in organometallic chemistry and play key roles in dozens of widely known industrial processes such as the Fischer-Tropsch process, Mobil Oil process, and Monsanto acetic acid process.[1, 2] Mechanistically, these organometallic hydride species helped scientists understand that there were discrete steps in catalytic cycles, beyond generality. In the early days of homogeneous catalysis, tetracarbonyldihydridoiron or $H_2Fe(CO)_4$, for example, was a known intermediate in the synthesis gas reaction, water-gas shift process, **Scheme 1.1**.[2] In this case, a hydroxide ion attacks at an electrophilic carbonyl carbon on $Fe(CO)_5$ and it is believed deprotonation of the carboxyl occurs before loss of carbon dioxide giving the iron hydride anion intermediate.[1] The iron hydride anion is then re-protonated giving the highly unstable dihydride species $H_2Fe(CO)_4$. $H_2Fe(CO)_4$ subsequently loses an H_2 molecule in the presence of carbon monoxide reforming the starting catalyst.[1] The water-gas shift process proposed mechanism helped describe the involvement of metal-hydride complexes in the production of precursors for several important industrial pathways of petroleum bulk materials.

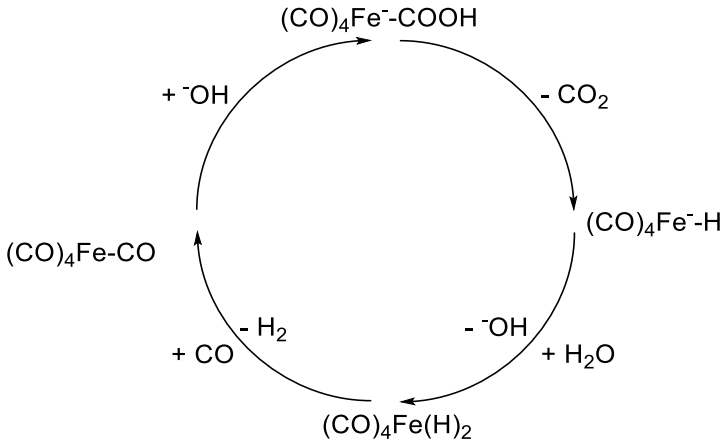

Scheme 1.1 Water-gas shift proposed mechanism.

1.2 Early Controversy in Metal-Hydrogen Bonding

Literary controversy for the bonding of hydrogen to a metal began with what is considered the first metal-hydride complex, $H_2Fe(CO)_4$. First reported in 1931 by Hieber and Leutert, $H_2Fe(CO)_4$ is a highly oxygen, light, and temperature sensitive complex.[3] In fact, because of its highly sensitive nature, the special reaction conditions for this complex were termed the "polar night synthesis" owing to the conditions of the first synthesis that took place: outside, at night, and below freezing temperatures.[4] After the initial synthesis was reported, through electron diffractometry, one group went so far as to say that $H_2Fe(CO)_4$ didn't seem to have a true Fe-H bond and that the complex formula should be written as $Fe(CO)_2(COH)_2$. The report continues by stating that the bound carbonyl groups are most closely represented by tetrahedral geometry to the Fe center making it *impossible* for hydrogen coordination![5]

The confusion over the formula for $H_2Fe(CO)_4$ stemmed from researcher's inability to properly describe the acidic nature of the complex.[6] So, it was thought that hydrogen was bound to an oxygen of the carbonyl group. However, upon decomposition, the complex was believed to release dihydrogen gas and this point left the metal-hydrogen behavior open to interpretation. The role of the hydrogen in $H_2Fe(CO)_4$ remained ambiguous for many years. Since $H_2Fe(CO)_4$ is highly unstable, solid-state crystals could not be grown for useful data from single crystal neutron diffractometry, a highly hydrogen sensitive technique.

However, the structure for $HMn(CO)_5$ was determined by neutron diffractometry, proving that the hydrogen was indeed bound directly to the Mn center, so it was again proposed that the hydrogens in $H_2Fe(CO)_4$ were directly bound to the iron center in an octahedral motif, **Figure 1.1**. In 1977, another group used gas phase electron diffractometry, in comparison with previously published data, to unambiguously establish the geometry and nature of the hydrogen bonding in $H_2Fe(CO)_4$.[7] In contrast to the tetrahedral sans metal-hydrogen geometry previously theorized**,** it was proven that the hydrogens are bound to iron where the structure is severely distorted from octahedral geometry, **Figure 1.1**.[8]

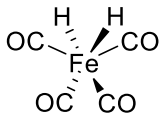

Figure 1.1 Representation of the distorted octahedral molecular geometry of $H_2Fe(CO)_4$.

1.3 Mechanism of Hydrogen Activation in Homogeneous Catalysis

It was originally theorized that organometallic hydrogenations proceeded through concerted mechanisms. On first inspection, a concerted process occurring in one concurrent movement at the metal center would seem to violate the principle of conservation of orbital symmetry (Woodward-Hoffman Rule). However, it has been well established that organometallic hydrogenations tend to occur by precise stepwise mechanisms. This point was first elucidated in the kinetic study of the mechanism of homogeneous catalysis for olefin hydrogenation.[9] Wilkinson's catalyst, $RhCl(PPh_3)_3$, discovered in 1964, is considered the quintessential homogeneous catalyst for the hydrogenation of olefins, **Figure 1.2**.[2] The general mechanism is shown below, **Scheme 1.2**.[1, 9] While scientists generally accepted that the reaction proceeded through a metal-hydride intermediate, the exact details of this cycle were unclear. The mechanism for this catalytic cycle is quite more complex than is generally described. Simply, the 4 coordinate (4C) square planar Rh^I, $RhCl(PPh_3)_3$, species is activated by addition of H_2 resulting in the 6C octahedral Rh^{III} species; metal-hydride bonding details will be discussed in a later paragraph. During this step, an olefin is added to the Rh^{III} species with the loss of a PPh_3 ligand. The olefin thereby "picks up" the hydrides and is released from the Rh^{III} species as the appropriate alkane, ethane in the example in **Scheme 1.2**, with the re-addition of the PPh_3 ligand regenerating the starting catalyst species.

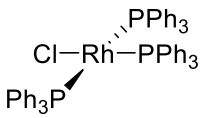

Figure 1.2 $RhCl(PPh_3)_3$, Wilkinson's catalyst.

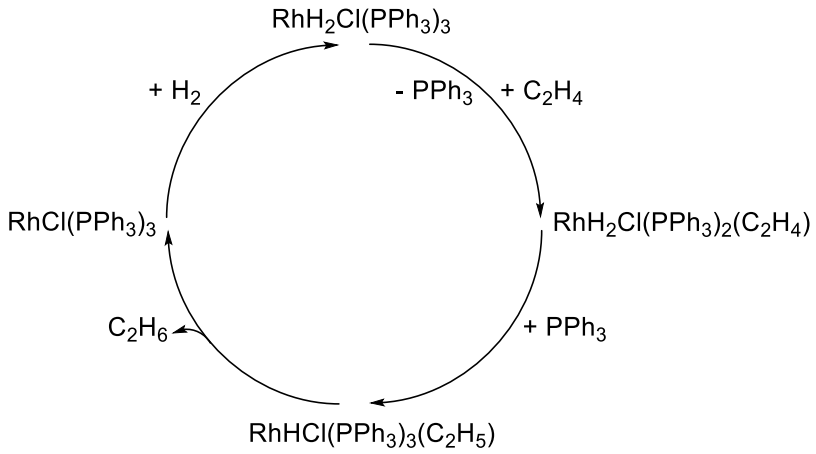

Scheme 1.2 Simplified cycle for olefin hydrogenation by Wilkinson's Catalyst.

In an essential report by Halpern, the individual steps during the mechanism in this catalytic cycle were precisely examined.[9] Through ^{31}P NMR spectroscopy experiments, it was found that an additional five Rh species were involved in the catalytic cycle for olefin hydrogenation that are not listed in the general scheme! Each general step described, **Scheme 1.2**, has been shown to be complicated by multiple intermediates and several stabilizing side reactions. It is important to note that this was the first study that clearly showed that the mechanism for olefin hydrogenation proceeds through discrete steps that included multiple metal-hydride intermediates.

Transition-metal hydride complexes mediate the hydroformylation (oxo-synthesis) synthesis in which olefins are converted to aldehydes. As with olefin hydrogenation, hydroformylation is used to produce important precursors for several industrial processes. The Rh-hydride catalyst is the most active for hydroformylation. However, it is relevant to further discuss the Ir-hydride catalyst since it is derived from a noteworthy complex in the determination of the oxidative addition mechanism of H_2 to metal complexes. Five coordinate Ir monohydrides (ex. $IrH(CO)_2(PPh_3)_2$) were found to be more stable analogues of the Rh intermediates believed formed during the hydroformylation synthesis. These stable Ir analogues made studying the hydroformylation mechanism easier.[10, 11, 12]

Vaska's complex, *trans*-$IrCl(CO)(PPh_3)_2$, is a deceptively simple 4C square planar complex, **Figure 1.3**. The discovery of which in 1961, was only after Vaska had unexpectedly synthesized the first iridium dihydride complexes, $IrH_2X(PPh_3)_3$.[12] Vaska's complex, in several accounts, has been cited as the most widely studied complex for the oxidative addition (OA)

mechanism.[1, 2, 10] Vaska's complex reacts with several substrates that oxidatively add to the 4C complex; H_2, CH_4, C_2H_6 and CH_3I, only to name a few. [2] The H_2 adduct will be used to discuss the oxidative addition reaction and this type of metal-hydrogen bonding.

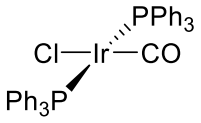

Figure 1.3 Vaska's complex, $IrCl(CO)(PPh_3)_2$.

Similar 4C Ir^I species of the type, $IrClL_2(CO)$, are highly active towards H_2 OA reaction. In 4C Ir^I complexes, there are open coordination sites, or an unsaturation at the metal center on the complexes which is highly beneficial and important for OA reactions. In the case of Vaska's complex, $IrCl(CO)(PPh_3)_2$, which is a d^8 16 electron Ir species, H_2 adds to the complex increasing Ir formal oxidation state by two from Ir^I to Ir^{III}. In turn, its coordination number also increases by two from 4 to 6, $Ir(H)_2Cl(CO)(PPh_3)_2$, now a d^6 18 electron complex, **Eqn. 1.1**.

$$MXL_n + H_2 \longrightarrow M(H)_2XL_n$$

Eqn. 1.1 Oxidative addition of H_2 to an unsaturated metal (M) complex.

1.4 M-H Bonding Considerations in Classical Dihydride Formation

The molecular orbital approach of H_2 to the open coordination site proceeds in a side-on fashion where the filled H_2 σ orbital (symmetric bonding orbital) donates to an appropriate vacant linear orbital of Ir. To complete the 3-center addition process, the then filled metal (M) d_π orbital back donates to the vacant H_2 σ^* orbital (anti-symmetric bonding orbital), **Figure 1.4**. As a result of stronger back donation from the M filled d_π orbital to the empty σ* orbital of H_2, the H-H bond is cleaved, forming metal-dihydride, $M(H)_2$, bonds. This type of metal-hydrogen bonding, as seen in the formation of a metal-hydride, is termed *classical* metal-hydrogen bonding. In the classical metal-hydrogen bonding scenario, the ML_n electronic environment is π basic enough for the

lengthening and eventual cleavage of the H-H bond. In other words, the ligand system will donate enough electron density to the metal for sufficient d_π back donation into the empty H_2 σ^* orbital for the H-H bond to break and oxidatively add to the metal. There is a delicate electronic balance at the metal center that can be manipulated by exchanging better acceptor ligands such as CO, with better donor ligands such as PR_3, in order to increase the basicity at the metal. This interaction is the necessary first step in catalytic cycles, as in the previously mentioned olefin hydrogenation. As shown in **Scheme 1.2**, molecular dihydrogen is oxidatively added to Winkinson's catalyst at the initial step in olefin hydrogenation.

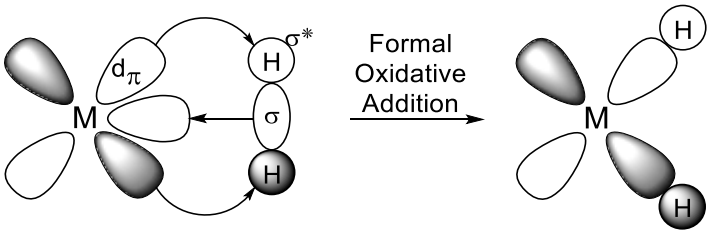

Figure 1.4. Molecular orbital depiction of classical (OA) M-$(H)_2$ coordination.

1.5 Kubas (Non-Classical) Bonding Model

The molecular dihydrogen approach to a metal center in the early stage of H_2 OA was a topic of much controversy. As mentioned above, the formation of a dihydride intermediate through a concerted oxidative addition of H_2 at a metal center for alkene hydrogenation directly violates the Woodward-Hoffman rules. However, a mechanism involving the formation of a coordinated H_2 sigma complex circumvents any such violation. It was suggested that metal complexes bind H_2 and form either an H_2 sigma complex intermediate or transition state before undergoing H_2 OA to metal to yield a dihydride complex. The H_2 molecule would need a close approach to the metal or M-H_2 bond before OA could occur.[2, 10] There were theoretical arguments for an H-H "end-on" approach (colinear with metal) and arguments for an H-H "side-on" approach (each hydrogen equi-distant to metal), **Figure 1.5**.[13, 14, 15, 16] In the event H_2 approaches the metal center in an end-on conformation, top **Figure 1.5**, the filled (basic) M d_σ orbital donation to an empty (acidic) H_2 σ^* orbital would be the dominant electronic characteristic. Alternately, if H_2 approaches a metal

center in a side-on conformation, bottom **Figure 1.5**, the filled (basic) H_2 σ orbital donation to an empty (acidic) M d_σ orbital would be the dominant electronic characteristic. These two assumptions lead to further calculations on theoretical M-H_2 model complexes.[16] The existence of M-H_2 complexes remained punitive until the seminal characterization of $W(\eta^2\text{-}H_2)(CO)_3(i\text{Pr}_3\text{P})_2$, **Figure 1.6**, the first M-(η^2-H_2) complex isolated by Kubas through neutron diffraction in 1984. This was followed by a 20-year eruption of research that established the fundamentals of metal-(η^2-H_2) bonding, *non-classical* or Kubas interaction.[16]

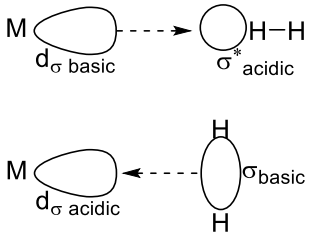

Figure 1.5 Simplified H_2 orbital approach to a metal center, (top) end-on H_2 approach, and (bottom) side-on H_2 approach.

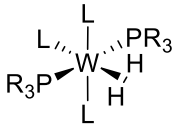

Figure 1.6 Kubas complex, $W(\eta^2\text{-}H_2)(L)_3(PR_3)_2$ (L= CO, R= *i*Pr)

Before Kubas's seminal discovery, it was believed that the H_2 σ bond was inert towards metal coordination. However, a stabilizing feature of the M-(η^2-H_2) bond, is the electron back donation from a filled M d_π orbital to the empty H_2 σ^* orbital, **Figure 1.7**. This stabilization is analogous to metal-olefin π coordination (Dewar-Chatt-Duncanson Model).[16] There is a necessary tandem effect of both H_2 σ donation to an empty M d_σ orbital and a M d_π back donation to an empty H_2 σ^* orbital in order to stabilize this 3-center 2-electron bond (3c $2e^-$), analogous to the H_3^+ molecule. In other words, the ML_n system is not sufficiently basic enough for metal back donation to dominate and cleave the H_2 bond as in the classical M-$(H)_2$ bonding scenario.[1, 10, 16] In the H_3^+

orbital correlation diagram, **Figure 1.8**, the H^+ atomic orbital, right side **Figure 1.8**, would represent the electron deficient σ orbital of the metal center and the two bonding electrons would come from the filled σ orbital of H_2, left side **Figure 1.8**. The 2-electron filled symmetric molecular orbital, center bottom, **Figure 1.8**, bond, and the empty molecular orbitals of the non-bonding, center middle, **Figure 1.8**, and anti-bonding, center top, **Figure 1.8**, together, represent the 3-center 2-electron bonding in non-classical (Kubas interaction) M-(η^2-H_2) bond.[16, 17]

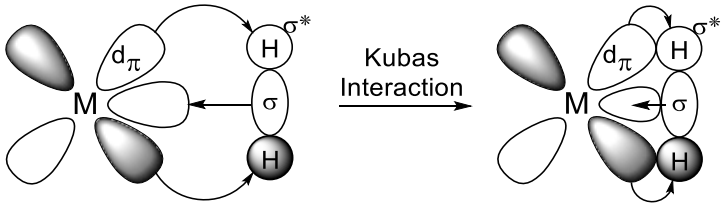

Figure 1.7 Molecular orbital depiction of non-classical (Kubas Interaction) metal-(η^2-H_2) coordination.

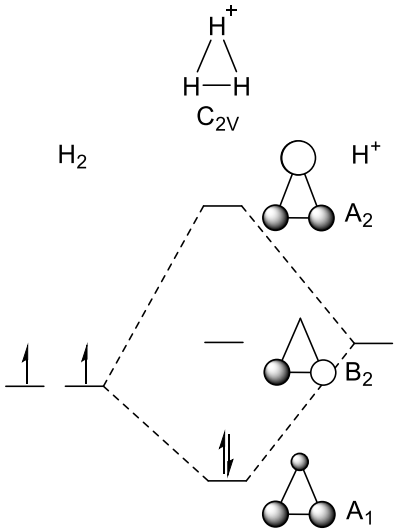

Figure 1.8 Representational H_3^+ orbital correlation diagram for 3c 2e$^-$ M-(η^2-H_2) bonding.

During the late 60's and early 70's, it was theorized that molecular dihydrogen may also approach the metal center and bind in an end-on motif as metal-(η^1-H_2).[16, 18, 19] This begs the

question of whether alternative metal-H_2 binding modes exist that were obscured as the Kubas dogma gained general acceptance. However, as was the case for Kubas complexes, acceptance and determination of (η^1-H_2) or unusual η^2-H_2 bonding awaits the isolation and characterization of complexes which provide examples of alternative metal-hydrogen bonding. It is the goal of this thesis to establish the existence of complexes that possess metal-(η^1-H_2) and unusual metal-(η^2-H_2) interactions.

CHAPTER 2. Neutron Structures for the Polyhydrogen Complexes $IrBrH_x(iPr_3P)_2 \cdot C_{10}H_8$ and $IrClH_x(iPr_3P)_2$: An Argument for a Cis Halide π Donor Effect on an Unexpected η^2-H_2 Conformation

2.1 Introduction

From the seminal characterization of the first metal-(η^2-H_2) complex by neutron diffraction in 1984, to the quintessential book on metal-dihydrogen complexes in 2001, the name Kubas hardly needs an introduction when discussing metal-dihydrogen structures. For nearly 20 years, the literature erupted with articles laying the groundwork for the fundamentals of metal-(η^2-H_2) bonding, or Kubas interaction. There was much controversy about the appropriate designation between formal oxidative addition of molecular H_2 to a dihydride and a Kubas type η^2-H_2 bond in metal-dihydrogen complexes. The distance between the metal bound hydrogens, $d_{H\text{-}H}$, has become essential in classifying the nature of hydrogen interaction at a metal center. Along this metal-hydrogen continuum, starting from the distance in free hydrogen, 0.74 Å, the $d_{H\text{-}H}$ placed these complexes in their currently accepted classifications. Approximately, 0.8-0.9 Å for a true Kubas non-classical M-(η^2-H_2) complex, ~1.0-1.2 Å for an elongated non-classical M-(η^2-H_2) complex, ~1.3-1.6 Å for a compressed classical M-$(H)_2$ or stretched non-classical M-(η^2-H_2), and >1.6 Å for a classical M-$(H)_2$.[16] Metal-hydrogen bonding designations are still ambiguous when classifying non-bonding and bonding character between the hydrogens on metal-polyhydrogen complexes. In fact, and only through neutron diffraction at 11 K, was the $[OsH_5(PPhMe_2)_3]^+$ structure finally resolved. It took scientists 25 years to establish that the 5 metal bound hydrogens most closely resemble a pentahydride assignment, even though the closest set of hydrogens are 1.49(4) Å from each other.[20]

Several techniques have been employed to establish metal-hydrogen character; NMR experiments, and X-ray diffractometry to name two. T_1 minimum (min) data and HD coupling in NMR experiments are used heavily to help determine the presence of a hydride or dihydrogen in metal-polyhydrogen complexes. However, we now know T_{1min} data can only help us determine the possible existence of either a hydride or dihydrogen ligand, not necessarily distinguish between the two.[16, 21] It was previously assumed that high T_{1min}, > 100 ms, was a distinguishing characteristic of a hydride and that a low T_{1min} value, < 40 ms, was a distinguishing characteristic

of an η^2-H_2 ligand. However, these parameters were solely based on homonuclear dipole-dipole interactions of metal-bound hydrogens.[21] T_{1min} values are not an infallible way to delineate the difference between a hydride or dihydrogen since T_{1min} values are highly dependent on the environment surrounding the hydrogens about a metal center; temperature, solvent effects, concentration, field strength and heteronuclear dipole-dipole interactions to name a few. There are more factors involved in interpreting T_{1min} values than just the distance between nuclei. In fact, T_1 values for dissolved H_2 in D_2O was found to be close to 2 seconds over a range of temperatures![22] In the case of some metal-polyhydrogen complexes, coupling data could not be determined because the exchange dynamics of these ligands were too fast to be seen even at low temperatures on the NMR time scale. In other words, HD coupling sometimes cannot be used to distinguish between hydride and dihydrogen ligands. X-ray diffraction cannot accurately locate or even determine the presence of hydrogens in most metal-polyhydrogen complexes. X-ray scattering cross sections of a transition metal vs. a hydrogen are too large to accurately distinguish metal-bound hydrogens or accurate d_{H-H}. In the case of $Cr(CO)_3(i Pr_3P)_2(H_2)$, X-ray diffraction results determined the distance between the hydrogens of the dihydrogen ligand to be 0.67(5) Å, an H-H bond distance less than that of molecular dihydrogen, 0.74 Å.[23]

While these techniques are still useful for complete structural analysis, they have their limits. It is well known that even neutron diffraction characterization for metal-polyhydrogen structural analysis has its issues. Even at low temperatures, if uncorrected, the rapid motion and exchange of multiple metal-bound hydrogens causes erroneous measurements of d_{H-H}. Even so, locating and determining metal-polyhydrogen orientations and bond lengths between hydrogens can only reliably be determined through corrected neutron diffraction structural studies. With the guiding principles well established to determine the ambiguity between hydride vs. dihydrogen bonding in metal complexes, however, there is still controversy over the bonding dynamics of metal-polyhydrogen interactions.

An explanation for the dynamical bonding of the metal-polyhydrogen interactions in the complex $Fe(H)_2(\eta^2\text{-}H_2)(EtPh_2P)_3$, whose structure was determined by neutron diffractometry in 1990 at 27 $\pm$ 0.5 K, is still a relevant topic of discussion.[24] The η^2-H_2 ligand in this polyhydrogen complex was found to exhibit an unexpected 43° twist from the expected P'-H'-H' plane, **Figure 2.1**. The orientation of the η^2-H_2 unit is typically found in the plane with ancillary ligands of least π acceptor ability and least steric hindrance. This is due to the metal's deemphasized electronic

back donation from a filled metal d_{π} orbital to the empty $H_{2\sigma*}$ orbital, which stabilizes an η^2 conformation of H_2.[16] In turn, a precise amount of metal to dihydrogen interaction should keep the η^2-H_2 unit confined to a plane.

The reasoning placed forth by this group is that because of the geometric distortion from the typical octahedron coordination, there is considerable orbital competition from the PR_3 ancillary ligands, sterics and a cis hydride interaction on the dihydrogen unit owing to its stabilization staggered between the P-Fe-H and P-Fe-P planes. The distance of the cis hydride is 1.862(13) Å from the closest hydrogen of the dihydrogen ligand, within Van der Waals radii, $d_{H\text{-}H}$ 2.4 Å, to account for some bonding character.[24] Recently, through high level calculations, it is reported that through a balance of crystal lattice dipole induced-dipole moments and molecular orbital interactions, the dihydrogen unit is arrested in the experimentally found staggered conformation. While the dihydrogen/dihydride exchange pathway is unresolved, the cis hydride attraction to the dihydrogen unit does not completely account for the intramolecular rearrangement of the metal bound hydrogens.[25]

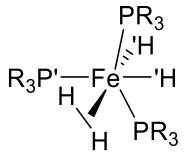

Figure 2.1 Representation of twisted η^2-H_2 unit found in $Fe(H)_2(\eta^2\text{-}H_2)PR_3$, where R = $EtPh_2$ and R_3P'-H'-H' represent the expected plane for the η^2-H_2 conformation.

To the author's knowledge, the last two neutron structures of interest and relevance to the current work were reported in 2005. The metal-polyhydrogen complex $RuH_2(\eta^2\text{-}H_2)_2(PCyp_3)_2$ was the first reported bis(dihydrogen) structure determined by neutron diffractometry at 20 K.[26] It was reported that the two dihydrogen ligands cis to each other are twisted out of their coordination plane by 24.6(5)° and 22.8(5)°, not unexpected because of steric allowances from the ancillary ligands. Most notably, they report each dihydrogen ligand is outside the acceptable range for any interaction with their cis hydride neighbors, > 2.1 Å. In other words, contrary to the case of $Fe(H)_2(\eta^2\text{-}H_2)(EtPh_2P)_3$, there is no cis hydride interaction on the dihydrogen units to explain the

exchange process between the 6 hydrogens on $RuH_2(\eta^2\text{-}H_2)_2(PCyp_3)_2$. Also, in 2005, the neutron diffraction determined structure for $OsClH_3(PPh_3)_3$ was resolved 30 years after being formulated as $OsClH(PPh_3)_3$![27] Neutron data was collected at 295 K and 5 K where they note "barely significant" changes in geometry between the two temperatures. Two hydrogens with $d_{H\text{-}H}$ of 1.48(2) Å are categorized on the continuum of dihydrogen complexes in the range of "compressed dihydride" or "severely stretched" dihydrogen complex. Not quite classical yet not quite a non-classical type of metal-hydrogen interaction. Most notably, the geometry about the metal center is severely distorted from an octahedron where the cis hydride is 1.67(2) Å away from dihydrogen unit displaying some bonding character. The dihydrogen is found in the expected plane, H-Os-Cl, trans to a chloride and cis to a hydride, in the plane where the ancillary ligands have the least π acceptor ability. It is suggested that the presence of a trans chloride, being more electronegative than hydride, is promoting closer H-H interactions causing the severe stretching in the dihydrogen unit.

The polyhydrogen complex $IrBrH_x(i\text{Pr}_3\text{P})_2\cdot C_{10}H_8$ **(1)**, who's structure was resolved by neutron diffractometry at 25(2) K and unpublished for nearly 25 years, will be reported and analyzed. **(1)** was found with two superimposed structures, one saturated species with an $\eta^2\text{-}H_2$ unit found in the expected Br-Ir-H plane and an unsaturated dihydride species. Neutron diffractometry results at 293(2) K for $IrClH_x(i\text{Pr}_3\text{P})_2$ **(2)** resolved with an $\eta^2\text{-}H_2$ unit with $d_{H\text{-}H}$ 0.7167(0.0142) Å, less than $d_{H\text{-}H}$ found in molecular dihydrogen, 0.74 Å! An alternate study at liquid helium temperatures for $IrClH_x(i\text{Pr}_3\text{P})_2$ **(3)** was conducted, where we also report the first metal-polyhydrogen complex with three superimposed structures found by neutron diffractometry. **(3)** contains two superimposed saturated iridium-polyhydrogen structures each with a different conformer of an $\eta^2\text{-}H_2$ unit and one unsaturated dihydride species. One saturated conformer resolves with a dihydrogen unit found in an unprecedented nearly 90° rotation from the expected Cl-Ir-H coordination plane!

2.2 P_2X Background

Coordinatively unsaturated complexes of the type $MX(H)_2P_2$ (P = PR_3, X = halide) were of interest for their reactions involving their basic metal centers.[28] Interest which evolved into $MX(H)_2P_2$ complexes' reactivity with hydrogen, forming their coordinatively saturated

complexes, $MX(H)_2(H_2)P_2$. Almost 30 years ago, this group isolated and characterized the first neutral iridium polyhydrogen compound $IrCl(H)_2(\eta^2\text{-}H_2)L_2\cdot C_{10}H_8$ (L = *i*Pr_3P) **(4)**.[29] A structure was reported, found by single crystal X-ray diffraction studies, for the core $IrClL_2$ structure, but the metal bound hydrogen designations could not be resolved for the chloro analogue.[29, 30] However, in 1995, a structure for the $IrI(H)_2(\eta^2\text{-}H_2)L_2\cdot C_{10}H_8$ **(5)** analogue was resolved by single crystal neutron diffractometry at 15 K while, in the $IrCl(H)_2(\eta^2\text{-}H_2)L_2\cdot C_{10}H_8$ analogue, there was still dynamic disordering found at 15 K and in turn, a neutron diffraction structure was not obtained.[31] This group is now able to verify, through single crystal neutron diffractometry, the hydride and dihydrogen distinction at the iridium metal center in $IrX(H)_2(\eta^2\text{-}H_2)L_2$ for X = Cl^-, and Br^-. What is the reasoning for the unexpected rotation found in one $\eta^2\text{-}H_2$ conformer of $IrCl(H)_2(\eta^2\text{-}H_2)$(*i*$Pr_3P)_2$? Some background and trends with regards to the energetics and computational studies for this halide series of metal-polyhydrogen complexes that have been previously reported and theorized needs to be recounted.

While trying to determine the type of hydrogen bonding about the iridium center, this group used alternate techniques to characterize and analyze the metal-polyhydrogen interactions of the type $IrX(H)_2(\eta^2\text{-}H_2)L_2$, (X = Cl^-, Br^-, and I^-). Through NMR studies, $IrCl(H)_2(\eta^2\text{-}H_2)L_2$ was found to exhibit rapid intermolecular dynamic exchange with free hydrogen down to 178 K, unlike similar iridium cationic species which displayed no intermolecular exchange with free H_2, and rapid intramolecular dihydride and dihydrogen exchange to the low temperature limit of NMR techniques, 77 K.[29, 30] Similar dynamics were found within $IrX(H)_2(\eta^2\text{-}H_2)L_2$ (X = Br^-, and I^-) analogues. Also through NMR studies, the barrier heights for the interconversion with free H_2 were calculated between the three analogues which resulted in the iodo analogue having the highest energy barrier, 45.6 kJ/mol, and the chloro analogue having the lowest energy barrier to interconversion, 40.0 kJ/mol (bromo analogue = 43.6 kJ/mol).[32] The iodo analogue displays the most difficulty, of the three halide analogues, exchanging with free H_2. Through INS studies, the barrier to H_2 rotation resulted in the iodo analogue also having the highest energy barrier, 3.8 kJ/mol, and the chloro analogue having also the lowest energy barrier 2.1 kJ/mol to H_2 rotation (bromo analogue = 2.2 kJ/mol).[32] The dihydrogen unit is labile but strong enough for some π back-bonding interaction from the metal center. These studies confirm that the π back-bonding strength from the metal d_π to $H_{2\sigma^*}$ among the three halide analogues increases down the halide period, Cl^- < Br^- < I^-. In other words, the iodo analogue is the most thermodynamically stable analogue as

opposed to the bromo which is slightly more thermodynamically stable than the chloro analogue. This could explain the dynamic disordering still found at 15 K during neutron diffraction studies for the $IrCl(H)_2(\eta^2\text{-}H_2)L_2$ complex. If we only consider the σ donor ability of the halide to metal, then this thermodynamic trend reflects their σ donor strengths which increases down the halide period, $Cl^- < Br^- < I^-$. As the electron density at the iridium center increases so too does the metal d_π to $H_{2\sigma^*}$ back-bonding interaction then too should the $d_{H\text{-}H}$ of the dihydrogen ligand increase. Considering metal d_π to $H_{2\sigma^*}$ strengths across the three halide analogues, the activation of the dihydrogen ligand should also reflect this trend. It is then implied, that the $d_{H\text{-}H}$ on each of the analogues must also increase down the halide period, $Cl^- < Br^- < I^-$. As such, from X-ray diffraction data, the Ir-Cl distance found in the chloro analogue, 2.427(2) Å, and the Ir-I distance found in the iodo analogue, 2.728(3) Å, from neutron diffraction data, lead to the implication that metal to halide distance should also increase down the halide period, $Cl^- < Br^- < I^-$.

Computational results were reported using data obtained from the neutron structure for $IrI(H)_2(\eta^2\text{-}H_2)L_2$ (L = *i*Pr_3) as a model to answer lingering questions about certain trends in the bromo and chloro analogues. Ancillary ligand effects, best theories for modeling these complexes, and transition states vs. intermediates proposed for the mechanism of intra-hydride dihydrogen exchange were discussed. To sum the relevant findings, only the data for the theoretical bond distances of the saturated and unsaturated species found between the bromo and chloro analogues will be used later for discussion, since we now have neutron data for comparison. The important implications of σ and π interactions about the metal center from the computational data that considered the H_2 unit in the same plane found as the saturated $IrI(H)_2(\eta^2\text{-}H_2)L_2$ species, about the X-Ir-H coordination plane. In the saturated species, geometry about Ir in the $IrX(H)_2(\eta^2\text{-}H_2)L_2$ (L = Me_3P) series was modeled as a transition state from two relevant reports.[33, 34] It was concluded that H_2 disrupts the π interaction between metal and halide, and that it would be more energetically disfavored to reach a transition state for a stronger Ir-X π interaction, in which π donor strength increases up the halide period, $Cl^- > Br^- > I^-$, as opposed to σ donor strength increasing down the halide period $Cl^- < Br^- < I^-$. As weakening of Ir-X π interaction increases, so the σ interactions at Ir center adjust to account for the change in geometry. Since a H^- has strong σ donor capabilities, it is more energetically favorable for I^- to be trans to H^-, as I^- has weaker σ donor potential in comparison, and so energy cost increases up the halide period, $Cl^- > Br^- > I^-$. It is thought, since I^-

is less electronegative among the three halides, it would donate more electron density to Ir, increasing the metal d_π to $H_{2\sigma^*}$ interaction. It is agreed in an alternate finding, that as the halide becomes less electronegative, $Cl^- > Br^- > I^-$, electron density on the metal should increase back donation from metal d_π to $H_{2\sigma^*}$, increasing the activation of H_2 where $d_{H\text{-}H}$ should increase down the halide period $Cl^- < Br^- < I^-$. Expected trends to follow, where $d_{H\text{-}H}$ increases down the halide period, $I^- > Br^- > Cl^-$, and metal to halide distance should increase down the period as well, $I^- > Br^- > Cl^-$. Calculated bond distances in $d_{H\text{-}H}$ and $d_{M\text{-}X}$ confirm these trends from both reports. However, if the influence of the trans hydride is also considered, since Cl^- and H^- both exhibit strong trans influence and are found trans to each other in all three of these complexes, the metal center in turn would then be more basic in the chloro analogue, while basicity at the metal center increases up the halide period, $Cl^- > Br^- > I^-$.

There is an awareness that slight changes to the electronic environment about a metal center has massive influence on an H_2 metal coordinated unit. The effects of ancillary ligands on the activation of the H_2 unit in the $IrX(H)_2(\eta^2\text{-}H_2)L_2$ series, is not quite as generic as previously discussed. We now know from available neutron data collected for the chloro and bromo analogues that not only is the $d_{H\text{-}H}$ in the $\eta^2\text{-}H_2$ ligand trend disproved, where $d_{H\text{-}H}$ was thought to be longest in the iodo analogue and shortest in the chloro analogue, there is also an unusual situation in the case of the chloro analogue where there are two superimposed conformers of an $\eta^2\text{-}H_2$ unit. One $\eta^2\text{-}H_2$ unit found in the expected Cl-Ir-H plane and one rotated nearly a full 90° from this coordination plane. In both conformers of the $\eta^2\text{-}H_2$ unit in the chloro analogue the $d_{H\text{-}H}$ is longer than in the iodo analogue, results and discussion to follow. The only change across the $IrX(H)_2(\eta^2\text{-}H_2)L_2$ series is the halide ligand from iodo to chloro, which produces an electronic influence that results in an unexpected rotation of the $\eta^2\text{-}H_2$. Discrepancies in the afore mentioned trends resulting in the unexpected distance between H-H from the halide replacement in the $IrX(H)_2(\eta^2\text{-}H_2)L_2$ series tells us that there is more that needs to be emphasized in the discussion of donor ability than σ ligand strength. Computational results were based on the neutron data for the iodo analogue, where L = Me_3P computationally, yet L = $i Pr_3P$ experimentally, this could have wild effects on results since basicity at the metal would increase from the computed $(Me_3P)_2$ ancillary unit to the experimental $(iPr_3P)_2$ ancillary unit. Now there is publishable data on the chloro and bromo structures to contrast results and trends. A 90° rotated H_2 unit was considered as a transition

state in one report.[33] Both σ donor and π donor strengths of the halides need to be emphasized in the discussion and weighted across the three halides. Some of these insights may help us to understand the 90° rotation of the η^2-H_2 unit in the chloro analogue. However, we do confirm the $d_{M\text{-}X}$ expected trend does hold true where $d_{M\text{-}X}$ is longest in the iodo and decreases up the halide period, $Cl^- < Br^- < I^-$. Loose generic trends do not account for the H_2 unit found out of the expected plane.

2.3 Experimental

General Considerations. All manipulations were carried out under 100 % H_2 (g) (Airgas USA) atmosphere with standard Schlenk and glove bag techniques. Any glove box manipulations were carried out under 100 % Ar (g) (Airgas USA) atmosphere. (*i*Pr)$_3$P (Strem Chemicals) and $IrCl_3$•xH_2O (Johnson-Mathey) were used as received. The complex $[IrCl(C_8H_{14})_2]_2$ was prepared according to literature.[35] All other solvents and reagents were purified, dried and deoxygenated using conventional methods. All synthesized complexes here within are highly air sensitive and stable only under H_2 (g) atmosphere.

Synthesis and Crystal Isolation. **$IrBrH_x(iPr_3P)_2 \cdot C_{10}H_8$**. Preparation of $IrBrH_x(iPr_3P)_2 \cdot C_{10}H_8$ was carried out with modification to the method of Le-Husebo.[32] A solution of $IrCl(H)_2(iPr_3P)_2$ and LiBr (xs) in toluene was added to a reaction vessel. The solution was heated to 50 °C and stirred under H_2 (g). The solvent was removed in vacuo and the subsequent product was co-crystallized with naphthalene in C_5H_{12} under approximately 1 atm. of H_2 (g) which yielded orange crystals large enough for neutron diffraction studies. An orange crystal was picked and mounted in a hydrogen filled glove bag.

Synthesis and Crystal Isolation. **$IrClH_x(iPr_3P)_2$**. Preparation of $IrClH_x(iPr_3P)_2$ was carried out with modification to the method of Mediati.[30] A solution of $[IrCl(C_8H_{14})_2]_2$ and (*i*Pr)$_3$P (1 mol: 4.5 mol) in C_5H_{12} was added to a 10 mL Schlenk bomb flask. The subsequent orange solution was freeze-pump-thaw degassed 3x before the addition of H_2 (g). The solution was stirred vigorously for 12 h under H_2 (g). The solvent was removed in vacuo until the product appeared as a red-orange oil. Fresh C_5H_{12} was added to the oil until first sign of dissolution and filtered through a Kimwipe

plug into a new Schlenk bomb flask. Approximately 1 atm. pressure of H_2 (g) was intermittently added to the solution over a period of one week for the reduction of the solvent before crystallization from evaporation could occur. The super saturated solution was heated to 100 °C and left to slowly return to ambient temperature over a period of 24 h after which a single orange crystal large enough for neutron diffraction studies had been obtained. The orange crystal was picked and mounted in a hydrogen filled glove bag.

2.4 Results

Table 2.1 Neutron diffraction data for $IrBrH_x(iPr_3P)_2 \cdot C_{10}H_8$ **(1)** at 25(2) K.

Empirical formula	$C_{28}H_{56}BrIrP_2$
Formula weight	726.83
Wavelength	1.3033 Å
Crystal System, Space group	Triclinic, C_i^1-Pī
a, Å	8.0029(10)
b, Å	13.6829(10)
c, Å	14.4094(10)
α, deg.	83.621(5)
β, deg.	83.959(5)
γ, deg.	72.225(5)
Vol., $Å^3$	1489.0(2)
Z, Calculated density; Mg/m^3	2, 1.621
Temp. of data collection, K	25(2)
linear abs. coeff., mm^{-1}	0.382
F(000)	9
Theta range for data collection, deg.	2.616 to 55.305
Limiting indices	-9<=*h*<=4, -16<=*k* <=14, -16<=*l*<=18
Reflections collected / unique	6203 / 4791 [R(int) = 0.0400]
Completeness to theta = 51.442	85.2 %
Refinement method	Full matrix least – squares on F^2
Data / Restraints / Parameters	4791 / 0 / 793
Goodness to fit on F^2	1.041
Final R indices [I>2σ(I)]	R1 = 0.0560, *w*R2 = 0.1370
R indices (all data)	R1 = 0.0621, *w*R2 = 0.1416
Largest diff. peak and hole	1.013 and -1.114 e.$Å^3$

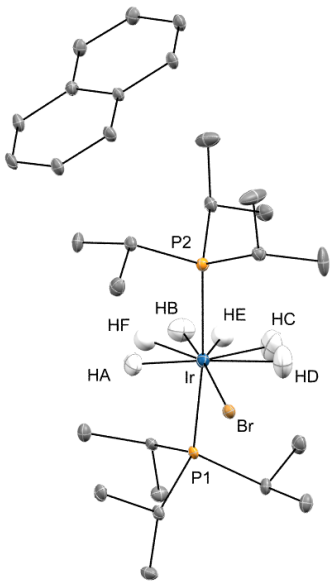

Figure 2.2 ORTEP diagram of the structure determined for $IrBrH_x(iPr_3P)_2 \cdot C_{10}H_8$ **(1)** by neutron diffraction analysis. Atoms in the iridium coordination sphere have been labeled. Coordinatively saturated high occupancy and unsaturated low occupancy superimposed structural hydride ligand sets, H(A), H(B) and H(F), H(E), respectively, have been included. Coordinatively saturated high occupancy dihydrogen ligand, H(C)-H(D), has been included. Alkane hydrogens have been omitted for clarity. Thermal ellipsoids at 50 % probability.

Table 2.2 Neutron diffraction data for $IrClH_x(iPr_3P)_2$ **(2)** at 293(2) K.

Empirical formula	$C_{18}H_{45}ClIrP_2$
Formula weight	551.18
Crystal system, Space group	Monoclinic, C_{2h}^5-$P2_1/c$
a, Å	15.7824(7)
b, Å	8.9511(3)
c, Å	16.2988(6)
α, deg.	90
β, deg.	94.954(3)
γ, deg.	90
Vol., $Å^3$	2293.93(15)
Z, Calculated density; Mg/m^3	4, 1.596
Temp. of data collection, K	293(2)
linear abs. coeff., mm^{-1}	0.446
F(000)	-73
Theta range for data collection, deg.	5.143 to 60.784
Limiting indices	-9<=*h*<=18, -10<=*k*<=10, -19<=*l*<=19
Reflections collected / unique	14313 / 3914 [R(int) = 0.0831]
Completeness to theta = 60.844	94.2 %
Refinement method	Full-matrix least-squares on F^2
Data / Restraints / Parameters	3914 / 0 / 631
Goodness to fit on F^2	1.094
Final R indices [I>2σ(I)]	R1 = 0.0669, *w*R2 = 0.1699
R indices (all data)	R1 = 0.0741, wR2 = 0.1767
Largest diff. peak and hole	0.811 and -0.920 e.$Å^3$

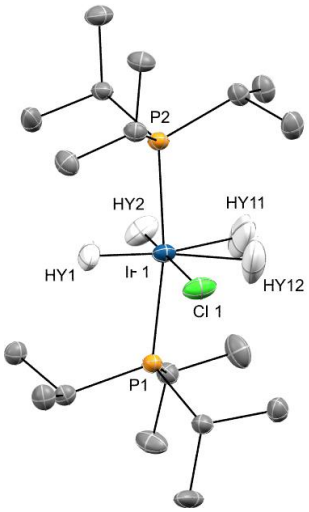

Figure 2.3 ORTEP diagram of the structure determined for $IrClH_x(i Pr_3P)_2$ **(2)** at 293(2) K by neutron diffraction analysis. Atoms in the iridium coordination sphere have been labeled. Coordinatively saturated structural hydrides, HY(1) and HY(2), have been included. Dynamically disordered dihydrogen ligand HY(11)-HY(12) has been included. Alkane hydrogens have been omitted for clarity. Thermal ellipsoids at 50 % probability.

Table 2.3 Neutron diffraction data $IrClH_x(iPr_3P)_2$ **(3)** at 5(2) K.

Empirical formula	$C_{18}H_{45}ClIrP_2$
Formula weight	551.18
Crystal system, Space group	Monoclinic, C_{2h}^5-$P2_1/c$
a, Å	15.7744(8)
b, Å	8.9542(4)
c, Å	16.2934(7)
α, deg.	90
β, deg.	94.980(3)
γ, deg.	90
Vol., $Å^3$	2292.71(18)
Z, Calculated density; Mg/m^3	4, 1.597
Temp. of data collection, K	5(2)
linear abs. coeff., mm^{-1}	0.4467
F(000)	-73
Theta range for data collection, deg.	5.143 to 60.823
Limiting indices	-9<=*h*<=17, -9<=*k*<=10, -19<=*l*<=19
Reflections collected / unique	10469 / 3628 [R(int) = 0.0623]
Completeness to theta = 60.844	87.3 %
Refinement method	Full-matrix least-squares on F^2
Data / Restraints / Parameters	3628 / 0 / 629
Goodness to fit on F^2	1.073
Final R indices [I>2σ(I)]	R1 = 0.0583, *w*R2 = 0.1429
R indices (all data)	R1 = 0.0717, *w*R2 = 0.1492
Largest diff. peak and hole	0.733 and -0.972 e.$Å^3$

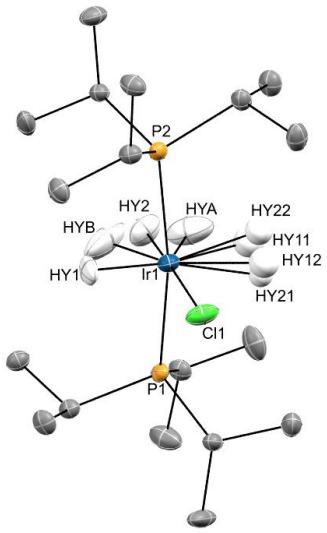

Figure 2.4 ORTEP diagram of the structure determined for $IrClH_x(iPr_3P)_2$ **(3)** at 5(2) K by neutron diffraction analysis. Atoms in the iridium coordination sphere have been labeled. Coordinatively saturated and unsaturated superimposed structural hydride ligand sets, HY(1), HY(2) and HY(A), HY(B), respectively, have been included. Coordinatively saturated high and low occupancy dihydrogen ligands, H(11)-H(12) and H(21)-H(22), respectively, have been included. Alkane hydrogens have been omitted for clarity. Thermal ellipsoids at 50 % probability.

Table 2.4 Selected bond distances (Å). Inside the metal coordination sphere only. Includes superimposed structures and high and low occupancy hydrogens except for the low occupancy η^2-H_2 from **(3)**. Refer to Figures 2.1-2.3 for labeling, see Appendices A-C for supplemental information.

$IrBrH_x(iPr_3P)_2 \cdot C_{10}H_8$ **(1)** Figure 2.1		$IrClH_x(iPr_3P)_2$ **(2)** Figure 2.2		$IrClH_x(iPr_3P)_2$ **(3)** Figure 2.3	
H(C)-H(D)	0.8231(0.0091)	HY(11)-HY(12)	0.7167(0.0142)	HY(11)-HY(12)	0.8727(0.0250)
P(1)-Ir	2.330(3)	P(1)-Ir	2.322(3)	P(1)-Ir	2.323(3)
P(2)-Ir	2.326(3)	P(2)-Ir	2.319(3)	P(2)-Ir	2.314(3)
H(A)-Ir	1.586(6)	HY(1)-Ir	1.548(7)	HY(1)-Ir	1.552(7)
H(B)-Ir	1.602(7)	HY(2)-Ir	1.581(9)	HY(2)-Ir	1.586(9)
H(C)-Ir	1.761(6)	HY(11)-Ir	1.773(12)	HY(11)-Ir	1.780(14)
H(D)-Ir	1.784(6)	HY(12)-Ir	1.821(13)	HY(12)-Ir	1.811(15)
Br-Ir	2.592(2)	Cl-Ir	2.4444(18)	Cl-Ir	2.4426(18)
H(E)-Ir	1.507(16)	HY(A)-Ir	1.474(17)	HY(A)-Ir	1.472(15)
H(F)-Ir	1.589(15)	HY(B)-Ir	1.578(14)	HY(B)-Ir	1.594(15)

Table 2.5 Low occupancy η^2-H_2 located on structure **(3)**, HY(21)-HY(22), bond distances (Å). Refer to Figure 2.3 for labeling.

$IrClH_x(iPr_3P)_2$ **(3)** Figure 2.3	
HY(21)-HY(22)	0.8812(0.0386)
HY(21)-Ir	1.85(2)
HY(22)-Ir	1.84(2)

Table 2.6 Selected bond angles (°). Inside the metal coordination sphere only. Includes superimposed structures and high and low occupancy hydrogens except for the 90° rotated low occupancy η^2-H_2 from **(3)**. Refer to Figures 2.1-2.3 for labeling, see Appendices A-C for supplemental information.

$IrBrH_x(iPr_3P)_2 \cdot C_{10}H_8$ **(1)** Figure 2.1		$IrClH_x(iPr_3P)_2$ **(2)** Figure 2.2		$IrClH_x(iPr_3P)_2$ **(3)** Figure 2.3	
P(1)-Ir-P(2)	172.87(10)	P(1)-Ir-P(2)	171.05(10)	P(1)-Ir-P(2)	170.79(10)
P(1)-Ir-H(A)	87.2(2)	P(1)-Ir-HY(1)	87.3(3)	P(1)-Ir-HY(1)	86.8(3)
P(1)-Ir-H(B)	87.1(3)	P(1)-Ir-HY(2)	86.8(4)	P(1)-Ir-HY(2)	86.6(4)
P(1)-Ir-H(C)	92.1(3)	P(1)-Ir-HY(11)	97.2(5)	P(1)-Ir-HY(11)	92.9(6)
P(1)-Ir-H(D)	93.1(3)	P(1)-Ir-HY(12)	88.5(6)	P(1)-Ir-HY(12)	92.4(7)
P(1)-Ir-Br	92.39(8)	P(1)-Ir-Cl	92.91(8)	P(1)-Ir-Cl	92.84(8)
P(2)-Ir-H(A)	88.4(2)	P(2)-Ir-HY(1)	85.0(3)	P(2)-Ir-HY(1)	85.2(3)
P(2)-Ir-H(B)	86.9(3)	P(2)-Ir-HY(2)	88.5(4)	P(2)-Ir-HY(2)	88.4(4)
P(2)-Ir-H(C)	90.4(3)	P(2)-Ir-HY(11)	89.2(5)	P(2)-Ir-HY(11)	93.3(6)
P(2)-Ir-H(D)	92.1(3)	P(2)-Ir-HY(12)	99.7(6)	P(2)-Ir-HY(12)	96.2(7)
H(A)-Ir-H(B)	83.5(4)	HY(1)-Ir-HY(2)	89.0(6)	HY(1)-Ir-HY(2)	86.7(6)
H(A)-Ir-Br	91.9(2)	HY(1)-Ir-Cl	91.5(3)	HY(1)-Ir-Cl	92.0(3)
H(A)-Ir-H(C)	161.7(4)	HY(1)-Ir-HY(11)	165.0(7)	HY(1)-Ir-HY(11)	161.5(6)
H(A)-Ir-H(D)	171.4(4)	HY(1)-Ir-HY(12)	171.9(6)	HY(1)-Ir-HY(12)	170.4(6)
H(B)-Ir-H(C)	78.2(5)	HY(2)-Ir-HY(11)	77.1(9)	HY(2)-Ir-HY(11)	74.8(8)
H(B)-Ir-H(D)	105.0(5)	HY(2)-Ir-HY(12)	97.7(8)	HY(2)-Ir-HY(12)	102.9(8)
H(B)-Ir-Br	175.5(4)	HY(2)-Ir-Cl	179.4(5)	HY(2)-Ir-Cl	178.6(5)
H(C)-Ir-H(D)	26.8(3)	HY(11)-Ir-HY(12)	23.0(5)	HY(11)-Ir-HY(12)	28.1(8)
H(C)-Ir-Br	106.3(4)	HY(11)-Ir-Cl	102.5(7)	HY(11)-Ir-Cl	106.5(6)
H(D)-Ir-Br	91.5(9)	HY(12)-Ir-Cl	81.8(5)	HY(12)-Ir-Cl	78.4(5)
H(E)-Ir-Br	149.8(10)	HY(A)-Ir-Cl	145.0(12)	HY(A)-Ir-Cl	148.7(10)
H(E)-Ir-H(F)	69.4(13)	HY(A)-Ir-HY(B)	67.6(14)	HY(A)-Ir-HY(B)	65.5(12)
H(F)-Ir-Br	140.6(9)	HY(B)-Ir-Cl	147.4(11)	HY(B)-Ir-Cl	145.7(10)

Table 2.7 Low occupancy η^2-H_2 located on structure **(3)**, HY(21)-HY(22), bond angles (°). Refer to Figure 2.3 for labeling.

$IrClH_x(iPr_3P)_2$ **(3)** Figure 2.3			
HY(21)-Ir-P(1)	79.6(8)	HY(22)-Ir-P(1)	106.9(8)
HY(21)-Ir-P(2)	108.4(8)	HY(22)-Ir-P(2)	80.8(8)
HY(21)-Ir-Cl	88.4(8)	HY(22)-Ir-Cl	91.5(9)
HY(21)-Ir-HY(1)	166.3(8)	HY(22)-Ir-HY(1)	165.7(9)
HY(21)-Ir-HY(2)	92.8(10)	HY(22)-Ir-HY(2)	89.9(10)
HY(21)-Ir-HY(22) 27.7(12)			

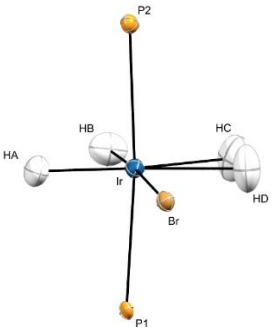

(1a)

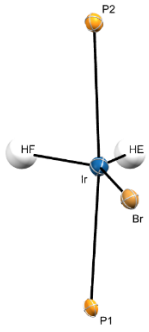

(1b)

Figure 2.5 ORTEP diagram for iridium coordination sphere of **(1)**. $IrBr(H)_2(\eta^2\text{-}H_2)(iPr_3P)_2\cdot C_{10}H_8$ **(1a)** high occupancy coordinatively saturated hydrides, H(A) and H(B), η^2-H_2, H(C)-H(D), ligand. $IrBr(H)_2(iPr_3P)_2\cdot C_{10}H_8$ **(1b)** low occupancy coordinatively unsaturated hydrides, H(E) and H(F). Alkane carbons and hydrogens have been removed for clarity.

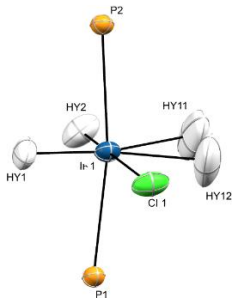

(2)

Figure 2.6 ORTEP diagram for iridium coordination sphere of $IrCl(H)_2(\eta^2\text{-}H_2)(i\text{Pr}_3\text{P})_2$ **(2)**. Coordinatively saturated hydrides, HY(1) and HY(2), and the dynamically disordered $\eta^2\text{-}H_2$, HY(11)-HY(12), ligand. Alkane carbons and hydrogens have been removed for clarity.

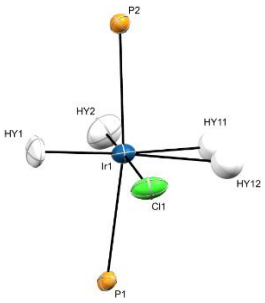

(3a)

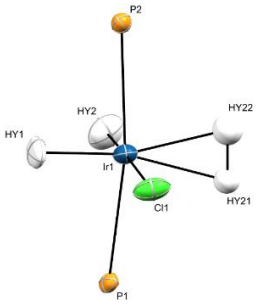

(3b)

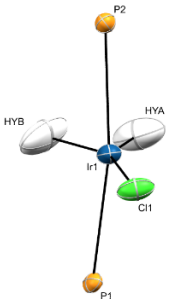

(3c)

Figure 2.7 ORTEP diagram for iridium coordination sphere of **(3)**. $IrCl(H)_2(\eta^2\text{-}H_2)(i\text{Pr}_3\text{P})_2$ **(3a)** coordinatively saturated hydrides, HY(1) and HY(2), and the high occupancy $\eta^2\text{-}H_2$, HY(11)-HY(12), ligand. $IrCl(H)_2(\eta^2\text{-}H_2)(i\text{Pr}_3\text{P})_2$ **(3b)** coordinatively saturated hydrides, HY(1) and HY(2), and the low occupancy $\eta^2\text{-}H_2$, HY(21)-HY(22), ligand. $IrCl(H)_2(i\text{Pr}_3\text{P})_2$ **(3c)** coordinatively unsaturated hydrides, HY(A) and HY(B). Alkane carbons and hydrogens have been removed for clarity.

2.5 Discussion

Solid State Structure. **$IrBrH_x(iPr_3P)_2 \cdot C_{10}H_8$ (1)**. The neutron diffraction analysis of **(1)**, **Figure 2.2**, refined to give two superimposed structures, one of higher occupancy, the non-classical polyhydrogen complex $IrBr(H)_2(\eta^2\text{-}H_2)(iPr_3P)_2 \cdot C_{10}H_8$ **(1a)**, **Figure 2.5**, and one of lower occupancy, the classical dihydride complex $IrBr(H)_2(iPr_3P)_2 \cdot C_{10}H_8$ **(1b)**, **Figure 2.5**. The non-classical polyhydrogen complex **(1a)** resolves with the highest occupied metal coordinated hydrogens, hydrides H(A) and H(B) and the dihydrogen ligand H(C)-H(D). The dihydride structure **(1b)** resolves with the lowest occupied metal coordinated hydrides, hydrides H(E) and H(F). In **(1a)**, the Ir-hydride distances (Ir-H(A) 1.586(6) and Ir-H(B) 1.602(7) Å) are significantly shorter than the Ir-H dihydrogen distances (Ir-H(C) 1.761(6) and Ir-H(D) 1.784(6) Å). This same relationship was found for the established neutron structure for $IrI(H)_2(\eta^2\text{-}H_2)(iPr_3P)_2 \cdot C_{10}H_8$ **(5)**, where the Ir-hydride distances (Ir-H(a) 1.579(6) and Ir-H(b) 1.589(6) Å) and the Ir-H dihydrogen distance (Ir-H(c) 1.764(7) and Ir-H(d) 1.748(7) Å) were similarly disproportionate.[31] The Ir-P distances found for **(1)**, (Ir-P(1) 2.330(3) and Ir-P(2) 2.326(3) Å), agree with comparable Ir-P distances in other iridium non-classical polyhydrogen structures.[31,36,37] Ir-P distances in **(1)** are slightly shorter than in **(5)**, (Ir-P(1) 2.334(4) and Ir-P(2) 2.338(4) Å), and slightly longer than in **(3)**, as mentioned below. The dihydrogen ligand in **(1a)**, H(C)-H(D), has a $d_{H\text{-}H}$ of 0.8231(0.0091) Å, which is an H-H separation in agreement with true $\eta^2\text{-}H_2$ type coordinated complexes, only slightly elongated from molecular dihydrogen (0.74 Å).[16] The $d_{H\text{-}H}$ for **(1a)** (H(C)-H(D) 0.8231(0.0091) Å), follows the anticipated trend shorter than **(5)** (H(c)-H(d) 0.856(9) Å).[31] The replacement of the iodo ligand in **(5)** with a bromo ligand in **(1)** decreases the electron density at the iridium center (less σ donor capability from iodo to bromo) thereby weakening the metal-d_π to $H_{2\sigma^*}$ back-bonding capability. In other words, there is an even weaker Ir-dihydrogen interaction in **(1)** than **(5)**. The expected trends from **(5)** to **(1)** continue with the metal-halide distance, in **(1)** (Ir-Br 2.592(2) Å) is shorter than in **(5)** (Ir-I 2.770(4) Å) due to the decrease in size of atomic radii from iodo to bromo.[31] The H(C)-H(D) ligand, almost completely eclipses the Br-Ir-H(B)-H(A) equatorial plane (arbitrarily assigned), **Figure 2.8**, with a dihedral angle between the equatorial plane Br-Ir-H(B)-H(A) and the axial plane H(A)-Ir-P(2)-P(1) of 89.6(8)°, **Figure 2.9**. The H(C)-H(D) eclipse of the equatorial plane in **(1)** is slightly more orthogonal to the axial plane than in

(5), which has a dihedral angle between the synonymous planes of 88.8(5)°.[31] As mentioned above, in both the cases of **(1)** and **(5)**, the dihydrogen ligand was located in the expected equatorial plane.

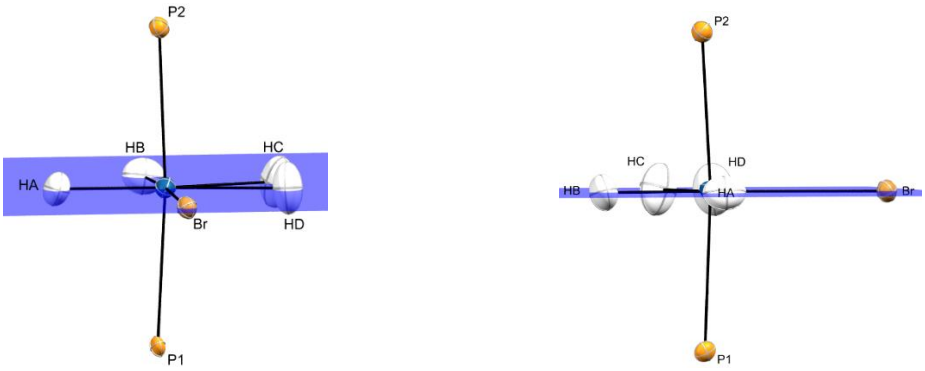

(1aα) **(1aβ)**

Figure 2.8 ORTEP diagram for iridium coordination sphere in **(1a)**. **(1aα)** equatorial plane, Br-Ir-H(B)-H(A) (blue). Tilted view down the Br-Ir-H(B) axis. **(1aβ)** equatorial plane, Br-Ir-H(B)-H(A) (blue). View down the H(A)-Ir-(H(C)-H(D)) axis. Alkane carbons and hydrogens have been removed for clarity.

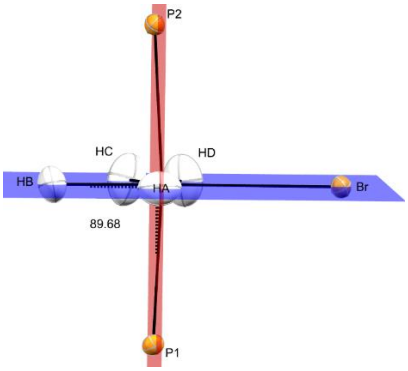

Figure 2.9 ORTEP diagram for iridium coordination sphere in **(1a)**. Equatorial plane, Br-Ir-H(B)-H(A) (blue). Axial plane, H(A)-Ir-P(1)-P(2) (red). View down the H(A)-Ir-(H(C)-H(D)) axis. Alkane carbons and hydrogens have been removed for clarity.

Solid State Structure. **$IrClH_x(iPr_3P)_2$ (2)**. The neutron diffraction analysis of **(2)**, **Figure 2.3**, at 293(2) K refined to give two superimposed structures, one of higher occupancy, the non-classical polyhydrogen complex $IrCl(H)_2(\eta^2\text{-}H_2)(iPr_3P)_2$ **(2)**, **Figure 2.3,** and one of lower occupancy, a classical dihydride complex, $IrCl(H)_2(iPr_3P)_2$, not depicted. Upon analysis, the $d_{H\text{-}H}$, HY(11)-HY(12), 0.7167(0.0142) Å (**Table 2.4**, highlighted in red) was troubling since the $d_{H\text{-}H}$ found in **(2)** is shorter than in free hydrogen (0.74 Å). However, in comparison to X-ray data collected for $IrCl(H)_2(\eta^2\text{-}H_2)(iPr_3P)_2\cdot C_{10}H_8$ **(4)**, the Ir-Cl distance found in **(2)**, 2.4444(18) Å, did agree with Ir-Cl distance from **(4)**, 2.427 Å. Ir-P(1) and Ir-P(2) found in **(4)**, 2.303 and 2.307 Å respectively, also agree with the Ir-P distances found in **(2)**, 2.322(3) and 2.319(3) Å, respectively. Since dynamic disordering of the metal bound hydrogens occurs at 293(2) K making the dihydrogen bond distance appear unusually and unreliably short, another attempt was made at 5(2) K for further confirmation of the structure.

Solid State Structure. **$IrClH_x(iPr_3P)_2$ (3)**. The neutron diffraction analysis of **(3)**, **Figure 2.4**, at 5(2) K refined to give three superimposed structures. Two coordinatively saturated non-classical polyhydrogen species, one refined with higher occupancy metal-$(\eta^2\text{-}H_2)$ ligand, HY(11)-HY(12), $IrCl(H)_2(\eta^2\text{-}H_2)(iPr_3P)_2$ **(3a)**, **Figure 2.7**, and one refined with lower occupancy metal-$(\eta^2\text{-}H_2)$ ligand, HY(21)-HY(22), $IrCl(H)_2(\eta^2\text{-}H_2)(iPr_3P)_2$ **(3b)**, **Figure 2.7**. One coordinatively unsaturated classical dihydride species with hydrides HY(A) and HY(B), $IrCl(H)_2(iPr_3P)_2$ **(3c), Figure 2.7**. In structures **(3a)** and **(3b)**, the Ir-hydride distances (Ir-HY(1) 1.552(7) and Ir-HY(2) 1.586(9) Å) are significantly shorter than the Ir-H dihydrogen distances in both conformers of $\eta^2\text{-}H_2$, in **(3a)**, Ir-HY(11) 1.780(14) and Ir-HY(12) 1.811(15) Å and in **(3b)**, Ir-HY(21) 1.85(2) and Ir-HY(22) 1.84(2). This same relationship was found for the established neutron structure for $IrI(H)_2(\eta^2\text{-}H_2)(iPr_3P)_2\cdot C_{10}H_8$ **(5)**, where the Ir-hydride distances (Ir-H(a) 1.579(6) and Ir-H(b) 1.589(6) Å) and the Ir-H dihydrogen distances (Ir-H(c) 1.764(7) and Ir-H(d) 1.748(7) Å) were similarly disproportionate.[31] The Ir-P distances found for **(3)**, not significantly different from **(2)**, Ir-P(1) 2.323(3) and Ir-P(2) 2.314(3) Å, vs Ir-P(1) 2.322(3) and Ir-P(2) 2.319(3). However, slightly longer than found from X-ray data for **(4)**, Ir-P(1) 2.303 and Ir-P(2) 2.307 Å. Ir-P distances are comparable to other iridium non-classical polyhydrogen structures.[31,36,37] It may be worth mentioning that the Ir-P distances in **(3)** are slightly shorter than in **(1),** Ir-P(1) 2.330(3) and Ir-P(2) 2.326(3) Å, and **(5)**, Ir-P(1) 2.334(4) and Ir-P(2) 2.338(4) Å. The dihydrogen ligand in **(3a)**,

HY(11)-HY(12), has a d_{H-H} of 0.8727(0.0250) Å and in **(3b)**, HY(21)-HY(22) d_{H-H} is 0.8812(0.0386) Å. Both **(3a)** and **(3b)** have an H-H separation in agreement with true η^2-H_2 type coordinated complexes, only slightly elongated from molecular dihydrogen (0.74 Å).[16] The d_{H-H} of **(3a)** and **(3b)** do not follow the trend expected considering the σ halide influence between the metal-polyhydrogen complexes **(1)** and **(5)**, where it was expected that d_{H-H} would be longest in **(5)** and shortest in **(1)**, I^- **(5)** > Br^- **(1)** > Cl^- **(3)**. Instead, both conformers **(3a)** and **(3b)** display the longest d_{H-H} between the three analogues, revising the trend for longest d_{H-H} to Cl^- **(3)** > I^- **(5)** > Br^- **(1)**, where the d_{H-H} are: **(3a)** 0.8727(0.0250), **(3b)** 0.8812(0.0386) Å, **(5)** 0.856(9) Å and **(1)** 0.8231(0.0091). All d_{H-H} are within 3 σ limits. The anticipated trend from **(3)** to **(1)** and **(5)** however, for metal-halide distance, d_{M-X}, is as expected. In **(3)** d(M-X), Ir-Cl 2.4426(18) Å, is shortest among the three analogues, and follows where in **(1)** d_{M-X}, 2.592(2) Å is shorter than **(5)** d_{M-X} 2.770(4) Å, I^- **(5)** > Br^- **(1)** > Cl^- **(3),** due to the decrease in size of atomic radii across I^- to Cl^-.[31] In **(3)**, d_{M-X}, 2.4426(18) Å, is also found to be slightly longer from the X-ray data set for **(4)** 2.427 Å. In **(3a)** the η^2-H_2 ligand, HY(11)-HY(12), is found in the expected plane with ancillary ligands of the least π acceptor ability, Cl-Ir-HY(2)-HY(1), arbitrarily taken as the equatorial plane, displayed in two separate rotations about the equatorial axis in **Figure 2.10**. However, in **(3b)** the η^2-H_2 ligand, HY(21)-HY(22), is unexpectedly found rotated out of the equatorial plane, Cl-Ir-HY(2)-HY(1), displayed in two separate rotations about the equatorial axis in **Figure 2.11**. The η^2-H_2 ligand of **(3b)** is rotated almost completely orthogonal to the equatorial plane, eclipsing the axial plane, arbitrarily set as HY(1)-Ir-P(1)-P(2), **Figure 3.12 (3b)**, versus the η^2-H_2 ligand in **(3a)** which completely eclipses the equatorial plane, Cl-Ir-HY(2)-HY(1), **Figure 3.12 (3a)**. The dihedral angle between the equatorial axis and the axial axis is 89.4(1)° which is taken as the degree to which η^2-H_2 in **(3b)** is located from the equatorial axis, **Figure 3.12**. The dihedral angle between the three analogues of the synonymous planes, 89.6(8)° in **(1)** and 88.8(5)° in **(5)**, suggests that **(1)** is most closely of pure octahedral geometry, 90°. The P(1)-Ir-P(2) angles among the three analogues also agrees with this statement, **(3)** P(1)-Ir-P(2) 170.79(10) Å, **(1)** 172.87(10) Å and **(5)** 171.8(1) Å, **(1)** is most closely of pure octahedral geometry, 180°. However, in the cases of **(1)** and **(5)**, the dihydrogen ligand was refined in the expected equatorial plane.

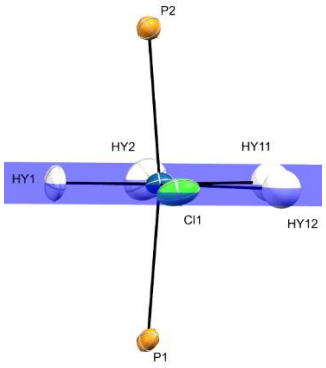

(3aα)

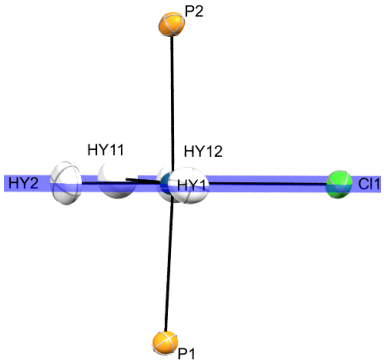

(3aβ)

Figure 2.10 ORTEP diagram for iridium coordination sphere in **(3a)**. **(3aα)** equatorial plane, Cl-Ir-HY(2)-HY(1) (blue). Tilted view down the Cl-Ir-HY(2) axis. **(3aβ)** equatorial plane, Cl-Ir-HY(2)-HY(1) (blue). View down the HY(1)-Ir-(HY(11)-HY(12)) axis. Alkane carbons and hydrogens have been removed for clarity.

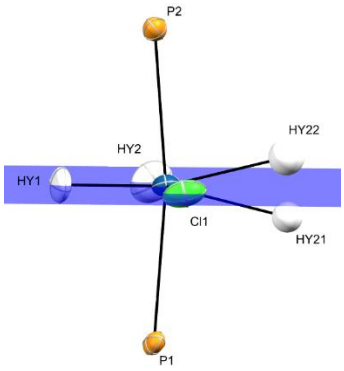

(3bα)

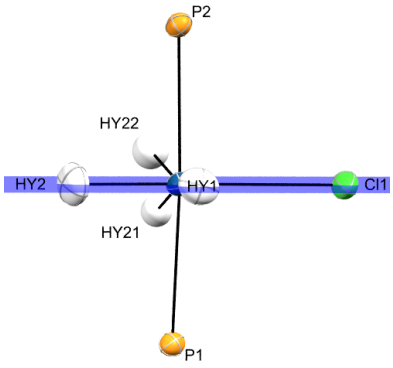

(3bβ)

Figure 2.11 ORTEP diagram for iridium coordination sphere in **(3b)**. **(3bα)** equatorial plane, Cl-Ir-HY(2)-HY(1) (blue). Tilted view down the Cl-Ir-HY(2) axis. **(3bβ)** equatorial plane, Cl-Ir-HY(2)-HY(1) (blue). View down the HY(1)-Ir-(HY(21)-HY(22)) axis. Alkane carbons and hydrogens have been removed for clarity.

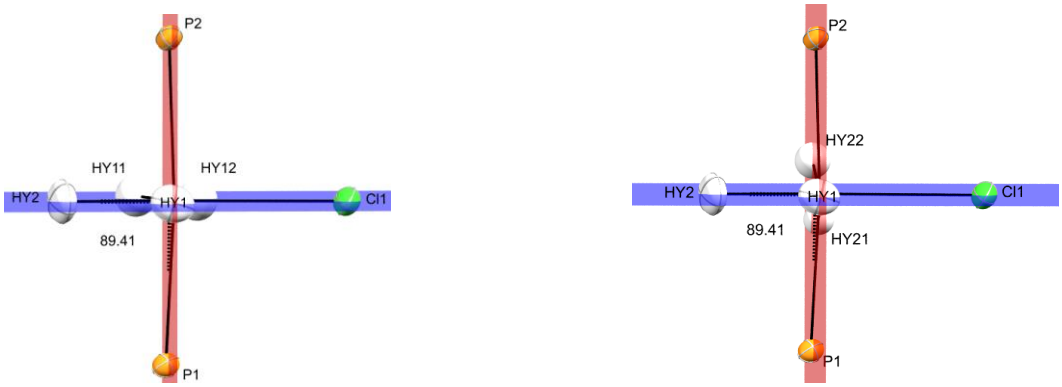

(3a) **(3b)**

Figure 2.12 ORTEP diagram for iridium coordination sphere in **(3a) and (3b)**. Equatorial plane, Cl-Ir-HY(2)-HY(1) (blue). Axial plane, HY(1)-Ir-P(1)-P(2) (red). View down the HY(1)-Ir-((HY(21)-HY(22)) axis. Alkane carbons and hydrogens have been removed for clarity.

2.6 Conclusions

The structures for $IrBrH_x(iPr_3P)_2 \cdot C_{10}H_8$ and $IrClH_x(iPr_3P)_2$ were resolved by neutron diffractometry. The structure for $IrBrH_x(iPr_3P)_2 \cdot C_{10}H_8$ resolved with two superimposed structures in the crystal lattice; the non-classical polyhydrogen complex $IrBr(H)_2(\eta^2\text{-}H_2)(iPr_3P)_2 \cdot C_{10}H_8$ and the classical dihydride complex $IrBr(H)_2(iPr_3P)_2 \cdot C_{10}H_8$. The structure for $IrClH_x(iPr_3P)_2$ resolved with three superimposed structures in the lattice crystal at 5(2) Kelvin. Two non-classical polyhydrogen complexes $IrCl(H)_2(\eta^2\text{-}H_2)(iPr_3P)_2$, where dihydrogen was found to be in two different orientations. The final third structure found was one classical dihydride complex $IrCl(H)_2(iPr_3P)_2$.

CHAPTER 3. Elucidation of the Nature of the Metal Bound Hydrogens in $IrH_x\{2,6\text{-}C_6H_3\text{-}(OAs(tBu_2))_2\}$ through NMR Spectroscopy: Agostic Hydrogen Interaction vs. "end-on" M-(η^1-H_2)

3.1 Background

As early as 1965, before the discovery of Kubas complexes, it had been suggested that the empty σ^* orbital of molecular H_2 could act as an acceptor for a filled linear metal orbital along the pathway to oxidative addition in an end-on motif, top **Figure 1.5**.[18] Wilkinson agreed that this scenario seemed more likely than if molecular H_2 entered the metal coordination sphere side-on, as an electron donor to an empty metal linear orbital, bottom **Figure 1.5**. In 1971, Vaska also agreed that molecular hydrogen must function as an acid on the metal in the OA process.[19] Dedieu and Strich in 1979 were the first to attempt a molecular orbital analysis of the end-on molecular H_2 approach to a metal center during the OA pathway.[13] Their calculations indicated that the H_2 preferred approach begins in an end-on orientation to the metal. As H_2 approaches the metal, the σ orbital becomes destabilized with an increase in H-H distance, and in turn the σ^* orbital becomes lower in energy, more stabilized. Albright confirms that as H-H distance increases, the bonding (σ) and antibonding (σ^*) orbitals become closer in energy levels.[17] In other words, as the H-H bond lengthens, the σ orbital increases in energy and the σ^* orbital decreases in energy. From a molecular orbital viewpoint, an end-on H_2 approach to metal is plausible, ergo it is then plausible for a M-(η^1-H_2) complex to exist.

There are two heavily cited reports where an η^1- H_2 orientation was suggested as the mode of coordination of H_2 to metal. In one report, a Pd/Kr matrix was doped with H_2 at low temperatures. It was found, through IR, that there was a possible mix of two orientations of H_2 bound to metal, Pd-(η^2-H_2) and Pd-(η^1-H_2), in this matrix. However, the Pd-(η^1-H_2) bond was not confirmed beyond these speculative IR results.[38] In an alternate report, asymmetric binding of Re to H_2 in the metal-hydrogen complex ($ReCl(H_2)(MePh_2P)_4$), found in single crystal X-ray diffractometry results, lead to the suggestion that the possible coordination to the metal center was in an η^1-H_2 orientation.[39] Variable temperature ^1H and ^{31}P NMR results proved inconclusive for the existence of an M-(η^1-H_2) bonding motif. Unfortunately, they were unable to obtain neutron diffraction data to conclusively confirm the end-on type of bonding. After the discovery of Kubas

complexes, Cotton claimed that since metal-hydrogen complexes can easily be tuned to delivery an H_2 OA type of bonding, M-$(H)_2$, and a dihydrogen type of bonding, M-(η^2-H_2), it goes that one should be able to prepare M-(η^1-H_2) complexes.[10] However, there have been no reports for the isolation of a discreet M-(η^1-H_2) complex.

3.2 M-(η^1-H_2) Bonding Precedent

A bonding model for the description of a M-(η^1-H_2) complex can be extrapolated from the first I_2 coordinated TM complex, PtI(η^1-I_2)(NCN^{Me2}), **Figure 3.1**.[40] X-ray diffractometry results from the reaction of PtI(NCN), a pincer type complex, with I_2 revealed an unexpected end-on η^1-I_2 complex. In this case, the I_2 molecule approaches the Pt center in an end-on conformation by which a filled linear Pt orbital donates electrons into the empty σ^* orbital of I_2. This approach mirrors the scenario where the σ^* acidic H_2 would approach a basic metal center in an end-on conformation best described as a 3-center 4-electron (3c 4e$^-$) bond, analogous to I_3^- or H_3^-, **Eqn. 3.1**.[17] This scenario contrasts the 3c 2e$^-$ bonding described in Kubas M-(η^2-H_2) complexes, Chapter 1.5. Using I_3^- as a model for 3c 4e$^-$ bonding, linear combinations have been treated in a representational orbital diagram for M-(η^1-H_2) bonding, **Figure 3.2**. In the I_3^- orbital correlation diagram, **Figure 3.2**, the I^- atomic orbital, right side **Figure 3.2**, would represent the filled linear metal orbital and the I_2 atomic orbitals, left side **Figure 3.2**, would represent the deficient orbital of H_2. The 2-electron filled symmetric molecular orbital, center bottom **Figure 3.2**, 2-electron filled non-bonding orbital, center middle **Figure 3.2**, and the empty σ^* anti-bonding orbital, center top **Figure 3.2**, together represent the 3c 4e$^-$ bonding in the metal-H_2 end-on bonding in M-(η^1-H_2) complexes.

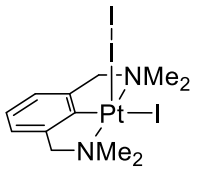

Figure 3.1 PtI(η^1-I_2)($NCN^{Me}{}_2$)

$$I^- + I_2 \longrightarrow I_3^-$$

$$M + H_2 \longrightarrow M\text{-}(\eta^1\text{-}H_2)$$

Eqn. 3.1 Linear I_3^- analogous to linear M-(η^1-H_2).

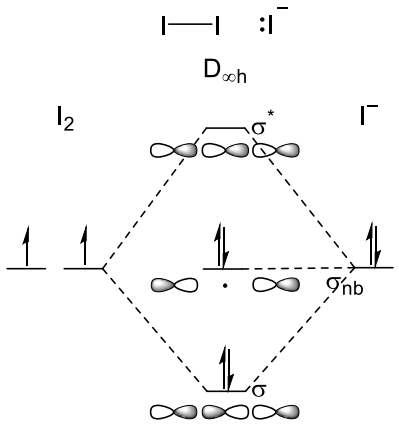

Figure 3.2 Representative I_3^- orbital correlation diagram for 3c 4e$^-$ M-(η^1-H_2) bonding.

3.3 Agostic Hydrogen Interaction at a Metal Center: Pincer Precedent

It was suggested by this lab in 1999 that the formation of an agostic interaction with a methyl C-H from a *t*Bu ligand of the pincer complex Ir(H)$_2${2,6-C_6H_3-(CH_2P(*t*Bu$_2$))$_2$} **(1)** coordinates to iridium **(2)** in solution and facilitates tert-Butylalkane (tba) elimination during the catalytic transfer dehydrogenation of alkanes, **Scheme 3.1**.[41] The dihydride species **(1)** is reacted in the presence of the hydrogen acceptor tert-Butylethylene (tbe) to give the tbe coordinated 18 e$^-$ species where hydrogen transfer takes place to give a 16 e$^-$ species. At this point in the cycle it is possible that an agostic C-H interaction at iridium facilitates hydride migration to form and eliminate tba which could give a mix in solution of the 14 e$^-$ complex **(3)** and the 16 e$^-$ agostic complex **(4)**. The suggestion of the agostic interaction was based on deuterium scrambling results seen with the dideuteride complex. There was exchange between the deuterides and methyl hydrogens of a *t*Bu group.

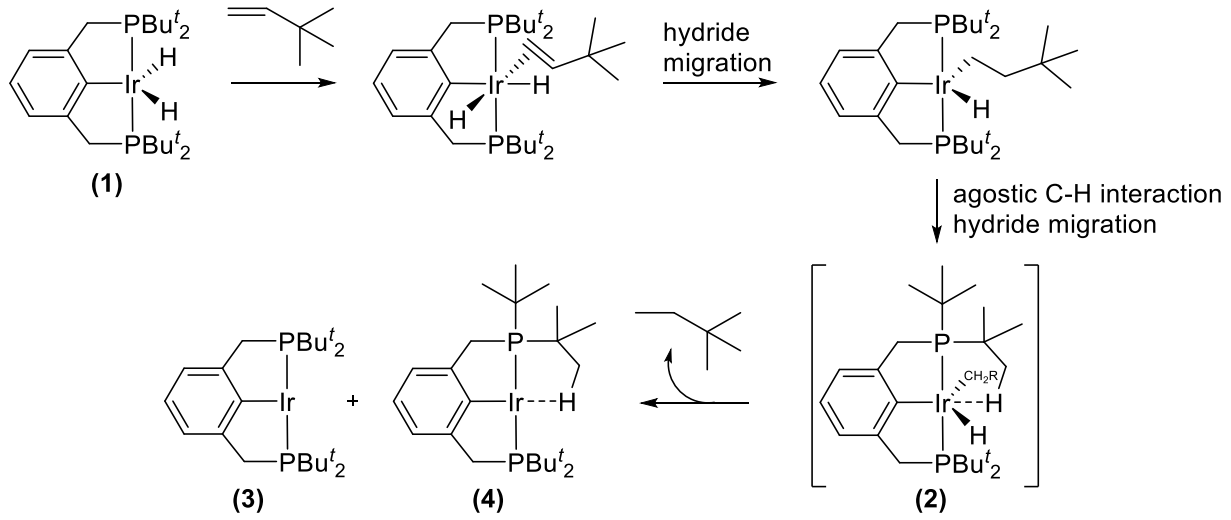

Scheme 3.1 Proposed agostic C-H interaction during transfer dehydrogenation of $Ir(H)_2\{2,6\text{-}C_6H_3\text{-}(CH_2P(tBu_2))_2\}$, R = CH_2CMe_3.

In 2004, similar alkane dehydrogenation experiments were run with an analogous pincer, $Ir(H)(Cl)\{2,6\text{-}C_6H_3\text{-}(OP(tBu_2))_2\}$ **(5)**.[42] In the article, it was found that the hydrido chloro species **(5)** when reacted with a base in the absence of hydrogen gas led to a species in fast exchange with the solvent. Rate measurements for facile exchange with free solvent suggests an intermediate species might be of the 14 e^- complex **(6)** or the 16 e^- agostic complex **(7)**, **Scheme 3.2**. While the same reaction run under hydrogen gas produces the desired dihydride catalyst **(8)**, **Scheme 3.3**. It is noteworthy to add to the discussion that the same article found that reaction with complex **(5)** and NaH, 1 mol % of PhOH, under 1 atm. of H_2 (g) in THF produces the anionic trihydride species **(9)**. The trihydride species was well flushed out and best characterized by their $^1H\{^{31}P\}$ NMR data from the hydride region where the lone hydride was found as a triplet at δ -13.33 with a $J_{H\text{-}H}$ coupling of 4.8 Hz and the trans dihydride was found as a doublet with a $J_{cisH\text{-}H}$ coupling of 4.8 Hz. The published spectroscopic data for complex **(9)** is similar and was useful in characterizing the current paper's findings. They also noted that the dihydride catalyst was best synthesized with NaO*t*Bu which acts as a base and hydrogen sponge under 1 atm. of H_2 (g).

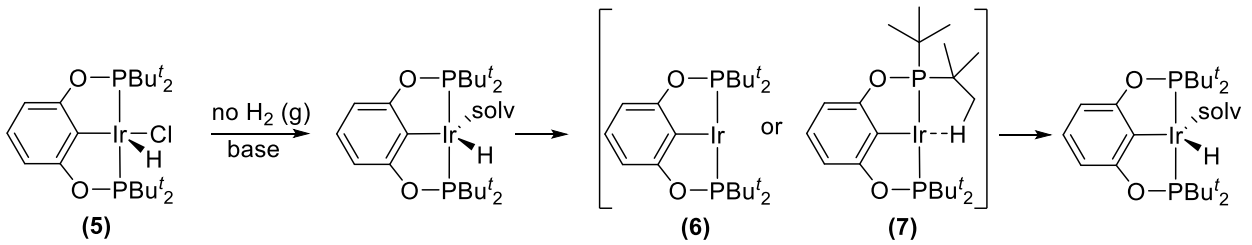

Scheme 3.2 Proposed agostic C-H interaction during dehydrochlorination of Ir(H)(Cl){2,6-C_6H_3-(OP(tBu$_2$))$_2$}.

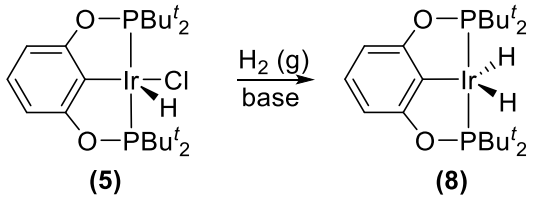

Scheme 3.3 Formation of Ir(H)$_2${2,6-C_6H_3-(OP(tBu$_2$))$_2$}.

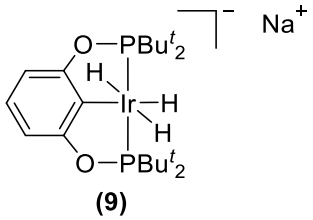

Figure 3.3 Anionic trihydride complex.

3.4. 2014 IrH$_x${2,6-C_6H_3-(OAs(tBu$_2$))$_2$} Results

In 2014, a paper was published from this lab which may mislead readers into assuming that, in the complex in question, IrH$_x${2,6-C_6H_3-(OAs(tBu$_2$))$_2$}, the hydrogen orientation about iridium is of the classical metal-dihydride, M-(H)$_2$, type **(10)**.[43] An analogous complex, Ir(H)$_2${2,6-C_6H_3-(OP(tBu$_2$))$_2$}, has previously been published and has been formulated as such, a M-(H)$_2$ complex.[42] However, X-ray crystallographic data was published for IrH$_x${2,6-C_6H_3-(OAs(tBu$_2$))$_2$}, which excluded data for the hydrogens about iridium. In actuality, the hydrogens

at iridium had been positionally refined and the occupancy refined to be in an end-on (η^1-H_2) type of orientation, a fact left out of the original 2014 report with good reason **(11)**. The distance of the metal bound hydrogen to Ir was found to be 2.027 Å and $d_{H\text{-}H}$ was found to be 0.863 Å.[44] It was the original intention of this author to purify and grow crystals of the material large enough for neutron diffractometry analysis, however there were many complications and as such this solid-state data could not be obtained. The following results will present an argument for the hydrogen orientation at iridium using multiple liquid NMR experiments.

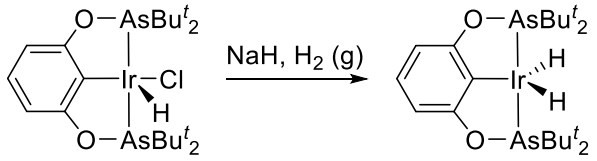

(10)

Scheme 3.4 $IrH_x\{2,6\text{-}C_6H_3\text{-}(OAs(t\text{Bu}_2))_2\}$ formulated as a classic dihydride.

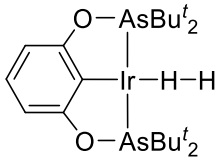

(11)

Figure 3.4 X-ray diffractometry refined structure for $IrH_x\{2,6\text{-}C_6H_3\text{-}(OAs(t\text{Bu}_2))_2\}$.

3.5 Experimental

General Considerations. Any glove box manipulations were carried out under technical grade Ar (g) (Airgas USA) atmosphere. All other manipulations were carried out using standard Schlenk techniques. Where H_2 (g) was used, 100% H_2 (g) (Airgas USA). Where D_2 (g) was used, (D, 99.9%) (Cambridge Isotopes). NMR experiments were conducted in Wilmad LPV NMR tubes (Aldrich). Where H_2 and D_2 gas was added to Wilmad LPV NMR tubes, less than 1 atm. Reagents $AsCl_3$ 99.99% trace metal basis (Aldrich), and *t*BuMgCl 1M in THF (Aldrich) were used as received. The complex $[IrCl(C_8H_{14})_2]_2$ was used instead of $[IrCl(C_8H_{12})]_2$ and prepared according

to literature.[35] The complex Ir(H)(Cl){2,6-C_6H_3-(OAs(tBu$_2$))$_2$} was prepared according to literature.[43] All other solvents and reagents were purified, dried and deoxygenated using conventional methods.

NMR Studies. Where deuterated solvents were used, toluene-d_8 99 + atom % D ampules (Aldrich) and benzene-d_6 D, 99.5% ampules (Cambridge Isotopes). All NMR experiments were recorded on a Varian-INOVA 500 MHz NMR spectrometer under hydrogen gas at ambient temperatures, unless otherwise stated. ^{1}H, ^{2}H and ^{13}C, were recorded at 500, 76 and 125 MHz. 1D-TOCSY experiments were conducted where the signal at δ -17.23 was irradiated. Gradient enhanced experiments used selective excitation with 90 degree quiet-sneeze pulse mixing time = 80 ms per Uhrin and Barlow protocol.[45] T_{1min} experiments were conducted with a standard inversion recovery (180°-τ-90°) pulse sequence and reported per Crabtree's protocol.[46] The ^{1}H NMR data are listed in ppm downfield from TMS at 0.00 ppm. The ^{2}H NMR data are listed in ppm relative to the methyl resonance of tol-d_8 at 2.09 ppm. The ^{13}C NMR data are listed in ppm relative to the solvents tol-d_8 and benzene-d_6 where noted. NOESY, 2D-TOCSY, HSQC and HETCOR experiments were conducted and yielded data that was too convoluted to be beneficial.

Synthesis IrH$_x${2,6-C_6H_3-(OAs(tBu$_2$))$_2$}. Preparation of IrH$_x${2,6-C_6H_3-(OAs(tBu$_2$))$_2$} was carried out with modification to the method of Brayton.[43] A solution of Ir(H)(Cl){2,6-C_6H_3-(OAs(tBu$_2$))$_2$} and NaH (xs) in benzene was charged in a reaction vessel and stirred under Ar (g) overnight. The Ar (g) was removed via f-p-t (3x) and H_2 (g) was then added. The solution was stirred for another 12 hours. The solvent was thereby removed via lyophilization and the remaining black-ish powder was re-dissolved in a *small* amount of toluene and filtered through a Kimwipe plug. Upon solvent evaporation, the recrystallized black material was rinsed with C_5H_{12}, an *absolute necessity*, yielding black crystalline material. Crystals large enough for neutron diffractometry could not be grown. ^{1}H{^{13}C} NMR (500 MHz, 23 °C, tol-d_8, H_2 (g)) δ 7.40 (d, J_{H-H} = 5 Hz, CH, 1 and 3), 7.19 (t, J_{H-H} = 5 Hz, CH, 2), δ 1.50 (br, 2CH_3, 4), 1.47 (m, 6) and 1.35 (br, 3tBu, 5) δ -14.28 (m, agostic hydrogen, 7), δ -17.23 (dvt, J = 9.05 Hz, dihydride, 8). See **Figure 3.5** and **Figure 3.6** for assignments. ^{13}C{^{1}H} NMR (125 MHz, 23 °C, tol-d_8): δ 172.68 (aryl), 153.76 (aryl), 149.63 (aryl), 114.30 (aryl), 108.39 (aryl), 42.07 (C_q), 31.04 (CH_3), 27.86 (CH_3),

27.44 (CH_3), 26.12 (CH_3).*NMR spectra does not change whether under 1 atm. of hydrogen pressure, argon pressure, or degassed.*

3.6 Results and Discussion

Solution ^1H Spectra. The *downfield* partial ^{1}H NMR spectrum of the sample reveals four shifts, **Figure 3.5**. One doublet at δ 7.40 with a $J_{H\text{-}H}$ value of 5 Hz was assigned to protons (1) and (3) of the aryl ring on the pincer complex in **Figure 3.5**. One triplet at δ 7.19 with a corresponding $J_{H\text{-}H}$ value of 5 Hz was assigned to proton (2) of the aryl ring on the pincer complex in **Figure 3.5**. Two signals were observed in the *t*Bu region of the spectrum. A broad singlet at δ 1.50 was assigned to the hydrogens of three equivalent *t*Bu, (4), and another broad singlet was assigned to the two methyl groups vicinal to the agostic methyl, (5), **Figure 3.5**.

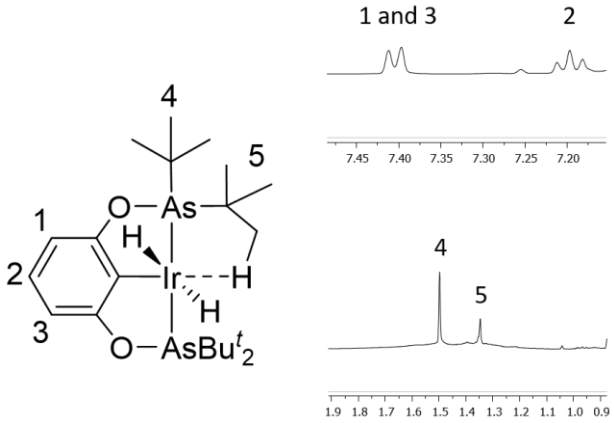

Figure 3.5 ^{1}H NMR assignments in the compound $IrH_x\{2,6\text{-}C_6H_3\text{-}(OAs(tBu_2))_2\}$, excluding metal bound hydrogens. $^1H\{^{13}C\}$ NMR (500 MHz, 23 °C, tol-d_8, H_2 (g)): top inset δ 7.40 (d, $J_{H\text{-}H}$ = 5 Hz, CH, 1 and 3), 7.19 (t, $J_{H\text{-}H}$ = 5 Hz, CH, 2); bottom inset δ (br, 1.50, 3*t*Bu, 4) and (br, 1.35, $2CH_3$, H5).

The ^{1}H NMR spectrum of the *hydride* region reveals a complicated multiplet at δ -14.28, left side **Figure 3.6**, that was assigned to the agostic hydrogen (7). The actual J_{cisH} cannot be obtained from simple inspection due to second order effects. This holds for the coupling to adjacent methylene protons, **Figure 3.6,** (6). The resonance for the trans hydride ligands is observed at δ -

17.23 (8). Accordingly, it has approximately double the intensity of the peak at δ -14.28. The resonance is a doublet of virtual triplets due to strong coupling of the agostic hydrogen with the methylene hydrogens, **Figure 3.6**. *J* coupling between the trans hydrides and the agostic hydrogen is observed to be 9.05 Hz.

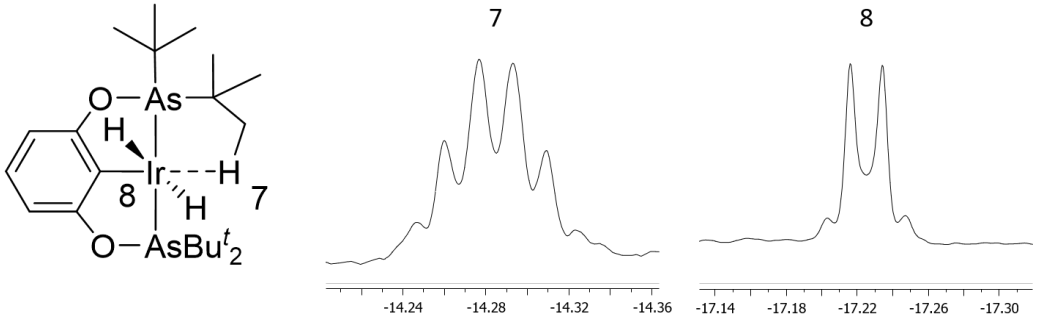

Figure 3.6 ^{1}H NMR assignments in the compound $IrH_x\{2,6\text{-}C_6H_3\text{-}(OAs(tBu_2))_2\}$, excluding aryl and alkyl hydrogens. $^1H\{^{13}C\}$ NMR (500 MHz, 23 °C, tol-d_8, H_2 (g)):left side δ -14.28 (m, 7) and right side δ -17.23 (dvt, $J_{agostic\text{-}H}$ = 9.05 Hz, dihydride, 8).

To determine if chemical shifts (7) and (8) were on the same molecule and coupled, a 2D homonuclear correlation spectroscopy (COSY) experiment was conducted. It was determined that indeed the two peaks are coupled and on the same molecule. **Figure 3.7** is the partial spectrum of the COSY experiment. Along the x-coordinate, ^{1}H (δ -14.28 and -17.23), and along the y-coordinate, ^{1}H (δ -14.28 and -17.23), shows the peaks' correlation.

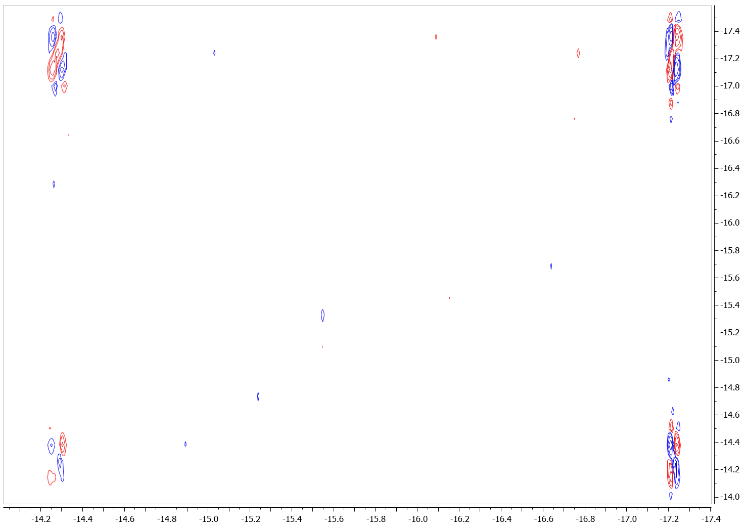

Figure 3.7 ^{1}H-^{1}H DQF-COSY NMR (500 MHz, 23 °C, tol-d_8), δ -14.28 and δ -17.23.

To confirm the correlation between the resonances for the hydride (7) and agostic hydrogen (8), 1D-total correlation (TOCSY) experiments were conducted and selectively decoupled spectra were obtained. **Figure 3.8** shows the effect of the multiplet at δ -14.28 under 1D-TOCSY and selectively decoupling of the δ -17.23 resonance. The resonance at δ -14.28 appears as broad singlet at room temperature 1D-TOCSY spectrum. However, the signal is observed to have slightly sharpened and appears to be broad multiplet and shifted slightly upfield to δ -14.40 in the 1D-TOCSY spectrum obtained at -80 °C, **Figure 3.9**. This may confirm the coupling to the methylene protons adjacent to the agostic hydrogen in the ^{1}H NMR spectrum.

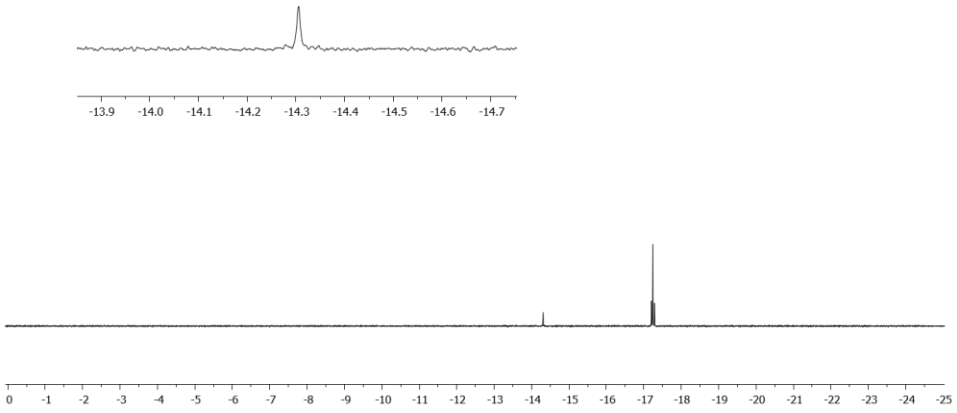

Figure 3.8 $^{1}H\{^{13}C, \delta\ -17.23\}$ 1D-TOCSY @ δ -17.23 NMR (500 MHz, 23 °C, tol-d_8, H_2 (g)), inset δ -14.28, (br, 7).

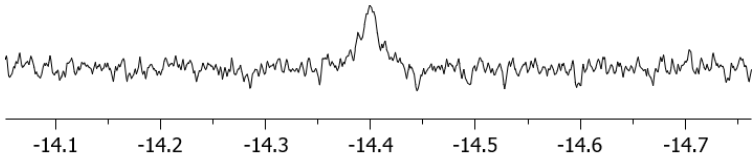

Figure 3.9 $^{1}H\{^{13}C, \delta\ -17.23\}$ 1D-TOCSY @ δ -17.23 NMR (500 MHz, -80 °C, tol-d_8, H_2 (g)), δ -14.40, (m, 7).

Figure 3.10 shows the effect of the doublet of virtual triplets at δ -17.23 under 1D-TOCSY and selectively decoupling δ -14.28. The peak at δ -17.23 goes from a doublet of virtual triplets to a broad singlet at room temperature. Using the same experiment, 1D-TOCSY and selectively decoupling δ -14.23, however at -80 °C the broad singlet remains a broad singlet, has shifted slightly downfield to δ -17.10 and appears to have lost intensity, **Figure 3.11**.

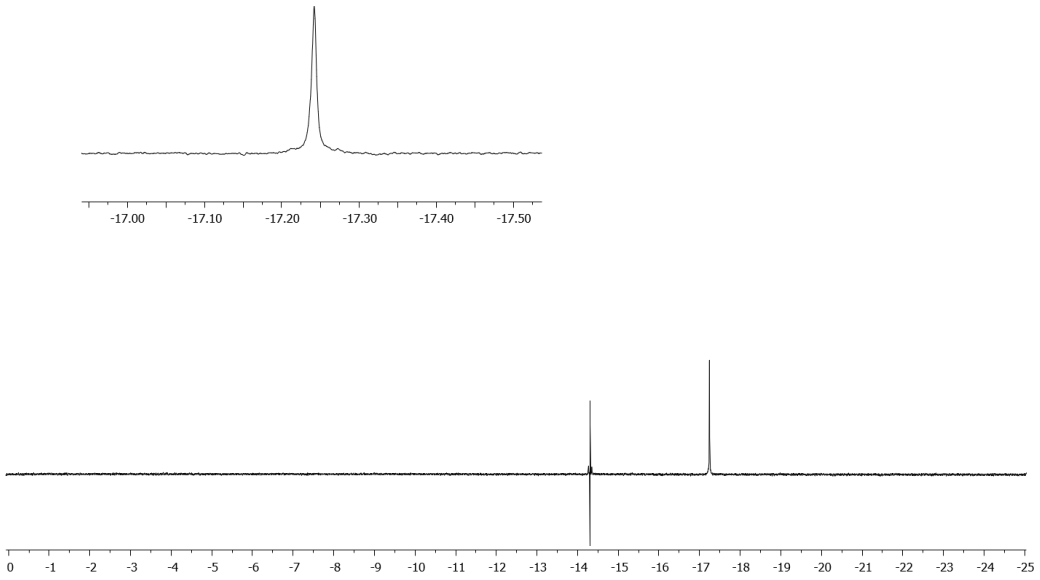

Figure 3.10 $^{1}H\{^{13}C, \delta\ -14.28\}$ 1D-TOCSY @ δ -17.23 NMR (500 MHz, 23 °C, tol-d_8, H_2 (g)), inset δ -17.23, (br, 8).

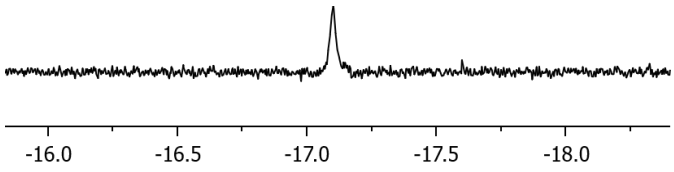

Figure 3.11 $^{1}H\{^{13}C, \delta\ -14.28\}$ 1D-TOCSY @ δ -17.23 NMR (500 MHz, -80 °C, tol-d_8, H_2 (g)), δ -17.10, (br, 8).

The 1D-TOCSY experiments also allowed the observation of the methylene protons that are obscured by the broad *t*Bu peak at δ 1.50 (4) in the standard ^{1}H NMR spectrum and the methyl peaks at δ 1.35 (5). There was difficulty getting complete suppression of the large *t*Bu peak at δ 1.50, as was evident by the presence of a remnant of the peak at δ 1.50 in the 1D-TOCSY, top and bottom **Figure 3.12**. However, a new broad multiplet at δ 1.47 appears and is attributed to the two remaining methylene protons, (6), top **Figure 3.12**. The bottom of **Figure 3.12** shows the effect of the broad multiplet at δ 1.47 under 1D-TOCSY and selectively decoupling δ -14.28, which goes to a broad singlet.

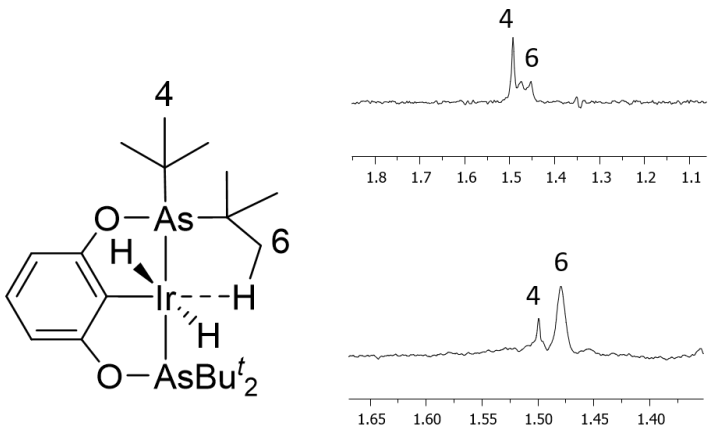

Figure 3.12 ^{1}H NMR assignments in the compound IrH$_x${2,6-C$_6$H$_3$-(OAs(*t*Bu$_2$))$_2$}, including *t*Bu (4) and methylene protons (6). Top, partial ^{1}H{^{13}C} 1D-TOCSY @ δ -17.23 NMR spectrum (500 MHz, 23 °C, tol-d_8, H$_2$ (g)) δ 1.47 (m, CH$_2$, 6); bottom, partial ^{1}H{^{13}C, δ -14.28} 1D-TOCSY @ δ -17.23 NMR spectrum (500 MHz, 25 °C, tol-d_8, H$_2$ (g)) δ 1.47 (br, CH$_2$, 6).

Solution ^{13}C Spectra. The partial ^{13}C NMR spectrum of the upfield shifts reveals four peaks, **Figure 3.14**. Four singlets, beginning with the furthest downfield: δ 31.04, δ 27.86, δ 27.44 and δ 26.12 located in the methyl region of the spectrum, **Figure 3.14**.

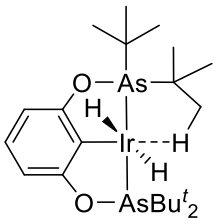

Figure 3.13. IrH$_x${2,6-C$_6$H$_3$-(OAs(*t*Bu$_2$))$_2$}.

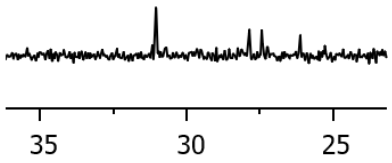

Figure 3.14 Upfield partial spectra $^{13}C\{^{1}H\}$ NMR (125 MHz, 23 °C, tol-d_8): δ 31.04 (CH_3), 27.86 (CH_3), 27.44 (CH_3), 26.12 (CH_3).

The partial ^{13}C NMR spectrum of the downfield shifts reveals five peaks, **Figure 3.15**. Five singlets, beginning with the furthest downfield: δ 172.68, δ 153.76, δ 149.63, δ 114.30 and δ 108.39 all in the aryl region of the spectrum, **Figure 3.15**.

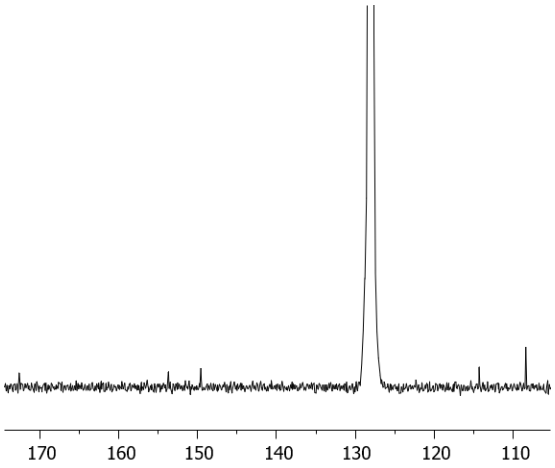

Figure 3.15 Downfield partial spectrum $^{13}C\{^{1}H\}$ NMR (125 MHz, 23 °C, C_6D_6): δ 172.68 (aryl), 153.76 (aryl), 149.63 (aryl), 114.30 (aryl), 108.39 (aryl).

Solution Deuterium Experiments. Upon replacement of H_2 (g) for D_2 (g) in the experiment, the following ^{1}H NMR spectrum were recorded. As per **Figure 3.5**, **Figure 3.16** shows the most downfield peaks with the exclusion of the hydride region of the spectrum. The shifts in the top inset; a doublet at δ 7.40, (1) and (3), and a triplet at δ 7.19 (2), appear to be unchanged by the

addition of D_2 (g). However, with the signals at δ 1.50 (4) and 1.35 (5), a noticeable broadening and slight splitting at the top of both peaks appears, indicative of deuterium scrambling into the methyls and *t*Bu regions of the complex. In the hydridic region of the spectrum, as per **Figure 3.6**, the middle of **Figure 3.17** shows the multiplet at δ -14.28 (7) for the agostic hydrogen shift and the bottom of **Figure 3.17** shows the doublet of virtual triplets at δ -17.23 (8) for the dihydride shift. There is slight agitation to the splitting, but both appear mostly unaffected by the addition of D_2 (g). There was an unexpected appearance for the signal of dissolved hydrogen deuteride (HD) (g) in the ^{1}H NMR, top **Figure 3.17**.

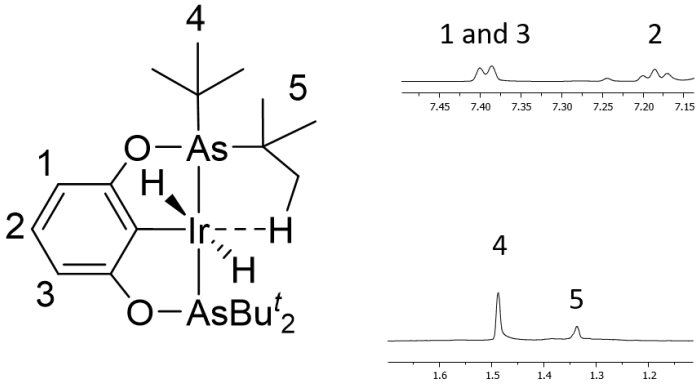

Figure 3.16 ^{1}H{^{13}C} NMR (500 MHz, 23 °C, tol-d_8, D_2 (g)): top inset δ 7.40 (d, $J_{H\text{-}H}$ = 5 Hz, CH, 1 and 3), 7.19 (t, $J_{H\text{-}H}$ = 5 Hz, CH, 2); bottom inset δ (br, 1.50, 2CH_3, 4) and (br, 1.35, 3*t*Bu, 5).

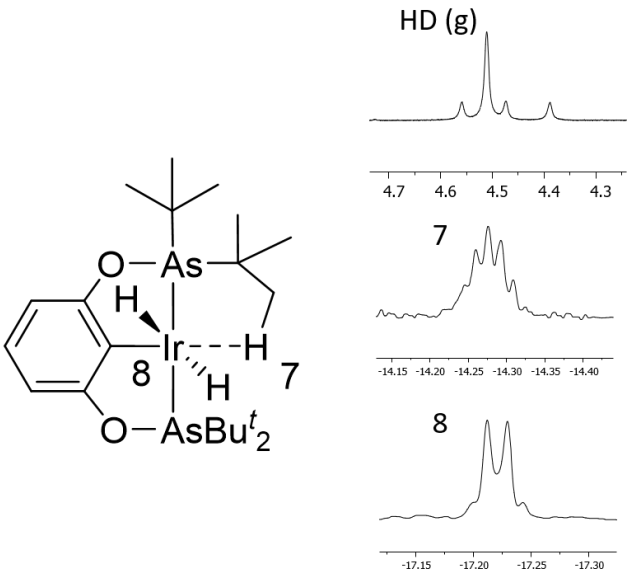

Figure 3.17 Partial spectrum $^{1}H\{^{13}C\}$ NMR (500 MHz, 23 °C, tol-d_8, D_2 (g)) top; dissolved H_2 gas δ 4.51 and dissolved HD gas δ 4.47, $J_{H\text{-}D}$ = 45 Hz, middle; δ -14.28 (m, agostic hydrogen, 7) and bottom; δ -17.23 (dvt, dihydride, 8).

Solution ^{2}H Spectra. The ^{2}H NMR decoupled ^{1}H spectrum reveals three useful shifts downfield, **Figure 3.18**, note there are no signals in the deuteride region present. The two largest signals belong to the solution toluene. A broad peak at δ 4.54 was assigned to hydrogen deuteride and two broad peaks at δ 1.58 and 1.48 which may be indicative of deuterium scrambling into the methyls and *t*Bu regions of the complex. A ^{2}H NMR coupled ^{1}H experiment would seem disadvantageous; however, it does confirm the presence of HD. **Figure 3.19** displays the spectrum for the coupled data and the top inset shows the appearance of the doublet from the hydrogen in HD. The bottom inset shows a further broadening at signals δ 1.58 and δ 1.48.

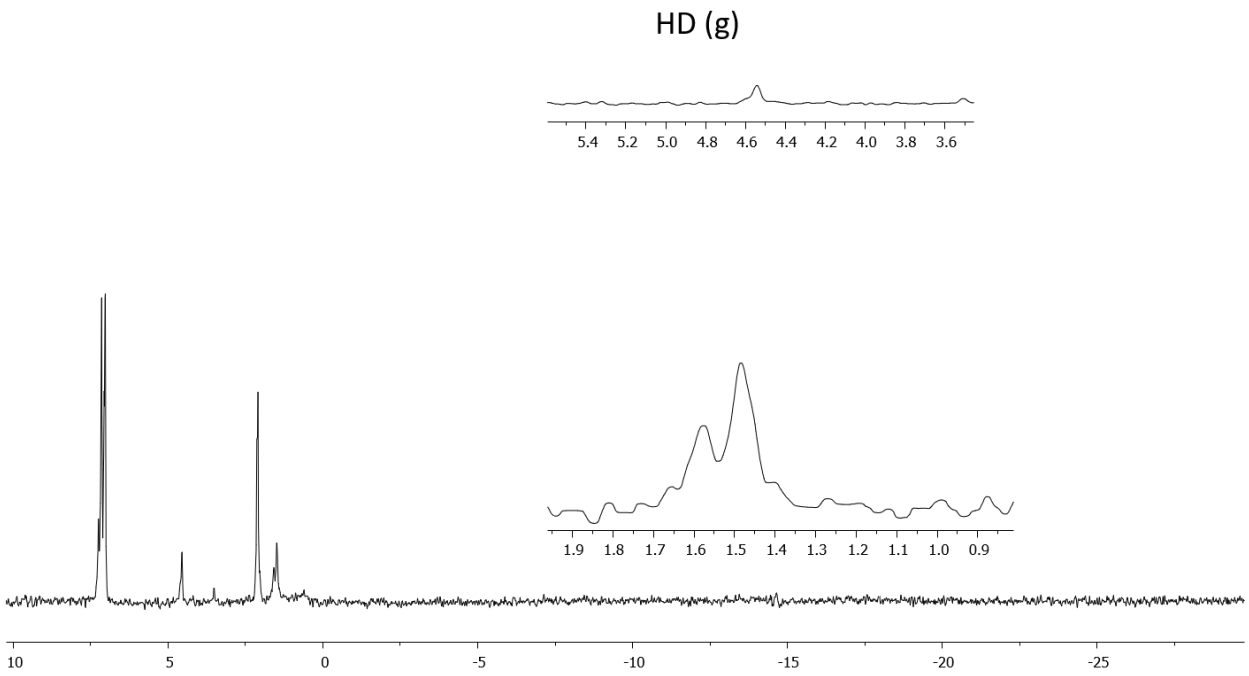

Figure 3.18 $^{2}H\{^{1}H\}$ NMR (76 MHz, 23 °C, tol-h_8, D_2 (g)): top inset; dissolved HD gas δ 4.54, bottom inset; δ 1.58 (br) and δ 1.48 (br).

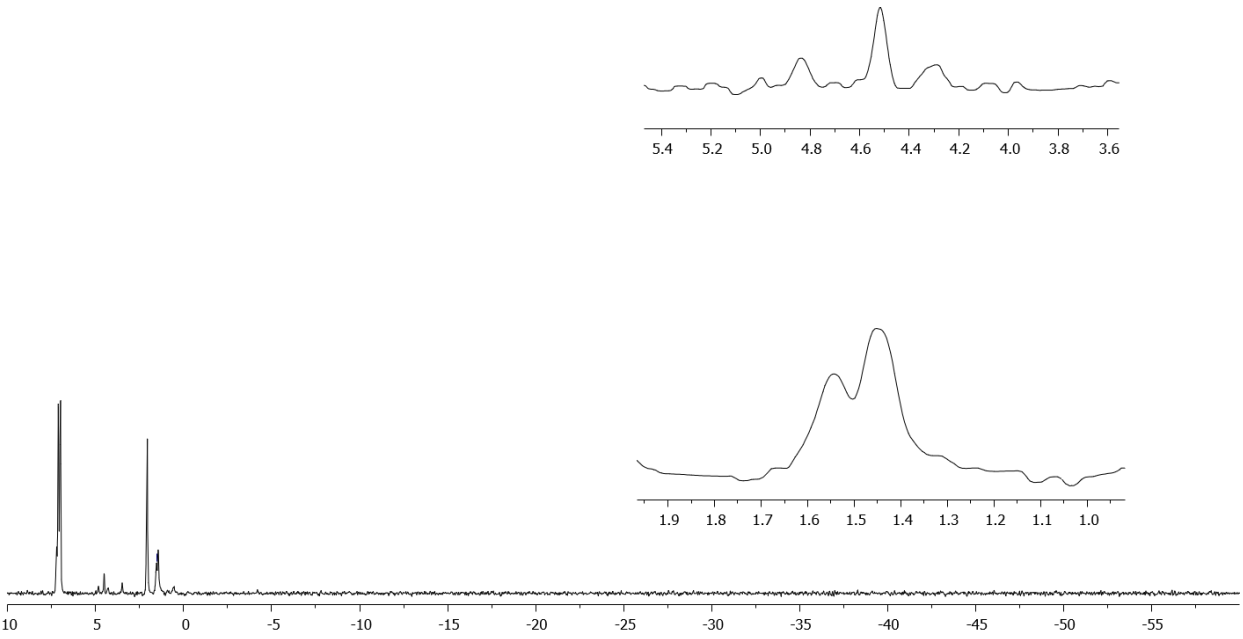

Figure 3.19 ^{2}H NMR (76 MHz, 23 °C, tol-h_8, D_2 (g)): top inset; dissolved HD gas, bottom inset; δ 1.58 (br) and δ 1.48 (br).

T_{1min} Experiments. T_{1min} data was obtained for the two hydridic hydrogen peaks obtained from ^{1}H NMR. For the multiplet at δ -14.28, a T_{1min} value of 220 ms was found and for the dvt at δ -17.23, a T_{1min} value of 278 ms was found. Below in **Figure 3.20** is the experimental curve for ln T_1 versus inverse temperature (Kelvin) for δ -14.28 and in **Figure 3.21** is the experimental curve for ln T_1 versus inverse temperature (Kelvin) for δ -17.23. Markings in red on both plots indicate the point at which T_1 is at a minimum. As per Chapter 2.1, a loose interpretation of T_{1min} assumes that high T_{1min}, > 100 ms, could be a distinguishing characteristic of a hydride and that a low T_{1min} value, < 40 ms, could be a distinguishing characteristic of an η^2-H_2 ligand. However, with both values over 200 ms, it is the belief of this author that an η^2-H_2 ligand is not present in this complex.

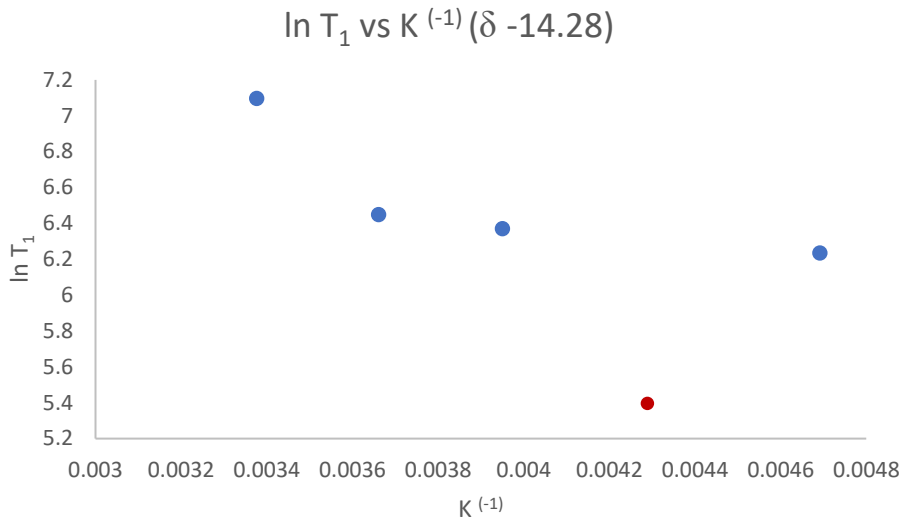

Figure 3.20 Experimental curve for ln T_1 versus inverse temperature for δ -14.28 in tol-d_8 T_1 minimum (red), 220 ms.

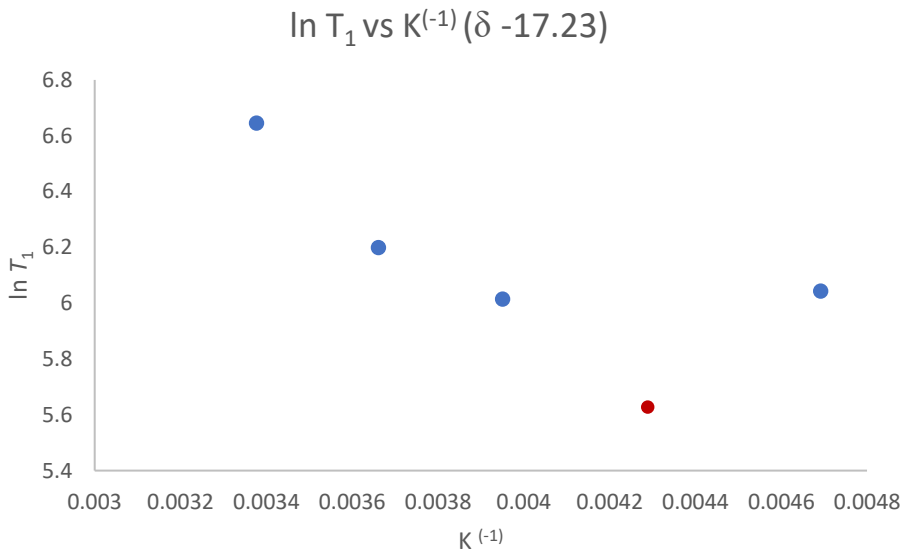

Figure 3.21 Experimental curve for ln T_1 versus inverse temperature for δ -17.23 in tol-d_8 T_1 minimum (red), 278 ms.

3.7 Plausible Structure

It is readily apparent from the number multiplicity of the hydride resonances in its solution ^{1}H NMR spectrum that, the metal-hydrogen bonding in the complex is more complicated than in the classical MH_2, dihydride complex depicted in structure **10**. The hydrides of structure **10**, would appear as a singlet where there would be no H-H coupling since the hydrides are equivalent and there are no other spin active nuclei in the complex, see **Figure 3.22** for all models considered.

Structure **11**, which contains the M-(η^1-H_2) interaction, raises the question as to what chemical shifts would be expected for the inequivalent hydrogens of the η^1 bound H_2. The hydrogen directly bound to the metal bound would ostensibly to be hydridic thus have a chemical shift upfield from zero, while the terminal hydrogen would be at least somewhat protic in nature and thus have a chemical shift downfield from that of free hydrogen. However, despite their chemical shifts, the two hydrogens of the η^1-H_2 in structure **11** should couple only to each other giving rises to 2 simple doublets, not the multiple splitting patterns seen in **Figure 3.6**. The hydride region of the ^{1}H spectrum of the anionic trihydride **9** should contain a discrete doublet and triplet signals rather than the observed complicated multiplets. Thus structures **9**, **10**, and **11** are clearly inconsistent with the NMR data and the three more complicated structures illustrated in **Figure 3.22** (structures **12**, **13** and **14)** were considered.

Structure **(12)** fits much of the criteria but not all the observed spectroscopic features. In this model the signal at δ -17.23 is assigned to the two equivalent trans hydrides and the signal at δ -14.28 is assigned to the metal bound hydrogen of the η^1 dihydrogen. The signal at δ -17.23 is affected by a highly mixed spin coupling system, **Figure 3.6**, giving rise to virtual coupling and the complex splitting pattern of this resonance. The splitting pattern can be understood as a doublet of virtual triplets, where the two unresolved peaks belonging to the triplets are overlapping. For structure **12**, δ the trans hydride resonance would appear as a virtual triplet if the spin states of both the hydrogens in the η^1-H_2 ligand were highly mixed. If this was not the case, the resonance would be a doublet of doublets. Thus, the NMR data is inconsistent with either of these possibilities. Moreover, the spectrum does not contain a resonance that is assignable to the protic hydrogen of the η^1-H_2 ligand. Upon selective decoupling, both the δ -17.23 and δ -14.28 multiplets convert to what appears to be broad singlet signals. For structure **12**, selectively decoupling of the trans hydrides, should render the metal bound hydrogen of the η^1-H_2 a doublet not a singlet.

Finally, the ^{13}C NMR data is completely inconsistent with structure **12** as there would be only two upfield signals in the ^{13}C NMR spectrum, one for the 12 equivalent methyl groups of the *t*Bu, and one for the 4 equivalent quaternary carbons of the *t*Bu.[42,43] **Figure 3.14** clearly shows four upfield signals in the methyl carbon region.

Structure **13** agrees the appearance of 4 distinct resonances in the methyl region of the ^{13}C NMR. However, the formal +4 oxidation state of iridium in structure **13** would render it paramagnetic and thus not observable by NMR spectroscopy. Having discarded structures **12** and **13,** structure **14** was brought into consideration as it is also in line with the observation of multiple methyl resonance in the methyl region of the ^{13}C NMR spectrum. Additionally, a selectively decoupled ^{1}H NMR spectrum was obtained at -80 °C in which the broad singlet for δ -14.28 in the room temperature spectrum was observed to shift slightly upfield (δ -14.40), and appears as a multiplet, **Figure 3.9**. This peak can be assigned to the agostic hydrogen of structure **14**. It is known that agostic hydrogens typically have upfield shifts from those of their non-agostic counterparts.[47] The resonance for the agostic hydrogen should either couple to two equivalent methylene hydrogens and appear as a triplet or to two inequivalent methylene hydrogens and appear as a doublet of doublets.[48] It is also possible that inequivalent methylene hydrogens could be rendered equivalent on the NMR time scale by a fast exchange. Finally, as mentioned above the TOCSY experiments found a peak underneath the *t*Bu and methyl peaks of the complex, **Figure 3.12**, which can be assigned to the methylene hydrogens. This broad multiplet at δ 1.47 converts to a broad singlet when decoupled from δ -14.28 which is also in accordance with structure **14**. Thus, among proposed structures **9-14**, structure **14** is the only one that is in general agreement with all or the ^{1}H and ^{13}C NMR spectroscopic data that has been obtained for the complex at hand, **Table 3.1**.

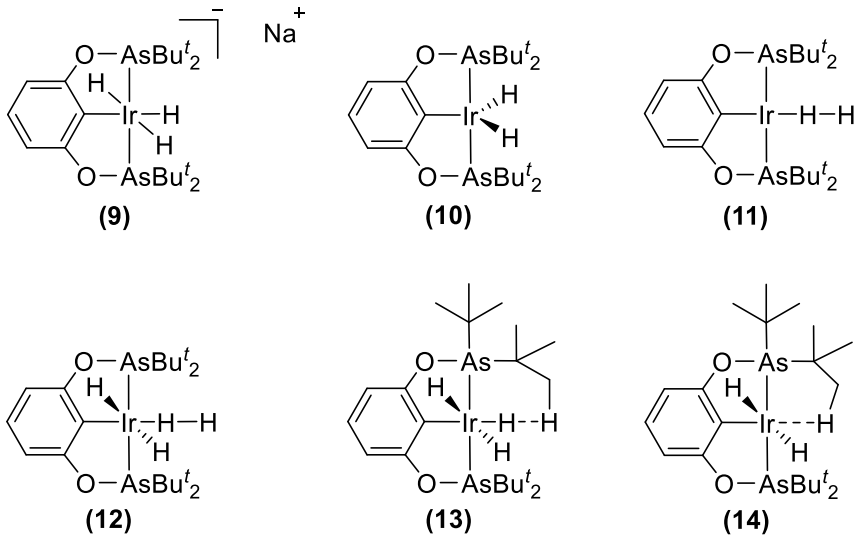

Figure 3.22 Structures considered for $IrH_x\{2,6\text{-}C_6H_3\text{-}(OAs(tBu_2))_2\}$.

Table 3.1 Expected ^1H and ^{13}C NMR signal multiplicities for structures **9-14**. Observed spectra are approximated by the spectra expected for structure **14**.

Structure	^1H NMR, hydride region	^{13}C NMR, methyl region
(9)	1 doublet, and 1 triplet	1 methyl signal
(10)	1 singlet	1 methyl signal
(11)	2 simple doublets	1 methyl signal
(12)	trans hydrides would yield 1 virtual triplet, or 1 doublet of doublets	1 methyl signal
(13)	paramagnetic	paramagnetic
(14)	2 multiplets	multiple methyl signals

3.8 Conclusion

The synthesis of "$IrH_x\{2,6\text{-}C_6H_3\text{-}(OAs(tBu_2))_2\}$" has been refined such that it can be obtained with regularity. Extensive ^1H and ^{13}C NMR studies were conducted to elucidate the nature of the metal bound hydrogens in this complex. These studies indicate that it is an "agostic complex" in accordance with structure **14**.

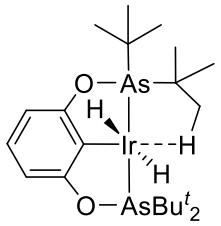

(14)

Figure 3.23 Structure for $IrH_x\{2,6\text{-}C_6H_3\text{-}(OAs(t\text{Bu}_2))_2\}$; Agostic complex- $Ir(H)_2\{2,6\text{-}C_6H_3\text{-}(OAs(t\text{Bu}_2))_2\}$.

CHAPTER 4. Reaction of Ir(H)(Cl){2,6-C_6H_3-(OAs(*t*Bu_2))$_2$} with the Hydrosilane Et_3SiH: OA vs. M-(η^2-H-SiR_3) vs M-(η^1-H-SiR_3) Bonding

4.1 Transition Metal-Hydrosilane Bonding Precedent for Dihydrogen Complexes

Hydrosilanes (R_3SiH) can bind to transition metals in variations of the following three motifs; R_3SiH can oxidatively add to the metal to give a classical metal hydrido-silyl complex (M-(H)(Si)), **Figure 4.1**, analogous to the classical metal dihydride complex (M-$(H)_2$) discussed in Chapter 1.4, **Figure 1.4**, R_3SiH can form a non-classical σ complex (M-η^2-$HSiR_3$) with a metal analogous to the non-classical Kubas complexes discussed in Chapter 1.5, **Figure 1.7** and R_3SiH can bind in a "bridging" type of complex (M-(η^1-$HSiR_3$)) much like the linear metal dihydrogen complex (M-η^1-H_2) discussed in Chapter 3.2.[16, 48]

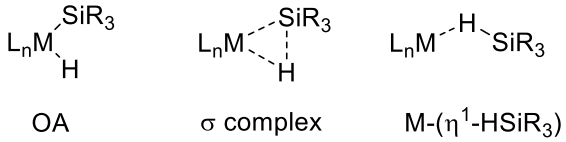

Figure 4.1 Three general TM bonding motifs with R_3SiH.

Silane complexes were known before Kubas's η^2-H_2 complex, but it was only after its discovery that the bonding principles for metal-silane complexes began to be understood. Hydrosilanes, like dihydrogen, have no non-bonding donor electrons or π electrons. Si-H bond elongates along a continuum upon metal coordination comparable to dihydrogen, discussed in Chapter 2.1. R_3SiH make good π acceptors and σ donors, similar to dihydrogen, discussed in Chapter 1.4 and 1.5. A difference between dihydrogen and hydrosilane is the variety of R groups to choose for hydrosilane which could give the scientist control over electronics and sterics of the reactions. Still, the chemistry is similar to dihydrogen chemistry.[16] The purpose of this Chapter was to gain insight into the hydrogen bonding at iridium for the complex from Chapter 3, IrH_x{2,6-C_6H_3-(OAs(*t*Bu_2))$_2$}.

X-ray diffractometry is the most definitive technique for characterizing these complexes. However, J_{SiH} values are used more often to distinguish between the 3 bonding motifs. Typically, the J_{SiH} values for (M-η^2-$HSiR_3$) complexes fall into the range of 20-70 Hz, though some claim out to 200 Hz.[16, 48, 47, 49] While uncoordinated hydrosilanes J_{SiH} values are greater than 155 Hz and the OA hydrido-silyl complexes have J_{SiH} values that are less than 10 Hz.[50]

4.2 Transition Metal-Hydrosilane: Pincer Bonding Precedent

Advantageously, in 2012, with the phosphorus analogue of Ir(H)(Cl){2,6-C_6H_3-(OAs(tBu$_2$))$_2$} mentioned in Chapter 3, Ir(H)(Cl){2,6-C_6H_3-(OP(tBu$_2$))$_2$}, similar chemistry was done.[49] It was found that the hydrido-chloro species when reacted with a base and excess Et_2SiH_2 yielded a mixture of the of the oxidative addition product **(1)** and either trihydride species **(2)** or η^2 species **(3)**. Species **(1)** ^{1}H signal was found at δ -16.9 with J_{SiH} value of 6.0 Hz, while species **(2)** and **(3)**, ^{1}H signal was found at δ -8.8 with J_{SiH} value of 10.5 Hz. Unfortunately, the scenario gets increasingly complicated when reacting using the dihydride complex as a starting material instead of the hydrido-chloro complex or reactions involving a hydrogen atmosphere.

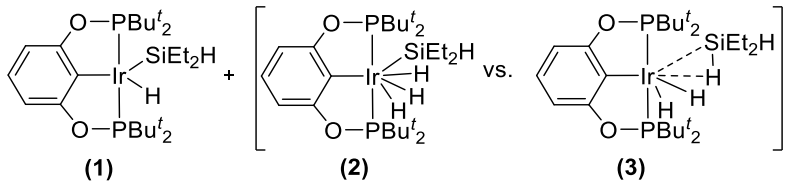

Figure 4.2 Products for the reaction of Ir(H)(Cl){2,6-C_6H_3-(OP(tBu$_2$))$_2$} and Et_2SiH_2.

4.3 Experimental

General Considerations. Any glove box manipulations were carried out under technical grade Ar (g) (Airgas USA) atmosphere. All other manipulations were carried out using standard Schlenk techniques. NMR Experiments conducted in Wilmad LPV NMR tubes (Aldrich). Reagents $AsCl_3$ 99.99% trace metal basis (Aldrich), and tBuMgCl 1M in THF (Aldrich) were used as received. The complex [IrCl(C_8H_{14})$_2$]$_2$ was used instead of [IrCl(C_8H_{12})]$_2$ and prepared

according to literature.[35] The complex Ir(H)(Cl){2,6-C_6H_3-(OAs(*t*Bu_2))$_2$} was prepared according to literature.[43] All other solvents and reagents were purified, dried and deoxygenated using conventional methods.

NMR Studies. Where deuterated solvents were used, benzene-d_6 D, 99.5% ampules (Cambridge Isotopes). All NMR experiments were recorded on a Varian-INOVA 500 MHz NMR spectrometer at ambient temperatures except for ^{29}Si experiments which were recorded on an Agilent DD2 400 MHz with 60 second relaxation delay. ^{1}H and ^{29}Si at 500 and 79 MHz. The ^{1}H NMR data are listed in ppm downfield from TMS at 0.00 ppm. The ^{29}Si NMR data are listed in ppm relative to the silicate resonance from the glass of the Wilmad LPV NMR tube at -110 ppm.

Synthesis Ir(η^2-H-SiEt$_3$){2,6-C_6H_3-(OAs(tBu$_2$))$_2$}. A solution of Ir(H)(Cl){2,6-C_6H_3-(OAs(*t*Bu_2))$_2$}[43] and NaH (xs) in benzene was charged in a reaction vessel and stirred under Ar (g) for 12 hr. Et_3SiH (1 mol) was added to the solution and stirred for another 12 hours. The solvent was thereby removed via lyophilization. The black/purple product was filtered through a Kimwipe plug with C_6D_6 to a Wilmad LPV NMR tube for the following NMR studies. Partial hydride region of NMR spectrum: ^{1}H{^{13}C} NMR (500 MHz, 23 °C, C_6D_6) δ -12.74 (br, J_{SiH} = 9.45 Hz, J_{SiH} = 32.95 Hz). ^{29}Si{^{1}H} NMR spectrum: (79 MHz, 23 °C, C_6D_6), δ 16.80 (s).

4.4 Results

Solution ^{1}H and ^{29}Si spectra. The partial ^{1}H NMR spectrum of the strongest signal, δ -12.74, in the hydride region can be seen in **Figure 4.3**. This is the only signal with noticeable ^{29}Si satellite peaks, and it happens to have two sets of these satellites with *J* values of 9.45 and 32.95 Hz. The J_{SiH} value of 9.45 Hz is consistent with coupling in the range for a hydrido-silyl complex (< 10 Hz). The J_{SiH} value of 32.95 Hz is consistent with coupling in the range for a (M-η^2-$HSiR_3$) complex (20-70 Hz). The rest of the ^{1}H NMR spectrum is too convoluted for interpretation. ^{29}Si NMR spectrum, **Figure 4.4**, reveals only one peak at δ 16.80 which is consistent with pincer type complexes of the hydrido-silyl type.[50]

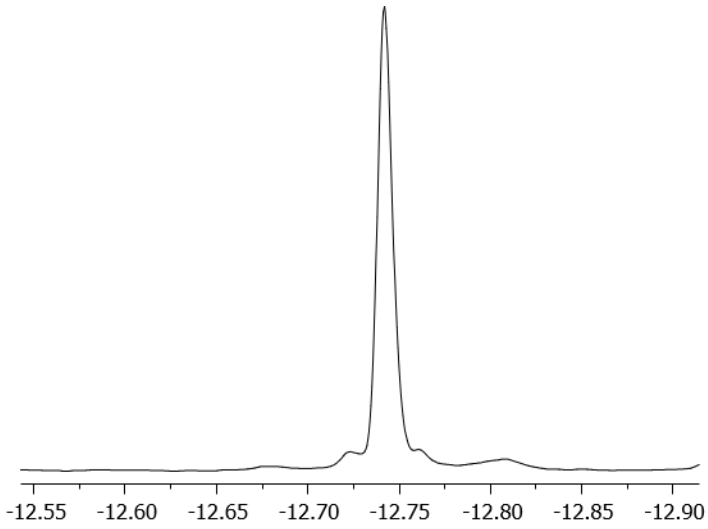

Figure 4.3 Partial NMR spectrum $^{1}H\{^{13}C\}$ NMR (500 MHz, 23 °C, C_6D_6) δ -12.74 (br, J_{SiH} = 9.45 Hz, J_{SiH} = 32.95 Hz).

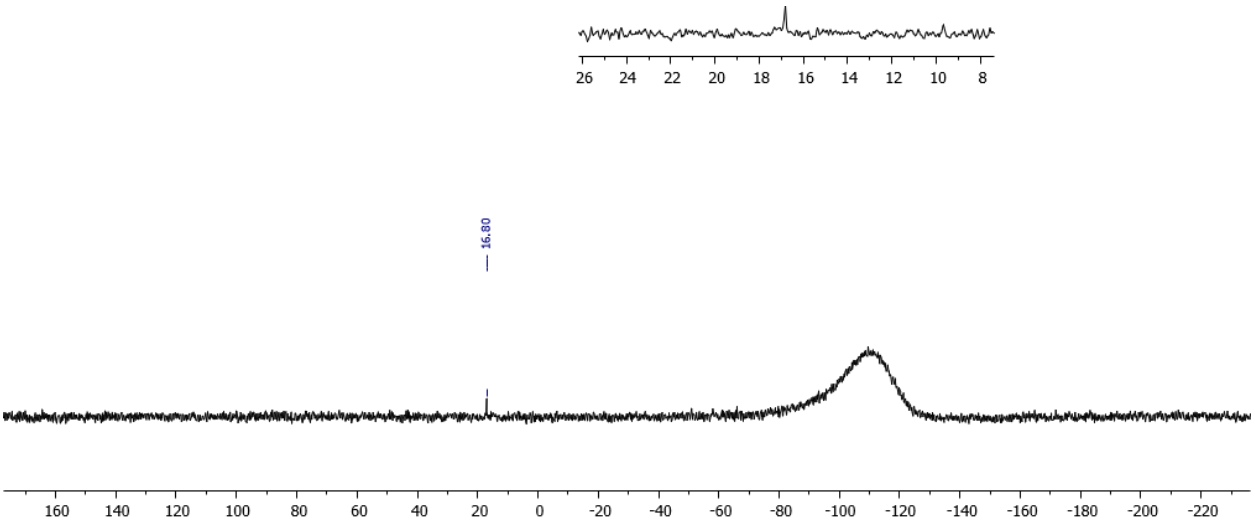

Figure 4.4 $^{29}Si\{^{1}H\}$ NMR spectrum (79 MHz, 23 °C, C_6D_6), δ 16.80 (s), -110 silicate glass; inset δ 16.80, (s).

4.5 Discussion

Results suggest an equilibrium between a hydrido-silyl complex and a (M-η^2-HSiR$_3$) complex in solution based on J_{Si-H} coupling values, **Scheme 4.1**. This scenario is not uncommon and has been seen in certain hydrido-silyl Kubas complexes.[48] [29]Si coupled to ^{1}H experiments were attempted but did not produce valuable information. These experiments were conducted in order to help shed light on the hydrogen bonding situation at iridium in Ir(H)$_2${2,6-C$_6$H$_3$-(OAs(*t*Bu$_2$))$_2$}. However, the results seem to open more doors of questions and added to the complexity of the situation instead of clarifying the results in Chapter 3.

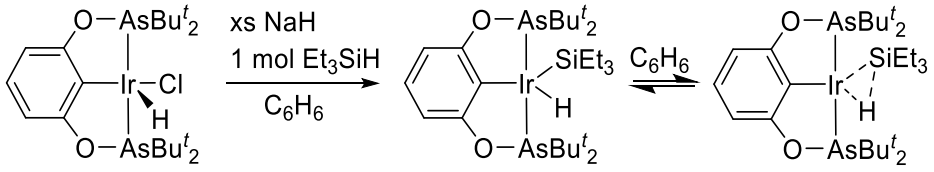

Scheme 4.1 Possible equilibrium in solution between hydrido-silyl product **(4)** and (M-η^2-HSiR$_3$) product **(5)**.

4.6 Conclusion

To conclude, the hydrosilane Et$_3$SiH was reacted with Ir(H)(Cl){2,6-C$_6$H$_3$-(OAs(*t*Bu$_2$))$_2$} in order to clarify the hydrogen bonding orientation in Ir(H)$_2${2,6-C$_6$H$_3$-(OAs(*t*Bu$_2$))$_2$} from Chapter 3. The results suggest a more complicated scenario, possibly an equilibrium in solution between a hydrido-silyl complex and a (M-η^2-HSiR$_3$) complex. To that end, this reaction was not helpful towards our goal.

APPENDIX A. Supplemental Data, Neutron Data Set for $IrBrH_x(iPr_3P)_2 \cdot C_{10}H_8$ @ 25(2) K

Table A.1 Crystal data and structure refinement for irh2ill.

Identification code	shelx
Empirical formula	C28 H56 Br Ir P2
Formula weight	726.83
Temperature	25(2) K
Wavelength	1.3033 A
Crystal system, space group	Triclinic, P -1
Unit cell dimensions	a = 8.0029(10) A alpha = 83.621(5) deg. b = 13.6829(10) A beta = 83.959(5) deg. c = 14.4094(10) A gamma = 72.225(5) deg.
Volume	1489.0(2) A^3
Z, Calculated density	2, 1.621 Mg/m^3
Absorption coefficient	0.382 mm^-1
F(000)	9
Crystal size	? x ? x ? mm
Theta range for data collection	2.616 to 55.305 deg.

Limiting indices -9<=h<=4, -16<=k<=14, -16<=l<=18

Reflections collected / unique 6203 / 4791 [R(int) = 0.0400]

Completeness to theta = 51.442 85.2 %

Refinement method Full-matrix least-squares on F^2

Data / restraints / parameters 4791 / 0 / 793

Goodness-of-fit on F^2 1.041

Final R indices [I>2sigma(I)] R1 = 0.0560, wR2 = 0.1370

R indices (all data) R1 = 0.0621, wR2 = 0.1416

Largest diff. peak and hole 1.013 and -1.114 e.A^-3

Table A.2 Atomic coordinates (x 10^4) and equivalent isotropic displacement parameters (A^2 x 10^3) for irh2ill.
U(eq) is defined as one third of the trace of the orthogonalized Uij tensor.

	x	y	z	U(eq)
Ir	3992(2)	2562(1)	7777(1)	10(1)
Br	2908(2)	4558(1)	7611(1)	10(1)

P(1)	2698(3)	2487(2)	9299(2)	8(1)
C(10)	536(2)	3476(2)	9491(1)	11(1)
C(11)	-738(3)	3555(2)	8740(1)	13(1)
C(12)	-380(3)	3413(2)	10477(1)	14(1)
C(20)	2483(2)	1179(2)	9668(1)	9(1)
C(21)	1043(3)	964(2)	9172(1)	14(1)
C(22)	2263(3)	884(2)	10725(1)	14(1)
C(30)	4010(2)	2692(2)	10207(1)	10(1)
C(31)	5813(3)	1881(2)	10205(2)	16(1)
C(32)	4214(3)	3778(2)	10103(1)	13(1)
P(2)	5187(3)	2455(2)	6236(2)	9(1)
C(40)	6144(3)	3509(2)	5792(1)	11(1)
C(41)	7678(3)	3508(2)	6337(2)	23(1)
C(42)	6589(4)	3632(2)	4735(2)	28(1)
C(50)	3559(2)	2549(2)	5374(1)	11(1)
C(51)	2117(3)	3587(2)	5390(2)	16(1)
C(52)	2757(3)	1654(2)	5543(2)	14(1)
C(60)	6834(2)	1181(2)	6044(1)	12(1)
C(61)	8284(3)	856(2)	6720(1)	16(1)
C(62)	7623(3)	1025(2)	5038(2)	22(1)
C(70)	4284(3)	1917(2)	2776(1)	11(1)
C(71)	2446(3)	2043(2)	2935(1)	12(1)
C(72)	1260(2)	3017(2)	2954(1)	13(1)
C(73)	1855(3)	3901(2)	2814(1)	13(1)
C(74)	3627(3)	3798(2)	2666(1)	12(1)
C(75)	4882(2)	2805(2)	2649(1)	9(1)
C(76)	6722(3)	2676(2)	2505(1)	11(1)
C(77)	7909(3)	1704(2)	2498(1)	13(1)
C(78)	7310(3)	822(2)	2612(1)	13(1)
C(79)	5537(3)	925(2)	2741(1)	12(1)

Table A.3 Bond lengths [A] and angles [deg] for irh2ill.

Ir-P(2)	2.326(3)
Ir-P(1)	2.330(3)
Ir-Br	2.592(2)
Ir-HA	1.586(6)
Ir-HB	1.602(7)
Ir-HC	1.761(6)
Ir-HD	1.784(6)
Ir-HE	1.507(16)
Ir-HF	1.589(15)
P(1)-C(30)	1.856(3)
P(1)-C(10)	1.859(3)
P(1)-C(20)	1.864(3)
C(10)-C(11)	1.536(2)
C(10)-C(12)	1.535(3)
C(10)-H(10)	1.103(4)
C(11)-H(11A)	1.087(5)
C(11)-H(11B)	1.091(5)
C(11)-H(11C)	1.084(5)
C(12)-H(12A)	1.088(5)
C(12)-H(12B)	1.093(5)
C(12)-H(12C)	1.086(5)
C(20)-C(21)	1.534(2)
C(20)-C(22)	1.538(3)
C(20)-H(20)	1.092(5)
C(21)-H(21A)	1.101(5)
C(21)-H(21B)	1.089(5)
C(21)-H(21C)	1.089(5)
C(22)-H(22A)	1.088(5)

C(22)-H(22B)	1.077(5)
C(22)-H(22C)	1.094(5)
C(30)-C(31)	1.528(3)
C(30)-C(32)	1.533(3)
C(30)-H(30)	1.095(5)
C(31)-H(31A)	1.082(6)
C(31)-H(31B)	1.089(6)
C(31)-H(31C)	1.095(5)
C(32)-H(32A)	1.087(5)
C(32)-H(32B)	1.087(4)
C(32)-H(32C)	1.095(5)
P(2)-C(40)	1.856(3)
P(2)-C(50)	1.860(3)
P(2)-C(60)	1.865(3)
C(40)-C(41)	1.525(3)
C(40)-C(42)	1.530(3)
C(40)-H(40)	1.095(5)
C(41)-H(41A)	1.095(7)
C(41)-H(41B)	1.078(7)
C(41)-H(41C)	1.086(5)
C(42)-H(42A)	1.079(9)
C(42)-H(42B)	1.084(5)
C(42)-H(42C)	1.079(9)
C(50)-C(52)	1.533(3)
C(50)-C(51)	1.533(3)
C(50)-H(50)	1.106(5)
C(51)-H(51A)	1.095(5)
C(51)-H(51B)	1.095(4)
C(51)-H(51C)	1.087(6)
C(52)-H(52A)	1.090(6)
C(52)-H(52B)	1.091(4)

C(52)-H(52C)	1.086(5)
C(60)-C(61)	1.524(3)
C(60)-C(62)	1.529(3)
C(60)-H(60)	1.095(5)
C(61)-H(61A)	1.088(6)
C(61)-H(61B)	1.082(5)
C(61)-H(61C)	1.073(6)
C(62)-H(62A)	1.083(5)
C(62)-H(62B)	1.088(7)
C(62)-H(62C)	1.093(6)
C(70)-C(71)	1.424(3)
C(70)-C(79)	1.422(3)
C(70)-C(75)	1.423(3)
C(71)-C(72)	1.381(3)
C(71)-H(71)	1.080(5)
C(72)-C(73)	1.417(3)
C(72)-H(72)	1.082(4)
C(73)-C(74)	1.377(3)
C(73)-H(73)	1.095(5)
C(74)-C(75)	1.423(3)
C(74)-H(74)	1.093(5)
C(75)-C(76)	1.424(3)
C(76)-C(77)	1.379(3)
C(76)-H(76)	1.090(5)
C(77)-C(78)	1.416(3)
C(77)-H(77)	1.087(4)
C(78)-C(79)	1.377(3)
C(78)-H(78)	1.079(5)
C(79)-H(79)	1.088(5)

H - H Distances

2.1232 (0.0104) HA - HB
3.3046 (0.0081) HA - HC
3.3600 (0.0080) HA - HD
2.6511 (0.0217) HA - HE
1.3087 (0.0231) HA - HF
2.1244 (0.0136) HB - HC
2.6887 (0.0123) HB - HD
0.9299 (0.0243) HB - HE
0.9557 (0.0231) HB - HF
0.8231 (0.0091) HC - HD
1.2406 (0.0289) HC - HE
2.7962 (0.0226) HC - HF
1.9130 (0.0257) HD - HE
3.1690 (0.0196) HD - HF
1.7643 (0.0323) HE - HF

P(2)-Ir-P(1)	172.87(10)
P(2)-Ir-Br	93.36(8)
P(1)-Ir-Br	92.39(8)
P(2)-Ir-HA	88.4(2)
P(1)-Ir-HA	87.2(2)
Br-Ir-HA	91.9(2)
P(2)-Ir-HB	86.9(3)
P(1)-Ir-HB	87.1(3)
Br-Ir-HB	175.5(4)
HA-Ir-HB	83.5(4)
P(2)-Ir-HC	90.4(3)
P(1)-Ir-HC	92.1(3)
Br-Ir-HC	106.3(4)
HA-Ir-HC	161.7(4)

HB-Ir-HC	78.2(5)
P(2)-Ir-HD	92.1(3)
P(1)-Ir-HD	93.1(3)
Br-Ir-HD	79.5(3)
HA-Ir-HD	171.4(4)
HB-Ir-HD	105.0(5)
HC-Ir-HD	26.8(3)
P(2)-Ir-HE	91.1(6)
P(1)-Ir-HE	86.0(6)
Br-Ir-HE	149.8(10)
HA-Ir-HE	118.0(11)
HB-Ir-HE	34.6(9)
HC-Ir-HE	43.8(11)
HD-Ir-HE	70.5(11)
P(2)-Ir-HF	86.3(6)
P(1)-Ir-HF	86.6(6)
Br-Ir-HF	140.6(9)
HA-Ir-HF	48.7(9)
HB-Ir-HF	34.9(8)
HC-Ir-HF	113.0(10)
HD-Ir-HF	139.9(9)
HE-Ir-HF	69.4(13)
C(30)-P(1)-C(10)	103.29(14)
C(30)-P(1)-C(20)	103.10(14)
C(10)-P(1)-C(20)	109.90(14)
C(30)-P(1)-Ir	114.38(13)
C(10)-P(1)-Ir	114.30(13)
C(20)-P(1)-Ir	111.07(13)
C(11)-C(10)-C(12)	110.87(16)
C(11)-C(10)-P(1)	113.55(15)
C(12)-C(10)-P(1)	115.29(15)

C(11)-C(10)-H(10)	106.1(3)
C(12)-C(10)-H(10)	109.1(3)
P(1)-C(10)-H(10)	100.9(3)
C(10)-C(11)-H(11A)	111.9(3)
C(10)-C(11)-H(11B)	109.3(3)
H(11A)-C(11)-H(11B)	108.3(4)
C(10)-C(11)-H(11C)	111.7(3)
H(11A)-C(11)-H(11C)	108.6(4)
H(11B)-C(11)-H(11C)	106.8(4)
C(10)-C(12)-H(12A)	113.5(3)
C(10)-C(12)-H(12B)	110.2(3)
H(12A)-C(12)-H(12B)	106.5(4)
C(10)-C(12)-H(12C)	111.2(3)
H(12A)-C(12)-H(12C)	108.2(4)
H(12B)-C(12)-H(12C)	106.9(4)
C(21)-C(20)-C(22)	109.79(16)
C(21)-C(20)-P(1)	111.80(15)
C(22)-C(20)-P(1)	117.36(15)
C(21)-C(20)-H(20)	107.5(3)
C(22)-C(20)-H(20)	108.3(3)
P(1)-C(20)-H(20)	101.3(3)
C(20)-C(21)-H(21A)	111.9(3)
C(20)-C(21)-H(21B)	109.7(3)
H(21A)-C(21)-H(21B)	108.3(4)
C(20)-C(21)-H(21C)	110.6(3)
H(21A)-C(21)-H(21C)	107.9(4)
H(21B)-C(21)-H(21C)	108.3(4)
C(20)-C(22)-H(22A)	112.8(3)
C(20)-C(22)-H(22B)	111.6(3)
H(22A)-C(22)-H(22B)	108.4(5)
C(20)-C(22)-H(22C)	109.1(3)

H(22A)-C(22)-H(22C)	106.8(4)
H(22B)-C(22)-H(22C)	107.9(5)
C(31)-C(30)-C(32)	110.47(16)
C(31)-C(30)-P(1)	110.75(15)
C(32)-C(30)-P(1)	112.72(14)
C(31)-C(30)-H(30)	108.1(3)
C(32)-C(30)-H(30)	107.9(3)
P(1)-C(30)-H(30)	106.6(3)
C(30)-C(31)-H(31A)	113.8(3)
C(30)-C(31)-H(31B)	111.7(3)
H(31A)-C(31)-H(31B)	106.8(5)
C(30)-C(31)-H(31C)	110.3(3)
H(31A)-C(31)-H(31C)	107.2(5)
H(31B)-C(31)-H(31C)	106.8(5)
C(30)-C(32)-H(32A)	112.3(3)
C(30)-C(32)-H(32B)	109.7(3)
H(32A)-C(32)-H(32B)	107.7(4)
C(30)-C(32)-H(32C)	111.6(3)
H(32A)-C(32)-H(32C)	107.6(4)
H(32B)-C(32)-H(32C)	107.8(4)
C(40)-P(2)-C(50)	103.12(14)
C(40)-P(2)-C(60)	110.07(15)
C(50)-P(2)-C(60)	102.49(14)
C(40)-P(2)-Ir	113.75(13)
C(50)-P(2)-Ir	113.96(13)
C(60)-P(2)-Ir	112.53(13)
C(41)-C(40)-C(42)	111.34(19)
C(41)-C(40)-P(2)	112.50(16)
C(42)-C(40)-P(2)	116.84(16)
C(41)-C(40)-H(40)	106.5(3)
C(42)-C(40)-H(40)	107.4(3)

P(2)-C(40)-H(40)	101.0(3)
C(40)-C(41)-H(41A)	112.1(4)
C(40)-C(41)-H(41B)	111.7(5)
H(41A)-C(41)-H(41B)	108.4(7)
C(40)-C(41)-H(41C)	109.4(3)
H(41A)-C(41)-H(41C)	107.8(5)
H(41B)-C(41)-H(41C)	107.2(5)
C(40)-C(42)-H(42A)	112.3(4)
C(40)-C(42)-H(42B)	110.1(3)
H(42A)-C(42)-H(42B)	106.9(6)
C(40)-C(42)-H(42C)	112.7(5)
H(42A)-C(42)-H(42C)	108.6(8)
H(42B)-C(42)-H(42C)	105.9(6)
C(52)-C(50)-C(51)	110.85(16)
C(52)-C(50)-P(2)	111.84(15)
C(51)-C(50)-P(2)	110.50(15)
C(52)-C(50)-H(50)	108.3(3)
C(51)-C(50)-H(50)	108.7(3)
P(2)-C(50)-H(50)	106.6(3)
C(50)-C(51)-H(51A)	111.0(3)
C(50)-C(51)-H(51B)	109.5(3)
H(51A)-C(51)-H(51B)	108.0(4)
C(50)-C(51)-H(51C)	112.5(3)
H(51A)-C(51)-H(51C)	108.3(5)
H(51B)-C(51)-H(51C)	107.5(4)
C(50)-C(52)-H(52A)	113.1(3)
C(50)-C(52)-H(52B)	109.2(3)
H(52A)-C(52)-H(52B)	106.8(4)
C(50)-C(52)-H(52C)	110.9(3)
H(52A)-C(52)-H(52C)	108.5(5)
H(52B)-C(52)-H(52C)	108.2(4)

C(61)-C(60)-C(62)	110.31(17)
C(61)-C(60)-P(2)	114.20(16)
C(62)-C(60)-P(2)	116.04(16)
C(61)-C(60)-H(60)	107.0(3)
C(62)-C(60)-H(60)	108.0(3)
P(2)-C(60)-H(60)	100.3(3)
C(60)-C(61)-H(61A)	111.5(4)
C(60)-C(61)-H(61B)	109.5(3)
H(61A)-C(61)-H(61B)	107.4(5)
C(60)-C(61)-H(61C)	112.0(3)
H(61A)-C(61)-H(61C)	109.9(6)
H(61B)-C(61)-H(61C)	106.4(5)
C(60)-C(62)-H(62A)	114.6(4)
C(60)-C(62)-H(62B)	110.9(4)
H(62A)-C(62)-H(62B)	107.1(6)
C(60)-C(62)-H(62C)	109.7(4)
H(62A)-C(62)-H(62C)	108.1(5)
H(62B)-C(62)-H(62C)	106.1(5)
C(71)-C(70)-C(79)	121.64(18)
C(71)-C(70)-C(75)	119.14(18)
C(79)-C(70)-C(75)	119.22(18)
C(72)-C(71)-C(70)	120.31(18)
C(72)-C(71)-H(71)	120.3(3)
C(70)-C(71)-H(71)	119.4(3)
C(71)-C(72)-C(73)	120.46(18)
C(71)-C(72)-H(72)	120.7(3)
C(73)-C(72)-H(72)	118.8(3)
C(74)-C(73)-C(72)	120.31(18)
C(74)-C(73)-H(73)	120.7(3)
C(72)-C(73)-H(73)	119.0(3)
C(73)-C(74)-C(75)	120.52(18)

C(73)-C(74)-H(74)	121.3(3)
C(75)-C(74)-H(74)	118.2(3)
C(74)-C(75)-C(70)	119.25(17)
C(74)-C(75)-C(76)	121.68(18)
C(70)-C(75)-C(76)	119.07(18)
C(77)-C(76)-C(75)	120.45(18)
C(77)-C(76)-H(76)	121.6(3)
C(75)-C(76)-H(76)	117.9(3)
C(76)-C(77)-C(78)	120.34(18)
C(76)-C(77)-H(77)	119.8(3)
C(78)-C(77)-H(77)	119.8(3)
C(79)-C(78)-C(77)	120.38(18)
C(79)-C(78)-H(78)	120.1(3)
C(77)-C(78)-H(78)	119.5(3)
C(78)-C(79)-C(70)	120.51(18)
C(78)-C(79)-H(79)	119.8(3)
C(70)-C(79)-H(79)	119.6(3)

Symmetry transformations used to generate equivalent atoms:

Table A.4 Anisotropic displacement parameters (A^2 x 10^3) for irh2ill.

The anisotropic displacement factor exponent takes the form:

-2 pi^2 [h^2 a*^2 U11 + ... + 2 h k a* b* U12]

U11	U22	U33	U23	U13	U12

Ir	10(1)	12(1)	10(1)	0(1)	-1(1)	-4(1)
Br	9(1)	10(1)	11(1)	0(1)	-2(1)	-3(1)
P(1)	5(1)	10(1)	10(1)	-1(1)	-1(1)	-2(1)
C(10)	8(1)	12(1)	11(1)	0(1)	-3(1)	-2(1)
C(11)	8(1)	17(1)	15(1)	-2(1)	-4(1)	-3(1)
C(12)	10(1)	16(1)	12(1)	-1(1)	0(1)	-1(1)
C(20)	7(1)	9(1)	11(1)	-2(1)	0(1)	-2(1)
C(21)	12(1)	13(1)	18(1)	0(1)	-4(1)	-6(1)
C(22)	16(1)	12(1)	12(1)	1(1)	0(1)	-5(1)
C(30)	9(1)	11(1)	12(1)	0(1)	-4(1)	-4(1)
C(31)	10(1)	16(1)	21(1)	-4(1)	-5(1)	-2(1)
C(32)	14(1)	12(1)	16(1)	1(1)	-4(1)	-7(1)
P(2)	9(1)	10(1)	11(1)	-1(1)	-1(1)	-4(1)
C(40)	10(1)	12(1)	12(1)	-1(1)	1(1)	-4(1)
C(41)	16(1)	19(1)	38(1)	7(1)	-14(1)	-11(1)
C(42)	52(2)	25(2)	16(1)	-9(1)	14(1)	-25(1)
C(50)	9(1)	14(1)	11(1)	-1(1)	-2(1)	-3(1)
C(51)	13(1)	16(1)	18(1)	-2(1)	-6(1)	-2(1)
C(52)	14(1)	17(1)	16(1)	0(1)	-5(1)	-9(1)
C(60)	9(1)	13(1)	13(1)	-1(1)	-2(1)	-3(1)
C(61)	11(1)	18(1)	17(1)	-2(1)	-4(1)	1(1)
C(62)	22(1)	22(1)	15(1)	-6(1)	-3(1)	6(1)

C(70)	10(1)	12(1)	12(1)	-1(1)	-2(1)	-4(1)
C(71)	8(1)	14(1)	15(1)	1(1)	-3(1)	-4(1)
C(72)	4(1)	18(1)	16(1)	-1(1)	-1(1)	-3(1)
C(73)	8(1)	14(1)	17(1)	0(1)	-2(1)	-2(1)
C(74)	7(1)	14(1)	15(1)	-1(1)	-2(1)	-2(1)
C(75)	6(1)	11(1)	11(1)	-1(1)	-1(1)	-2(1)
C(76)	7(1)	11(1)	16(1)	0(1)	-2(1)	-2(1)
C(77)	7(1)	14(1)	17(1)	-1(1)	-2(1)	-2(1)
C(78)	11(1)	12(1)	15(1)	-1(1)	-4(1)	-3(1)
C(79)	11(1)	11(1)	15(1)	0(1)	-5(1)	-2(1)
H(10)	22(2)	20(2)	29(2)	-3(2)	-6(2)	-7(2)
H(11A)	27(2)	51(3)	21(2)	0(2)	-2(2)	-14(2)
H(11B)	24(2)	31(3)	43(3)	-8(2)	-12(2)	4(2)
H(11C)	32(2)	30(3)	48(3)	4(2)	-18(2)	-15(2)
H(12A)	25(2)	47(3)	27(2)	-2(2)	-7(2)	-7(2)
H(12B)	24(2)	26(3)	38(2)	-2(2)	4(2)	6(2)
H(12C)	37(3)	34(3)	34(2)	-2(2)	5(2)	-17(2)
H(20)	17(2)	22(2)	24(2)	-2(2)	2(2)	-2(2)
H(21A)	37(3)	39(3)	23(2)	2(2)	-10(2)	-19(2)
H(21B)	34(2)	20(3)	48(3)	0(2)	-8(2)	-15(2)
H(21C)	15(2)	38(3)	44(3)	-9(2)	1(2)	-4(2)
H(22A)	38(3)	43(3)	26(2)	3(2)	-10(2)	-21(2)
H(22B)	33(3)	37(3)	28(2)	-2(2)	9(2)	9(2)

H(22C)	49(3)	15(3)	32(2)	4(2)	-1(2)	-13(2)
H(30)	22(2)	33(2)	19(2)	-1(2)	-2(2)	-10(2)
H(31A)	26(2)	20(3)	66(4)	-2(2)	-13(2)	-1(2)
H(31B)	22(2)	52(3)	43(3)	-8(2)	10(2)	-3(2)
H(31C)	26(2)	41(3)	55(3)	-9(2)	-26(2)	-1(2)
H(32A)	27(3)	24(2)	51(3)	-9(2)	-4(2)	-3(2)
H(32B)	29(2)	32(2)	40(2)	-1(2)	-18(2)	-14(2)
H(32C)	46(3)	38(3)	24(2)	0(2)	6(2)	-24(2)
H(40)	22(2)	20(2)	32(2)	-2(2)	-2(2)	-5(2)
H(41A)	74(4)	75(4)	33(3)	18(3)	-28(3)	-49(4)
H(41B)	18(3)	32(3)	130(7)	9(3)	-10(3)	-2(2)
H(41C)	38(3)	26(3)	58(3)	7(2)	-18(2)	-18(2)
H(42A)	93(5)	89(5)	28(3)	5(3)	-3(3)	-66(5)
H(42B)	62(3)	36(3)	32(2)	-2(2)	9(2)	-34(3)
H(42C)	115(7)	36(4)	76(5)	-34(4)	65(5)	-25(4)
H(50)	26(2)	27(2)	19(2)	0(2)	0(2)	-12(2)
H(51A)	30(2)	40(3)	29(3)	-10(2)	3(2)	5(2)
H(51B)	28(2)	35(3)	39(3)	-1(2)	-21(2)	-1(2)
H(51C)	37(3)	23(3)	63(3)	-1(2)	-13(2)	-10(2)
H(52A)	28(2)	24(3)	58(3)	-2(2)	-6(2)	-6(2)
H(52B)	31(2)	39(3)	34(2)	2(2)	-18(2)	-16(2)
H(52C)	47(3)	51(3)	25(2)	-4(2)	4(2)	-33(3)
H(60)	23(2)	23(2)	53(3)	-3(2)	2(2)	-11(2)

H(61A)	44(3)	90(5)	24(3)	-4(3)	-4(2)	17(3)
H(61B)	27(2)	25(3)	51(3)	-1(2)	-11(2)	2(2)
H(61C)	39(3)	34(3)	87(5)	8(3)	-34(3)	-19(2)
H(62A)	38(3)	73(4)	31(3)	-21(3)	-18(3)	20(3)
H(62B)	44(3)	41(3)	38(3)	4(2)	14(2)	-7(3)
H(62C)	39(3)	30(3)	42(3)	-15(2)	0(2)	4(2)
H(71)	27(2)	28(3)	43(3)	3(2)	-5(2)	-16(2)
H(72)	10(2)	41(3)	44(3)	-8(2)	0(2)	-9(2)
H(73)	18(2)	23(2)	44(3)	-1(2)	-4(2)	2(2)
H(74)	25(2)	19(2)	39(2)	-1(2)	0(2)	-8(2)
H(76)	23(2)	24(2)	38(2)	-1(2)	-3(2)	-13(2)
H(77)	11(2)	34(2)	43(3)	-2(2)	-2(2)	-6(2)
H(78)	26(2)	21(2)	42(3)	-4(2)	-5(2)	2(2)
H(79)	29(2)	19(2)	44(3)	1(2)	-4(2)	-9(2)
HA	21(3)	41(4)	23(3)	-4(3)	-6(2)	-13(3)
HB	29(4)	23(3)	31(3)	0(3)	-5(3)	-4(3)
HC	26(4)	33(5)	53(4)	-6(4)	-20(3)	-3(3)
HD	30(4)	33(5)	55(5)	-3(4)	-16(3)	-17(3)
HE	35(10)	23(9)	20(7)	10(7)	0(8)	10(9)
HF	57(14)	12(8)	30(8)	-12(7)	3(9)	-21(8)

Table A.5 Hydrogen coordinates (x 10^4) and isotropic displacement parameters (A^2 x 10^3) for irh2ill.

	x	y	z	U(eq)
H(10)	929(6)	4188(3)	9379(3)	23(1)
H(11A)	-112(6)	3598(4)	8036(3)	33(1)
H(11B)	-1853(6)	4247(4)	8811(4)	34(1)
H(11C)	-1269(6)	2907(4)	8821(4)	35(1)
H(12A)	471(6)	3359(4)	11033(3)	34(1)
H(12B)	-1495(6)	4103(4)	10569(4)	33(1)
H(12C)	-901(7)	2760(4)	10589(4)	34(1)
H(20)	3749(5)	690(3)	9393(3)	22(1)
H(21A)	1079(7)	1236(4)	8424(3)	31(1)
H(21B)	1215(6)	140(4)	9230(4)	32(1)
H(21C)	-254(6)	1348(4)	9490(4)	33(1)
H(22A)	3326(7)	950(4)	11102(3)	33(1)
H(22B)	1034(7)	1348(4)	11036(4)	38(1)
H(22C)	2271(7)	78(4)	10836(3)	32(1)
H(30)	3291(6)	2595(4)	10883(3)	24(1)
H(31A)	5752(6)	1097(4)	10271(4)	38(1)
H(31B)	6628(7)	1968(5)	9566(4)	42(1)
H(31C)	6525(7)	1959(4)	10787(4)	41(1)
H(32A)	2964(6)	4370(4)	10212(4)	34(1)
H(32B)	5073(6)	3838(4)	10616(4)	32(1)
H(32C)	4797(7)	3955(4)	9407(3)	34(1)
H(40)	5054(6)	4185(3)	5974(3)	25(1)
H(41A)	7367(10)	3436(6)	7096(4)	54(2)
H(41B)	8847(7)	2894(5)	6163(7)	62(2)
H(41C)	7994(7)	4227(4)	6160(4)	38(1)

H(42A)	5467(12)	3730(6)	4340(4)	62(2)
H(42B)	7027(8)	4309(4)	4554(4)	40(1)
H(42C)	7651(13)	2993(6)	4489(6)	78(3)
H(50)	4285(6)	2504(3)	4676(3)	24(1)
H(51A)	1434(7)	3688(4)	6088(3)	36(1)
H(51B)	1146(6)	3617(4)	4897(4)	35(1)
H(51C)	2631(7)	4235(4)	5186(4)	40(1)
H(52A)	3719(7)	908(4)	5438(4)	37(1)
H(52B)	1760(6)	1765(4)	5048(3)	33(1)
H(52C)	2130(7)	1624(4)	6247(3)	37(1)
H(60)	6004(6)	673(4)	6225(4)	32(1)
H(61A)	7743(9)	856(6)	7445(4)	61(2)
H(61B)	9098(6)	79(4)	6610(4)	37(1)
H(61C)	9142(8)	1334(4)	6605(5)	50(2)
H(62A)	6678(8)	1289(5)	4511(4)	53(2)
H(62B)	8618(8)	1421(5)	4860(4)	44(1)
H(62C)	8299(7)	208(4)	4971(4)	40(1)
H(71)	1988(6)	1371(4)	3043(4)	31(1)
H(72)	-138(6)	3119(4)	3075(4)	31(1)
H(73)	885(6)	4665(4)	2819(4)	30(1)
H(74)	4111(6)	4471(3)	2565(3)	28(1)
H(76)	7151(6)	3366(3)	2403(3)	27(1)
H(77)	9312(5)	1614(4)	2396(4)	30(1)
H(78)	8254(6)	66(4)	2599(4)	31(1)
H(79)	5087(6)	244(3)	2806(4)	30(1)
HA	2218(8)	2491(5)	7434(4)	27(1)
HB	4512(12)	1330(5)	7858(5)	29(1)
HC	6118(9)	2213(8)	8176(6)	37(2)
HD	5845(10)	2846(8)	8140(6)	37(2)
HE	5340(30)	1574(14)	8083(12)	31(4)
HF	3370(30)	1597(13)	7632(13)	31(4)

Table A.6 Torsion angles [deg] for irh2ill.

C(30)-P(1)-C(10)-C(11)	172.95(15)
C(20)-P(1)-C(10)-C(11)	-77.59(19)
Ir-P(1)-C(10)-C(11)	48.1(2)
C(30)-P(1)-C(10)-C(12)	-57.57(19)
C(20)-P(1)-C(10)-C(12)	51.9(2)
Ir-P(1)-C(10)-C(12)	177.54(13)
C(30)-P(1)-C(20)-C(21)	164.82(15)
C(10)-P(1)-C(20)-C(21)	55.23(19)
Ir-P(1)-C(20)-C(21)	-72.25(17)
C(30)-P(1)-C(20)-C(22)	36.7(2)
C(10)-P(1)-C(20)-C(22)	-72.90(19)
Ir-P(1)-C(20)-C(22)	159.62(14)
C(10)-P(1)-C(30)-C(31)	175.61(16)
C(20)-P(1)-C(30)-C(31)	61.16(19)
Ir-P(1)-C(30)-C(31)	-59.55(19)
C(10)-P(1)-C(30)-C(32)	-60.06(19)
C(20)-P(1)-C(30)-C(32)	-174.51(16)
Ir-P(1)-C(30)-C(32)	64.78(19)
C(50)-P(2)-C(40)-C(41)	-173.76(17)
C(60)-P(2)-C(40)-C(41)	-65.0(2)
Ir-P(2)-C(40)-C(41)	62.3(2)
C(50)-P(2)-C(40)-C(42)	-43.1(2)
C(60)-P(2)-C(40)-C(42)	65.6(2)
Ir-P(2)-C(40)-C(42)	-167.05(18)
C(40)-P(2)-C(50)-C(52)	173.15(16)
C(60)-P(2)-C(50)-C(52)	58.79(19)

Ir-P(2)-C(50)-C(52)	-63.07(19)
C(40)-P(2)-C(50)-C(51)	-62.85(19)
C(60)-P(2)-C(50)-C(51)	-177.21(15)
Ir-P(2)-C(50)-C(51)	60.93(19)
C(40)-P(2)-C(60)-C(61)	75.3(2)
C(50)-P(2)-C(60)-C(61)	-175.58(16)
Ir-P(2)-C(60)-C(61)	-52.75(19)
C(40)-P(2)-C(60)-C(62)	-54.8(2)
C(50)-P(2)-C(60)-C(62)	54.4(2)
Ir-P(2)-C(60)-C(62)	177.22(15)
C(79)-C(70)-C(71)-C(72)	-179.19(18)
C(75)-C(70)-C(71)-C(72)	0.8(3)
C(70)-C(71)-C(72)-C(73)	0.1(3)
C(71)-C(72)-C(73)-C(74)	-0.6(3)
C(72)-C(73)-C(74)-C(75)	0.1(3)
C(73)-C(74)-C(75)-C(70)	0.8(3)
C(73)-C(74)-C(75)-C(76)	-179.46(18)
C(71)-C(70)-C(75)-C(74)	-1.3(3)
C(79)-C(70)-C(75)-C(74)	178.76(17)
C(71)-C(70)-C(75)-C(76)	178.99(17)
C(79)-C(70)-C(75)-C(76)	-1.0(3)
C(74)-C(75)-C(76)-C(77)	179.59(18)
C(70)-C(75)-C(76)-C(77)	-0.7(3)
C(75)-C(76)-C(77)-C(78)	1.5(3)
C(76)-C(77)-C(78)-C(79)	-0.7(3)
C(77)-C(78)-C(79)-C(70)	-1.0(3)
C(71)-C(70)-C(79)-C(78)	-178.15(18)
C(75)-C(70)-C(79)-C(78)	1.8(3)

Least-squares planes (x,y,z in crystal coordinates) and deviations from them

(* indicates atom used to define plane)

- 2.5453 (0.0330) x - 0.2633 (0.0212) y + 13.1029 (0.0261) z = 9.1106 (0.0356)

* -0.0036 (0.0029) Ir

* 0.0015 (0.0012) Br

* -0.0002 (0.0002) HA

* 0.0024 (0.0019) HB

-0.0073 (0.0125) HD

-0.0128 (0.0130) HC

0.0785 (0.0180) HE

-0.0084 (0.0184) HF

2.3213 (0.0037) P1

-2.3249 (0.0038) P2

Rms deviation of fitted atoms = 0.0023

7.5661 (0.0020) x + 4.3281 (0.0101) y + 6.1031 (0.0088) z = 8.8197 (0.0070)

Angle to previous plane (with approximate esd) = 89.527 (0.231)

* 0.0561 (0.0013) Ir

* -0.0268 (0.0006) P1

* -0.0268 (0.0006) P2

* -0.0025 (0.0001) Br

Rms deviation of fitted atoms = 0.0339

- 2.5680 (0.0238) x - 0.1950 (0.0335) y + 13.0844 (0.0189) z = 9.1089 (0.0311)

Angle to previous plane (with approximate esd) = 89.699 (0.168)

* -0.0080 (0.0033) Ir

* 0.0135 (0.0036) Br

* -0.0117 (0.0077) HB

* -0.0004 (0.0070) HA

* -0.0146 (0.0072) HD

* -0.0250 (0.0079) HC

* 0.0638 (0.0131) HE

* -0.0177 (0.0124) HF

2.3166 (0.0042) P1

-2.3298 (0.0042) P2

Rms deviation of fitted atoms = 0.0265

APPENDIX B. Supplemental Data, Neutron Data Set for $IrClH_x(iPr_3P)_2$ @ 293(2) K

Table B.1 Crystal data and structure refinement for ir.

Identification code	shelx
Empirical formula	C18 H45 Cl Ir P2
Formula weight	551.18
Temperature	293(2) K
Wavelength	1.45549 A
Crystal system, space group	Monoclinic, P 21/c
Unit cell dimensions	a = 15.7824(7) A alpha = 90 deg. b = 8.9511(3) A beta = 94.954(3) deg. c = 16.2988(6) A gamma = 90 deg.
Volume	2293.93(15) A^3
Z, Calculated density	4, 1.596 Mg/m^3
Absorption coefficient	0.446 mm^-1
F(000)	-73
Crystal size	? x ? x ? mm
Theta range for data collection	5.143 to 60.784 deg.

Limiting indices	-9<=h<=18, -10<=k<=10, -19<=l<=19
Reflections collected / unique	14313 / 3914 [R(int) = 0.0831]
Completeness to theta = 60.844	94.2 %
Refinement method	Full-matrix least-squares on F^2
Data / restraints / parameters	3914 / 0 / 631
Goodness-of-fit on F^2	1.094
Final R indices [I>2sigma(I)]	R1 = 0.0669, wR2 = 0.1699
R indices (all data)	R1 = 0.0741, wR2 = 0.1767
Extinction coefficient	n/a
Largest diff. peak and hole	0.811 and -0.920 e.A^-3

Table B.2 Atomic coordinates (x 10^4) and equivalent isotropic displacement parameters (A^2 x 10^3) for ir.
U(eq) is defined as one third of the trace of the orthogonalized Uij tensor.

	x	y	z	U(eq)

Ir(1)	7406(1)	5030(1)	113(1)	18(1)
Cl(1)	7632(1)	7010(2)	1141(1)	29(1)
P(1)	6834(2)	6668(3)	-893(2)	17(1)
P(2)	8132(2)	3305(3)	972(2)	17(1)
C(1)	8983(1)	4185(2)	1663(1)	19(1)
C(2)	7642(1)	7381(2)	-1553(1)	18(1)
C(3)	8549(1)	1725(2)	397(1)	18(1)
C(4)	6396(1)	8386(2)	-460(1)	19(1)
C(5)	6045(1)	5776(2)	-1648(1)	20(1)
C(6)	7478(1)	2350(2)	1703(1)	20(1)
C(7)	8322(1)	8293(2)	-1057(1)	23(1)
C(8)	5728(2)	6717(3)	-2391(2)	31(1)
C(9)	9646(2)	4972(3)	1183(1)	25(1)
C(10)	5687(2)	8083(2)	95(1)	24(1)
C(11)	8042(1)	6113(2)	-2011(1)	21(1)
C(12)	9412(2)	3231(2)	2355(1)	24(1)
C(13)	9110(2)	2209(2)	-270(1)	28(1)
C(14)	5293(2)	5106(3)	-1249(2)	34(1)
C(15)	6151(2)	9657(3)	-1062(2)	34(1)
C(16)	7107(2)	3461(3)	2284(1)	27(1)
C(18)	6781(2)	1385(3)	1255(1)	25(1)
C(19)	8987(2)	480(2)	916(1)	27(1)

Table B.3 Bond lengths [A] and angles [deg] for ir.

Ir(1)-P(2)	2.319(3)
Ir(1)-P(1)	2.322(3)
Ir(1)-Cl(1)	2.4444(18)

Ir(1)-HY1	1.548(7)
Ir(1)-HY2	1.581(9)
Ir(1)-HY11	1.773(12)
Ir(1)-HY12	1.821(13)
Ir(1)-HYA	1.474(17)
Ir(1)-HYB	1.578(14)
P(1)-C(4)	1.850(3)
P(1)-C(2)	1.852(3)
P(1)-C(5)	1.854(3)
P(2)-C(3)	1.850(3)
P(2)-C(6)	1.851(3)
P(2)-C(1)	1.853(3)
C(1)-C(12)	1.526(3)
C(1)-C(9)	1.530(3)
C(1)-H(4)	1.092(5)
C(2)-C(7)	1.524(3)
C(2)-C(11)	1.526(3)
C(2)-H(2)	1.096(5)
C(3)-C(13)	1.523(3)
C(3)-C(19)	1.528(3)
C(3)-H(29)	1.097(5)
C(4)-C(10)	1.522(3)
C(4)-C(15)	1.531(3)

C(4)-H(27)	1.095(5)
C(5)-C(14)	1.524(3)
C(5)-C(8)	1.524(3)
C(5)-H(6)	1.083(5)
C(6)-C(16)	1.525(3)
C(6)-C(18)	1.533(3)
C(6)-H(5)	1.081(5)
C(7)-H(9)	1.077(5)
C(7)-H(36)	1.082(5)
C(7)-H(38)	1.082(6)
C(8)-H(8)	1.083(8)
C(8)-H(34)	1.086(6)
C(8)-H(42)	1.085(7)
C(9)-H(21)	1.084(5)
C(9)-H(22)	1.078(6)
C(9)-H(23)	1.094(6)
C(10)-H(1)	1.077(5)
C(10)-H(28)	1.077(5)
C(10)-H(46)	1.078(6)
C(11)-H(12)	1.082(5)
C(11)-H(31)	1.085(5)
C(11)-H(35)	1.080(5)
C(12)-H(10)	1.072(6)

C(12)-H(26)	1.084(5)
C(12)-H(37)	1.082(6)
C(13)-H(7)	1.075(6)
C(13)-H(33)	1.081(7)
C(13)-H(40)	1.085(5)
C(14)-H(25)	1.066(9)
C(14)-H(32)	1.079(5)
C(14)-H(47)	1.072(7)
C(15)-H(3)	1.083(5)
C(15)-H(43)	1.050(8)
C(15)-H(48)	1.093(9)
C(16)-H(18)	1.073(6)
C(16)-H(41)	1.078(5)
C(16)-H(45)	1.096(6)
C(18)-H(19)	1.081(6)
C(18)-H(20)	1.089(5)
C(18)-H(39)	1.073(6)
C(19)-H(24)	1.076(6)
C(19)-H(30)	1.081(5)
C(19)-H(44)	1.092(7)

******** H-H distances

HY11 - HY12	0.7167 (0.0142)
HYA - HYB	1.7001 (0.0328)
HY2 - HYA	0.9126 (0.0262)
HY11 - HYA	1.2112 (0.0350)
HY12 - HYA	1.7600 (0.0303)

P(2)-Ir(1)-P(1)	171.05(10)
P(2)-Ir(1)-Cl(1)	91.90(8)
P(1)-Ir(1)-Cl(1)	92.91(8)
P(2)-Ir(1)-HY1	85.0(3)
P(1)-Ir(1)-HY1	87.3(3)
Cl(1)-Ir(1)-HY1	91.5(3)
P(2)-Ir(1)-HY2	88.5(4)
P(1)-Ir(1)-HY2	86.8(4)
Cl(1)-Ir(1)-HY2	179.4(5)
HY1-Ir(1)-HY2	89.0(6)
P(2)-Ir(1)-HY11	89.2(5)
P(1)-Ir(1)-HY11	97.2(5)
Cl(1)-Ir(1)-HY11	102.5(7)
HY1-Ir(1)-HY11	165.0(7)
HY2-Ir(1)-HY11	77.1(9)
P(2)-Ir(1)-HY12	99.7(6)
P(1)-Ir(1)-HY12	88.5(6)
Cl(1)-Ir(1)-HY12	81.8(5)
HY1-Ir(1)-HY12	171.9(6)
HY2-Ir(1)-HY12	97.7(8)
HY11-Ir(1)-HY12	23.0(5)
P(2)-Ir(1)-HYA	89.6(6)
P(1)-Ir(1)-HYA	90.8(6)
Cl(1)-Ir(1)-HYA	145.0(12)
HY1-Ir(1)-HYA	123.4(13)

HY2-Ir(1)-HYA	34.5(10)
HY11-Ir(1)-HYA	42.6(13)
HY12-Ir(1)-HYA	63.6(13)
P(2)-Ir(1)-HYB	86.1(5)
P(1)-Ir(1)-HYB	85.8(5)
Cl(1)-Ir(1)-HYB	147.4(11)
HY1-Ir(1)-HYB	55.9(12)
HY2-Ir(1)-HYB	33.1(9)
HY11-Ir(1)-HYB	110.0(13)
HY12-Ir(1)-HYB	130.7(12)
HYA-Ir(1)-HYB	67.6(14)
C(4)-P(1)-C(2)	103.52(14)
C(4)-P(1)-C(5)	111.10(16)
C(2)-P(1)-C(5)	102.67(14)
C(4)-P(1)-Ir(1)	113.01(13)
C(2)-P(1)-Ir(1)	112.47(14)
C(5)-P(1)-Ir(1)	113.20(13)
C(3)-P(2)-C(6)	102.43(14)
C(3)-P(2)-C(1)	111.19(16)
C(6)-P(2)-C(1)	102.75(14)
C(3)-P(2)-Ir(1)	112.47(13)
C(6)-P(2)-Ir(1)	114.99(14)
C(1)-P(2)-Ir(1)	112.24(13)
C(12)-C(1)-C(9)	110.86(18)
C(12)-C(1)-P(2)	117.62(16)
C(9)-C(1)-P(2)	112.16(16)
C(12)-C(1)-H(4)	108.7(3)
C(9)-C(1)-H(4)	106.1(3)
P(2)-C(1)-H(4)	100.3(3)
C(7)-C(2)-C(11)	110.86(17)
C(7)-C(2)-P(1)	111.42(15)

C(11)-C(2)-P(1)	111.30(16)
C(7)-C(2)-H(2)	108.7(3)
C(11)-C(2)-H(2)	107.7(3)
P(1)-C(2)-H(2)	106.6(3)
C(13)-C(3)-C(19)	109.91(18)
C(13)-C(3)-P(2)	113.46(16)
C(19)-C(3)-P(2)	116.19(16)
C(13)-C(3)-H(29)	107.4(3)
C(19)-C(3)-H(29)	107.9(3)
P(2)-C(3)-H(29)	101.1(3)
C(10)-C(4)-C(15)	110.79(18)
C(10)-C(4)-P(1)	113.34(16)
C(15)-C(4)-P(1)	117.06(16)
C(10)-C(4)-H(27)	106.5(3)
C(15)-C(4)-H(27)	108.1(3)
P(1)-C(4)-H(27)	99.8(3)
C(14)-C(5)-C(8)	109.96(19)
C(14)-C(5)-P(1)	112.93(16)
C(8)-C(5)-P(1)	116.44(17)
C(14)-C(5)-H(6)	106.6(3)
C(8)-C(5)-H(6)	108.7(3)
P(1)-C(5)-H(6)	101.4(3)
C(16)-C(6)-C(18)	111.40(18)
C(16)-C(6)-P(2)	111.33(16)
C(18)-C(6)-P(2)	111.81(16)
C(16)-C(6)-H(5)	107.8(3)
C(18)-C(6)-H(5)	107.7(3)
P(2)-C(6)-H(5)	106.6(3)
C(2)-C(7)-H(9)	112.9(3)
C(2)-C(7)-H(36)	109.3(3)
H(9)-C(7)-H(36)	106.9(4)

C(2)-C(7)-H(38)	110.8(3)
H(9)-C(7)-H(38)	108.0(5)
H(36)-C(7)-H(38)	108.7(5)
C(5)-C(8)-H(8)	111.1(4)
C(5)-C(8)-H(34)	110.1(4)
H(8)-C(8)-H(34)	106.8(5)
C(5)-C(8)-H(42)	112.8(4)
H(8)-C(8)-H(42)	108.7(7)
H(34)-C(8)-H(42)	107.0(5)
C(1)-C(9)-H(21)	110.0(3)
C(1)-C(9)-H(22)	111.6(4)
H(21)-C(9)-H(22)	107.7(5)
C(1)-C(9)-H(23)	111.7(3)
H(21)-C(9)-H(23)	107.0(4)
H(22)-C(9)-H(23)	108.7(5)
C(4)-C(10)-H(1)	111.9(3)
C(4)-C(10)-H(28)	109.9(3)
H(1)-C(10)-H(28)	107.7(5)
C(4)-C(10)-H(46)	112.3(3)
H(1)-C(10)-H(46)	107.8(5)
H(28)-C(10)-H(46)	107.1(5)
C(2)-C(11)-H(12)	109.5(3)
C(2)-C(11)-H(31)	111.7(3)
H(12)-C(11)-H(31)	107.0(4)
C(2)-C(11)-H(35)	111.2(3)
H(12)-C(11)-H(35)	108.4(5)
H(31)-C(11)-H(35)	108.8(5)
C(1)-C(12)-H(10)	113.9(4)
C(1)-C(12)-H(26)	109.2(3)
H(10)-C(12)-H(26)	107.4(5)
C(1)-C(12)-H(37)	111.6(3)

H(10)-C(12)-H(37)	108.0(5)
H(26)-C(12)-H(37)	106.4(5)
C(3)-C(13)-H(7)	111.6(4)
C(3)-C(13)-H(33)	111.8(4)
H(7)-C(13)-H(33)	108.4(6)
C(3)-C(13)-H(40)	109.9(3)
H(7)-C(13)-H(40)	108.4(5)
H(33)-C(13)-H(40)	106.6(5)
C(5)-C(14)-H(25)	111.3(5)
C(5)-C(14)-H(32)	111.0(4)
H(25)-C(14)-H(32)	105.6(5)
C(5)-C(14)-H(47)	111.9(5)
H(25)-C(14)-H(47)	108.2(8)
H(32)-C(14)-H(47)	108.6(6)
C(4)-C(15)-H(3)	109.4(3)
C(4)-C(15)-H(43)	112.8(4)
H(3)-C(15)-H(43)	107.1(6)
C(4)-C(15)-H(48)	110.6(4)
H(3)-C(15)-H(48)	106.2(5)
H(43)-C(15)-H(48)	110.4(7)
C(6)-C(16)-H(18)	112.0(3)
C(6)-C(16)-H(41)	109.4(3)
H(18)-C(16)-H(41)	107.4(5)
C(6)-C(16)-H(45)	111.6(3)
H(18)-C(16)-H(45)	107.2(5)
H(41)-C(16)-H(45)	109.0(5)
C(6)-C(18)-H(19)	112.3(4)
C(6)-C(18)-H(20)	109.8(3)
H(19)-C(18)-H(20)	105.9(5)
C(6)-C(18)-H(39)	111.3(3)
H(19)-C(18)-H(39)	109.8(5)

H(20)-C(18)-H(39)	107.5(5)
C(3)-C(19)-H(24)	113.5(4)
C(3)-C(19)-H(30)	110.0(3)
H(24)-C(19)-H(30)	106.6(5)
C(3)-C(19)-H(44)	110.5(4)
H(24)-C(19)-H(44)	110.0(6)
H(30)-C(19)-H(44)	105.8(5)

********** Lsq planes

* -0.0015 (0.0034) Ir1

* 0.0234 (0.0044) Cl1

* 0.0083 (0.0071) HY1

* -0.0199 (0.0113) HYB

* -0.0268 (0.0094) HY2

* 0.0242 (0.0134) HYA

* 0.1458 (0.0137) HY11

* -0.1535 (0.0138) HY12

Rms deviation of fitted atoms = 0.0768

15.7180 (0.0048) x - 0.5845 (0.0245) y - 2.4129 (0.0387) z = 11.3132 (0.0216)

Angle to previous plane (with approximate esd) = 68.082 (0.288)

* 0.0061 (0.0059) Ir1

* -0.0024 (0.0023) Cl1

* -0.0037 (0.0036) HY2

Rms deviation of fitted atoms = 0.0044

5.6670 (0.1107) x - 2.5939 (0.3390) y + 13.9006 (0.2387) z = 3.0487 (0.1400)

Angle to previous plane (with approximate esd) = 71.259 (0.471)

* 0.0000 (0.0000) Ir1

* 0.0000 (0.0000) HY11

* 0.0000 (0.0000) HY12

Rms deviation of fitted atoms = 0.0000

Table B.4 Anisotropic displacement parameters (A^2 x 10^3) for ir.
The anisotropic displacement factor exponent takes the form:
-2 pi^2 [h^2 a*^2 U11 + ... + 2 h k a* b* U12]

U11	U22	U33	U23	U13	U12

Ir(1)	23(1)	14(1)	19(1)	0(1)	0(1)	2(1)
Cl(1)	40(1)	19(1)	27(1)	-6(1)	-8(1)	7(1)
P(1)	17(1)	14(1)	20(1)	2(1)	2(1)	1(1)
P(2)	20(1)	13(1)	18(1)	1(1)	2(1)	2(1)
C(1)	22(1)	17(1)	19(1)	0(1)	-1(1)	-1(1)
C(2)	20(1)	15(1)	18(1)	-3(1)	1(1)	0(1)
C(3)	21(1)	14(1)	19(1)	2(1)	2(1)	1(1)
C(4)	22(1)	16(1)	20(1)	2(1)	4(1)	1(1)
C(5)	21(1)	21(1)	20(1)	1(1)	1(1)	-2(1)
C(6)	24(1)	16(1)	20(1)	-2(1)	4(1)	-3(1)
C(7)	24(1)	21(1)	23(1)	-5(1)	3(1)	-4(1)
C(8)	30(1)	31(1)	29(1)	11(1)	-12(1)	-7(1)
C(9)	25(1)	26(1)	24(1)	1(1)	1(1)	-6(1)
C(10)	25(1)	21(1)	27(1)	-2(1)	9(1)	0(1)
C(11)	24(1)	19(1)	19(1)	-4(1)	3(1)	2(1)
C(12)	29(1)	21(1)	22(1)	3(1)	-4(1)	-1(1)
C(13)	35(2)	18(1)	33(1)	-1(1)	18(1)	1(1)
C(14)	32(1)	41(1)	28(1)	-3(1)	4(1)	-16(1)
C(15)	57(2)	22(1)	26(1)	8(1)	13(1)	19(1)
C(16)	31(1)	24(1)	28(1)	-7(1)	10(1)	-2(1)
C(18)	26(1)	24(1)	26(1)	-5(1)	6(1)	-7(1)
C(19)	36(1)	21(1)	23(1)	2(1)	0(1)	9(1)
H(1)	62(3)	39(3)	51(3)	19(2)	26(3)	7(2)
H(2)	35(2)	26(2)	33(2)	5(2)	5(2)	4(2)
H(3)	78(4)	25(2)	48(3)	4(2)	13(3)	15(2)
H(4)	38(2)	27(2)	37(2)	-6(2)	4(2)	-1(2)
H(5)	38(2)	28(2)	32(2)	1(2)	4(2)	0(2)
H(6)	40(3)	32(2)	41(2)	-10(2)	0(2)	5(2)
H(7)	96(5)	36(3)	60(3)	20(3)	42(3)	23(3)
H(8)	74(4)	36(3)	87(5)	-1(3)	-34(4)	11(3)
H(9)	43(3)	34(3)	60(3)	-23(2)	15(2)	-3(2)

H(10)	43(3)	67(4)	43(3)	24(3)	-1(2)	-13(3)
H(12)	44(3)	39(2)	39(2)	-1(2)	17(2)	-2(2)
H(19)	50(3)	42(3)	56(3)	-24(2)	17(2)	-11(2)
H(18)	42(3)	45(3)	57(3)	-20(2)	16(2)	-14(2)
H(20)	56(3)	45(3)	41(3)	-5(2)	14(2)	-22(2)
H(21)	40(3)	42(3)	39(2)	-7(2)	2(2)	-15(2)
H(22)	50(3)	52(3)	47(3)	22(3)	-1(2)	-13(2)
H(23)	38(3)	47(3)	55(3)	-9(2)	14(2)	-6(2)
H(24)	88(5)	52(3)	51(3)	22(3)	33(3)	24(3)
H(25)	47(4)	95(6)	88(5)	-48(4)	29(3)	-21(4)
H(26)	56(3)	40(3)	34(2)	-3(2)	-13(2)	-9(2)
H(27)	32(2)	31(2)	41(2)	-8(2)	0(2)	-7(2)
H(28)	50(3)	32(2)	48(3)	-13(2)	18(2)	1(2)
H(29)	29(2)	33(2)	38(2)	-6(2)	1(2)	-2(2)
H(30)	56(3)	28(2)	41(2)	-7(2)	-1(2)	6(2)
H(31)	39(3)	43(3)	45(3)	-24(2)	0(2)	-4(2)
H(32)	46(3)	50(3)	52(3)	-15(2)	3(2)	-22(2)
H(33)	48(4)	59(4)	80(4)	-25(3)	33(3)	-25(3)
H(34)	53(3)	52(3)	42(3)	2(2)	-14(2)	-10(3)
H(35)	53(3)	34(2)	42(3)	7(2)	3(2)	18(2)
H(36)	39(3)	41(3)	46(3)	-8(2)	12(2)	-14(2)
H(37)	62(3)	36(3)	45(3)	-4(2)	-9(2)	20(3)
H(38)	54(3)	40(3)	44(3)	3(2)	-14(2)	-10(2)
H(39)	51(3)	46(3)	53(3)	6(2)	-15(3)	-10(2)
H(40)	54(3)	30(2)	45(3)	-10(2)	18(2)	0(2)
H(41)	68(4)	43(3)	48(3)	-6(2)	32(3)	-15(3)
H(42)	58(4)	106(6)	49(3)	41(4)	-14(3)	-40(4)
H(43)	122(7)	51(4)	79(5)	30(3)	64(5)	34(4)
H(44)	57(4)	40(3)	67(4)	-7(2)	-24(3)	8(2)
H(45)	51(3)	43(3)	52(3)	-3(2)	8(2)	18(2)
H(46)	31(3)	58(3)	65(3)	-18(3)	14(3)	-9(2)

H(47)	72(5)	115(7)	70(4)	51(5)	-14(4)	-53(5)
H(48)	91(5)	55(4)	52(3)	1(3)	-21(4)	28(4)
HY1	20(4)	47(4)	35(4)	5(3)	8(3)	6(3)
HY2	31(6)	35(4)	48(5)	-9(4)	-5(5)	9(5)
HY11	31(6)	58(8)	133(13)	0(8)	39(7)	-4(6)
HY12	55(8)	58(8)	103(9)	-19(7)	52(6)	-4(7)
HYA	52(12)	44(9)	93(14)	17(9)	-21(11)	-5(8)
HYB	94(15)	62(11)	34(7)	-13(7)	-2(9)	58(11)

Table B.5 Hydrogen coordinates (x 10^4) and isotropic displacement parameters (A^2 x 10^3) for ir.

	x	y	z	U(eq)
H(1)	5850(4)	7195(6)	525(3)	50(1)
H(2)	7306(3)	8112(5)	-2013(3)	31(1)
H(3)	6060(4)	10674(6)	-721(3)	50(1)
H(4)	8622(3)	5071(5)	1934(3)	34(1)
H(5)	7901(3)	1615(5)	2069(3)	33(1)
H(6)	6408(3)	4846(5)	-1858(3)	38(1)
H(7)	8822(5)	3098(7)	-640(4)	62(2)
H(8)	5329(5)	7627(7)	-2213(5)	68(2)
H(9)	8069(3)	9270(6)	-778(3)	45(1)
H(10)	8975(4)	2673(7)	2720(3)	51(1)
H(12)	8517(3)	6563(6)	-2384(3)	40(1)
H(19)	7036(4)	410(6)	973(4)	49(1)
H(18)	7593(3)	4079(6)	2638(3)	47(1)

H(20)	6357(4)	963(6)	1695(3)	47(1)
H(21)	10039(3)	5695(6)	1592(3)	41(1)
H(22)	9351(4)	5654(7)	694(3)	50(1)
H(23)	10071(3)	4173(6)	920(3)	46(1)
H(24)	8622(5)	86(7)	1400(4)	62(2)
H(25)	4880(4)	5954(10)	-1058(5)	76(2)
H(26)	9813(4)	3937(6)	2766(3)	44(1)
H(27)	6949(3)	8746(5)	-56(3)	35(1)
H(28)	5566(4)	9071(5)	444(3)	43(1)
H(29)	7960(3)	1268(5)	88(3)	34(1)
H(30)	9095(4)	-475(5)	533(3)	42(1)
H(31)	7575(3)	5540(6)	-2426(3)	43(1)
H(32)	4908(4)	4428(7)	-1683(3)	49(1)
H(33)	9728(4)	2578(7)	-13(4)	61(2)
H(34)	5340(4)	6040(7)	-2831(3)	50(1)
H(35)	8346(4)	5309(6)	-1588(3)	43(1)
H(36)	8785(3)	8680(6)	-1460(3)	42(1)
H(37)	9825(4)	2396(6)	2122(3)	49(1)
H(38)	8644(4)	7624(6)	-572(3)	47(1)
H(39)	6403(4)	2019(7)	801(4)	51(1)
H(40)	9218(4)	1273(5)	-671(3)	42(1)
H(41)	6746(4)	2865(6)	2712(3)	51(1)
H(42)	6241(4)	7176(10)	-2714(4)	72(2)
H(43)	6620(6)	9878(8)	-1465(5)	81(3)
H(44)	9616(4)	839(6)	1173(4)	56(2)
H(45)	6691(4)	4276(6)	1948(3)	48(1)
H(46)	5098(3)	7787(7)	-251(4)	51(1)
H(47)	5494(5)	4435(11)	-724(5)	87(3)
H(48)	5542(5)	9421(8)	-1410(4)	68(2)
HY1	8283(4)	5332(9)	-212(4)	34(2)
HY2	7250(9)	3754(10)	-554(7)	38(2)

HY11	6433(8)	4227(19)	359(12)	72(4)
HY12	6369(9)	4958(18)	522(10)	69(4)
HYA	6825(15)	3837(19)	-210(15)	64(5)
HYB	7764(17)	4150(20)	-620(9)	64(5)

Table B.6 Torsion angles [deg] for ir.

C(3)-P(2)-C(1)-C(12)	-62.9(2)
C(6)-P(2)-C(1)-C(12)	46.0(2)
Ir(1)-P(2)-C(1)-C(12)	170.09(16)
C(3)-P(2)-C(1)-C(9)	67.4(2)
C(6)-P(2)-C(1)-C(9)	176.32(16)
Ir(1)-P(2)-C(1)-C(9)	-59.6(2)
C(4)-P(1)-C(2)-C(7)	59.2(2)
C(5)-P(1)-C(2)-C(7)	174.87(16)
Ir(1)-P(1)-C(2)-C(7)	-63.13(19)
C(4)-P(1)-C(2)-C(11)	-176.53(15)
C(5)-P(1)-C(2)-C(11)	-60.83(19)
Ir(1)-P(1)-C(2)-C(11)	61.17(19)
C(6)-P(2)-C(3)-C(13)	179.02(17)
C(1)-P(2)-C(3)-C(13)	-71.8(2)
Ir(1)-P(2)-C(3)-C(13)	55.0(2)
C(6)-P(2)-C(3)-C(19)	-52.2(2)
C(1)-P(2)-C(3)-C(19)	57.0(2)
Ir(1)-P(2)-C(3)-C(19)	-176.16(16)
C(2)-P(1)-C(4)-C(10)	178.23(16)
C(5)-P(1)-C(4)-C(10)	68.7(2)
Ir(1)-P(1)-C(4)-C(10)	-59.8(2)
C(2)-P(1)-C(4)-C(15)	47.4(2)

C(5)-P(1)-C(4)-C(15)	-62.2(2)
Ir(1)-P(1)-C(4)-C(15)	169.30(18)
C(4)-P(1)-C(5)-C(14)	-69.1(2)
C(2)-P(1)-C(5)-C(14)	-179.24(18)
Ir(1)-P(1)-C(5)-C(14)	59.3(2)
C(4)-P(1)-C(5)-C(8)	59.5(2)
C(2)-P(1)-C(5)-C(8)	-50.6(2)
Ir(1)-P(1)-C(5)-C(8)	-172.11(17)
C(3)-P(2)-C(6)-C(16)	176.62(17)
C(1)-P(2)-C(6)-C(16)	61.2(2)
Ir(1)-P(2)-C(6)-C(16)	-61.1(2)
C(3)-P(2)-C(6)-C(18)	-58.1(2)
C(1)-P(2)-C(6)-C(18)	-173.49(16)
Ir(1)-P(2)-C(6)-C(18)	64.3(2)

APPENDIX C. Supplemental Data, Neutron Data Set for $IrClH_x(iPr_3P)_2$ @ 5(2) K

Table C.1 Crystal data and structure refinement for ir 5K.

Identification code	shelx
Empirical formula	C18 H45 Cl Ir P2
Formula weight	551.18
Temperature	5(2) K
Wavelength	1.45549 A
Crystal system, space group	Monoclinic, P 21/c
Unit cell dimensions	a = 15.7744(8) A alpha = 90 deg. b = 8.9542(4) A beta = 94.980(3) deg. c = 16.2934(7) A gamma = 90 deg.
Volume	2292.71(18) A^3
Z, Calculated density	4, 1.597 Mg/m^3
Absorption coefficient	0.447 mm^-1
F(000)	-73
Crystal size	? x ? x ? mm
Theta range for data collection	5.145 to 60.823 deg.

Limiting indices	-9<=h<=17, -9<=k<=10, -19<=l<=19
Reflections collected / unique	10469 / 3628 [R(int) = 0.0623]
Completeness to theta = 60.844	87.3 %
Refinement method	Full-matrix least-squares on F^2
Data / restraints / parameters	3628 / 0 / 629
Goodness-of-fit on F^2	1.073
Final R indices [I>2sigma(I)]	R1 = 0.0583, wR2 = 0.1429
R indices (all data)	R1 = 0.0717, wR2 = 0.1492
Extinction coefficient	n/a
Largest diff. peak and hole	0.733 and -0.972 e.A^-3

Table C.2 Atomic coordinates (x 10^4) and equivalent isotropic displacement parameters (A^2 x 10^3) for ir.

U(eq) is defined as one third of the trace of the orthogonalized Uij tensor.

	x	y	z	U(eq)

Ir(1)	7404(1)	5030(1)	116(1)	16(1)
Cl(1)	7635(1)	7013(2)	1140(1)	25(1)
P(1)	6836(2)	6669(3)	-892(2)	13(1)
P(2)	8130(2)	3309(3)	972(1)	14(1)
C(1)	8985(1)	4183(2)	1663(1)	17(1)
C(2)	7639(1)	7378(2)	-1551(1)	14(1)
C(3)	8548(1)	1723(2)	394(1)	15(1)
C(4)	6397(1)	8390(2)	-460(1)	16(1)
C(5)	6041(1)	5776(2)	-1649(1)	18(1)
C(6)	7478(1)	2353(2)	1705(1)	17(1)
C(7)	8323(2)	8298(2)	-1055(1)	20(1)
C(8)	5732(2)	6717(3)	-2396(2)	29(1)
C(9)	9646(2)	4970(3)	1183(1)	21(1)
C(10)	5691(2)	8086(3)	99(1)	21(1)
C(11)	8039(2)	6113(2)	-2009(1)	17(1)
C(12)	9418(2)	3225(3)	2353(1)	21(1)
C(13)	9108(2)	2203(3)	-274(1)	24(1)
C(14)	5288(2)	5122(3)	-1249(2)	29(1)
C(15)	6145(2)	9658(3)	-1060(2)	31(1)
C(16)	7106(2)	3462(3)	2286(1)	24(1)
C(18)	6776(2)	1387(3)	1260(1)	21(1)

C(19)	8990(2)	479(2)	916(1)	24(1)

Table C.3 Bond lengths [A] and angles [deg] for ir.

Ir(1)-P(2)	2.314(3)
Ir(1)-P(1)	2.323(3)
Ir(1)-Cl(1)	2.4426(18)
Ir(1)-HY1	1.552(7)
Ir(1)-HY2	1.586(9)
Ir(1)-HY11	1.780(14)
Ir(1)-HY12	1.811(15)
Ir(1)-HYA	1.472(15)
Ir(1)-HYB	1.594(15)
Ir(1)-HY21	1.85(2)
Ir(1)-HY22	1.84(2)
P(1)-C(2)	1.843(3)
P(1)-C(4)	1.854(3)
P(1)-C(5)	1.861(3)
P(2)-C(1)	1.853(3)
P(2)-C(6)	1.852(3)
P(2)-C(3)	1.858(3)
C(1)-C(12)	1.527(3)
C(1)-C(9)	1.529(3)
C(1)-H(4)	1.101(5)
C(2)-C(11)	1.524(3)
C(2)-C(7)	1.531(3)
C(2)-H(2)	1.107(5)
C(3)-C(13)	1.521(3)

C(3)-C(19)	1.532(3)
C(3)-H(29)	1.090(6)
C(4)-C(10)	1.523(3)
C(4)-C(15)	1.528(3)
C(4)-H(27)	1.097(6)
C(5)-C(14)	1.522(3)
C(5)-C(8)	1.525(3)
C(5)-H(6)	1.091(5)
C(6)-C(16)	1.524(3)
C(6)-C(18)	1.536(3)
C(6)-H(5)	1.093(5)
C(7)-H(9)	1.089(5)
C(7)-H(36)	1.084(5)
C(7)-H(38)	1.085(6)
C(8)-H(8)	1.090(9)
C(8)-H(34)	1.080(6)
C(8)-H(42)	1.085(7)
C(9)-H(21)	1.083(6)
C(9)-H(22)	1.077(6)
C(9)-H(23)	1.098(6)
C(10)-H(1)	1.079(6)
C(10)-H(28)	1.082(5)
C(10)-H(46)	1.089(7)
C(11)-H(12)	1.079(5)
C(11)-H(31)	1.093(6)
C(11)-H(35)	1.092(5)
C(12)-H(10)	1.084(5)
C(12)-H(26)	1.088(6)
C(12)-H(37)	1.075(7)
C(13)-H(7)	1.084(7)
C(13)-H(33)	1.105(8)

C(13)-H(40)	1.077(5)
C(14)-H(25)	1.065(9)
C(14)-H(32)	1.091(6)
C(14)-H(47)	1.077(7)
C(15)-H(3)	1.080(6)
C(15)-H(43)	1.063(6)
C(15)-H(48)	1.094(9)
C(16)-H(18)	1.090(6)
C(16)-H(41)	1.075(5)
C(16)-H(45)	1.091(7)
C(18)-H(19)	1.090(6)
C(18)-H(20)	1.070(6)
C(18)-H(39)	1.091(6)
C(19)-H(24)	1.077(6)
C(19)-H(30)	1.084(5)
C(19)-H(44)	1.086(8)

HY2 - HY11	2.0512 (0.0212)
HY11 - HY12	0.8727 (0.0250)
HY12 - HY1	3.3507 (0.0155)
HY21 - HY22	0.8812 (0.0386)

P(2)-Ir(1)-P(1)	170.79(10)
P(2)-Ir(1)-Cl(1)	92.02(8)
P(1)-Ir(1)-Cl(1)	92.84(8)
P(2)-Ir(1)-HY1	85.2(3)
P(1)-Ir(1)-HY1	86.8(3)
Cl(1)-Ir(1)-HY1	92.0(3)
P(2)-Ir(1)-HY2	88.4(4)
P(1)-Ir(1)-HY2	86.6(4)
Cl(1)-Ir(1)-HY2	178.6(5)

HY1-Ir(1)-HY2	86.7(6)
P(2)-Ir(1)-HY11	93.3(6)
P(1)-Ir(1)-HY11	92.9(6)
Cl(1)-Ir(1)-HY11	106.5(6)
HY1-Ir(1)-HY11	161.5(6)
HY2-Ir(1)-HY11	74.8(8)
P(2)-Ir(1)-HY12	96.2(7)
P(1)-Ir(1)-HY12	92.4(7)
Cl(1)-Ir(1)-HY12	78.4(5)
HY1-Ir(1)-HY12	170.4(6)
HY2-Ir(1)-HY12	102.9(8)
HY11-Ir(1)-HY12	28.1(8)
P(2)-Ir(1)-HYA	89.2(6)
P(1)-Ir(1)-HYA	90.7(6)
Cl(1)-Ir(1)-HYA	148.7(10)
HY1-Ir(1)-HYA	119.2(10)
HY2-Ir(1)-HYA	32.6(8)
HY11-Ir(1)-HYA	42.3(11)
HY12-Ir(1)-HYA	70.4(12)
P(2)-Ir(1)-HYB	86.5(6)
P(1)-Ir(1)-HYB	85.1(6)
Cl(1)-Ir(1)-HYB	145.7(10)
HY1-Ir(1)-HYB	53.7(11)
HY2-Ir(1)-HYB	32.9(8)
HY11-Ir(1)-HYB	107.8(12)
HY12-Ir(1)-HYB	135.8(12)
HYA-Ir(1)-HYB	65.5(12)
P(2)-Ir(1)-HY21	108.4(8)
P(1)-Ir(1)-HY21	79.6(8)
Cl(1)-Ir(1)-HY21	88.4(8)
HY1-Ir(1)-HY21	166.3(8)

HY2-Ir(1)-HY21	92.8(10)
HY11-Ir(1)-HY21	23.0(7)
HY12-Ir(1)-HY21	15.8(7)
HYA-Ir(1)-HY21	61.7(12)
HYB-Ir(1)-HY21	124.5(13)
P(2)-Ir(1)-HY22	80.8(8)
P(1)-Ir(1)-HY22	106.9(8)
Cl(1)-Ir(1)-HY22	91.5(9)
HY1-Ir(1)-HY22	165.7(9)
HY2-Ir(1)-HY22	89.9(10)
HY11-Ir(1)-HY22	19.8(7)
HY12-Ir(1)-HY22	19.9(7)
HYA-Ir(1)-HY22	57.8(13)
HYB-Ir(1)-HY22	121.8(14)
HY21-Ir(1)-HY22	27.7(12)
C(2)-P(1)-C(4)	103.48(15)
C(2)-P(1)-C(5)	102.66(14)
C(4)-P(1)-C(5)	110.88(16)
C(2)-P(1)-Ir(1)	112.80(14)
C(4)-P(1)-Ir(1)	112.98(13)
C(5)-P(1)-Ir(1)	113.17(13)
C(1)-P(2)-C(6)	102.67(14)
C(1)-P(2)-C(3)	111.01(17)
C(6)-P(2)-C(3)	102.43(15)
C(1)-P(2)-Ir(1)	112.40(13)
C(6)-P(2)-Ir(1)	115.05(15)
C(3)-P(2)-Ir(1)	112.48(13)
C(12)-C(1)-C(9)	110.74(18)
C(12)-C(1)-P(2)	117.76(17)
C(9)-C(1)-P(2)	112.13(15)
C(12)-C(1)-H(4)	108.7(3)

C(9)-C(1)-H(4)	105.9(3)
P(2)-C(1)-H(4)	100.4(3)
C(11)-C(2)-C(7)	110.78(18)
C(11)-C(2)-P(1)	111.35(16)
C(7)-C(2)-P(1)	111.47(15)
C(11)-C(2)-H(2)	107.7(3)
C(7)-C(2)-H(2)	108.5(3)
P(1)-C(2)-H(2)	106.9(3)
C(13)-C(3)-C(19)	109.79(19)
C(13)-C(3)-P(2)	113.62(17)
C(19)-C(3)-P(2)	116.02(16)
C(13)-C(3)-H(29)	107.2(3)
C(19)-C(3)-H(29)	108.7(3)
P(2)-C(3)-H(29)	100.6(3)
C(10)-C(4)-C(15)	110.62(19)
C(10)-C(4)-P(1)	113.27(16)
C(15)-C(4)-P(1)	117.35(16)
C(10)-C(4)-H(27)	106.4(3)
C(15)-C(4)-H(27)	108.6(3)
P(1)-C(4)-H(27)	99.3(3)
C(14)-C(5)-C(8)	110.3(2)
C(14)-C(5)-P(1)	112.83(16)
C(8)-C(5)-P(1)	116.24(18)
C(14)-C(5)-H(6)	106.8(3)
C(8)-C(5)-H(6)	108.6(3)
P(1)-C(5)-H(6)	101.2(3)
C(16)-C(6)-C(18)	111.07(19)
C(16)-C(6)-P(2)	111.37(16)
C(18)-C(6)-P(2)	111.98(16)
C(16)-C(6)-H(5)	107.8(3)
C(18)-C(6)-H(5)	108.0(3)

P(2)-C(6)-H(5)	106.3(3)
C(2)-C(7)-H(9)	112.6(3)
C(2)-C(7)-H(36)	109.4(3)
H(9)-C(7)-H(36)	107.2(4)
C(2)-C(7)-H(38)	110.8(3)
H(9)-C(7)-H(38)	108.1(5)
H(36)-C(7)-H(38)	108.6(5)
C(5)-C(8)-H(8)	111.1(4)
C(5)-C(8)-H(34)	110.0(3)
H(8)-C(8)-H(34)	107.2(5)
C(5)-C(8)-H(42)	113.1(4)
H(8)-C(8)-H(42)	108.0(7)
H(34)-C(8)-H(42)	107.1(5)
C(1)-C(9)-H(21)	110.4(3)
C(1)-C(9)-H(22)	112.4(4)
H(21)-C(9)-H(22)	108.0(5)
C(1)-C(9)-H(23)	111.9(3)
H(21)-C(9)-H(23)	106.3(5)
H(22)-C(9)-H(23)	107.6(5)
C(4)-C(10)-H(1)	112.4(3)
C(4)-C(10)-H(28)	109.8(3)
H(1)-C(10)-H(28)	107.1(5)
C(4)-C(10)-H(46)	111.7(3)
H(1)-C(10)-H(46)	108.5(5)
H(28)-C(10)-H(46)	107.1(4)
C(2)-C(11)-H(12)	109.5(3)
C(2)-C(11)-H(31)	111.8(3)
H(12)-C(11)-H(31)	106.0(4)
C(2)-C(11)-H(35)	111.0(3)
H(12)-C(11)-H(35)	109.2(4)
H(31)-C(11)-H(35)	109.2(5)

C(1)-C(12)-H(10)	114.0(4)
C(1)-C(12)-H(26)	109.2(3)
H(10)-C(12)-H(26)	106.4(4)
C(1)-C(12)-H(37)	111.8(3)
H(10)-C(12)-H(37)	108.0(5)
H(26)-C(12)-H(37)	107.0(5)
C(3)-C(13)-H(7)	111.6(4)
C(3)-C(13)-H(33)	111.5(4)
H(7)-C(13)-H(33)	108.7(6)
C(3)-C(13)-H(40)	109.9(3)
H(7)-C(13)-H(40)	108.2(5)
H(33)-C(13)-H(40)	106.7(5)
C(5)-C(14)-H(25)	111.5(5)
C(5)-C(14)-H(32)	110.8(3)
H(25)-C(14)-H(32)	105.3(5)
C(5)-C(14)-H(47)	112.3(4)
H(25)-C(14)-H(47)	108.5(7)
H(32)-C(14)-H(47)	108.2(6)
C(4)-C(15)-H(3)	109.9(3)
C(4)-C(15)-H(43)	113.0(4)
H(3)-C(15)-H(43)	108.0(5)
C(4)-C(15)-H(48)	110.8(4)
H(3)-C(15)-H(48)	106.8(5)
H(43)-C(15)-H(48)	108.0(6)
C(6)-C(16)-H(18)	111.9(3)
C(6)-C(16)-H(41)	109.7(3)
H(18)-C(16)-H(41)	107.2(5)
C(6)-C(16)-H(45)	111.7(3)
H(18)-C(16)-H(45)	106.9(5)
H(41)-C(16)-H(45)	109.3(5)
C(6)-C(18)-H(19)	112.0(4)

C(6)-C(18)-H(20)	110.0(3)
H(19)-C(18)-H(20)	106.5(5)
C(6)-C(18)-H(39)	111.3(3)
H(19)-C(18)-H(39)	109.0(5)
H(20)-C(18)-H(39)	107.9(5)
C(3)-C(19)-H(24)	113.3(4)
C(3)-C(19)-H(30)	109.8(3)
H(24)-C(19)-H(30)	106.9(5)
C(3)-C(19)-H(44)	110.5(4)
H(24)-C(19)-H(44)	109.8(6)
H(30)-C(19)-H(44)	106.1(5)

Table C.4 Anisotropic displacement parameters (A^2 x 10^3) for ir.

The anisotropic displacement factor exponent takes the form:

-2 pi^2 [h^2 a*^2 U11 + ... + 2 h k a* b* U12]

	U11	U22	U33	U23	U13	U12
Ir(1)	17(1)	13(1)	16(1)	1(1)	0(1)	2(1)
Cl(1)	33(1)	16(1)	24(1)	-5(1)	-9(1)	7(1)
P(1)	8(1)	13(1)	18(1)	1(1)	0(1)	0(1)
P(2)	14(2)	13(1)	15(1)	0(1)	3(1)	1(1)
C(1)	17(1)	15(1)	17(1)	0(1)	-1(1)	1(1)
C(2)	14(1)	13(1)	15(1)	-1(1)	-1(1)	0(1)
C(3)	17(1)	12(1)	15(1)	1(1)	2(1)	1(1)
C(4)	19(1)	12(1)	17(1)	2(1)	4(1)	2(1)
C(5)	18(1)	16(1)	19(1)	0(1)	-1(1)	-3(1)

C(6)	18(1)	15(1)	19(1)	-2(1)	4(1)	-2(1)
C(7)	20(1)	19(1)	19(1)	-3(1)	1(1)	-6(1)
C(8)	27(2)	29(1)	30(1)	11(1)	-10(1)	-8(1)
C(9)	17(1)	24(1)	21(1)	1(1)	1(1)	-5(1)
C(10)	18(2)	21(1)	26(1)	0(1)	7(1)	0(1)
C(11)	19(1)	15(1)	18(1)	-2(1)	-1(1)	2(1)
C(12)	21(1)	20(1)	20(1)	5(1)	-3(1)	-3(1)
C(13)	24(2)	18(1)	31(1)	0(1)	15(1)	-3(1)
C(14)	24(2)	40(1)	24(1)	-4(1)	3(1)	-16(1)
C(15)	49(2)	20(1)	24(1)	8(1)	13(1)	18(1)
C(16)	24(1)	22(1)	25(1)	-7(1)	9(1)	-3(1)
C(18)	19(1)	21(1)	23(1)	-4(1)	2(1)	-5(1)
C(19)	32(2)	18(1)	20(1)	3(1)	2(1)	10(1)
H(1)	57(4)	44(3)	44(3)	19(2)	18(2)	6(3)
H(2)	31(3)	24(2)	25(2)	3(2)	-2(2)	5(2)
H(3)	71(4)	30(3)	47(3)	4(2)	15(3)	16(3)
H(4)	31(3)	27(2)	34(2)	-7(2)	5(2)	3(2)
H(5)	37(3)	23(2)	29(2)	4(2)	-1(2)	1(2)
H(6)	35(3)	34(3)	40(2)	-11(2)	4(2)	-1(2)
H(7)	92(5)	35(3)	55(3)	17(3)	38(3)	22(3)
H(8)	76(5)	38(3)	77(4)	2(3)	-31(4)	12(3)
H(9)	36(3)	40(3)	54(3)	-21(2)	9(2)	-5(2)
H(10)	47(3)	54(3)	41(3)	24(2)	4(2)	-12(3)
H(12)	36(3)	37(3)	37(2)	-3(2)	15(2)	1(2)
H(19)	49(3)	43(3)	52(3)	-25(2)	12(2)	-8(3)
H(18)	38(3)	48(3)	47(3)	-21(2)	10(2)	-14(3)
H(20)	46(3)	43(3)	47(3)	-7(2)	14(3)	-16(3)
H(21)	37(3)	37(2)	40(2)	-4(2)	0(2)	-16(2)
H(22)	53(3)	47(3)	38(3)	20(2)	-3(2)	-13(3)
H(23)	32(3)	45(3)	59(3)	-14(2)	20(2)	-1(2)
H(24)	78(4)	57(3)	48(3)	26(3)	35(3)	30(3)

H(25)	38(4)	87(5)	91(5)	-48(4)	21(3)	-18(4)
H(26)	46(3)	34(2)	36(2)	-4(2)	-7(2)	-7(2)
H(27)	21(3)	29(2)	39(2)	-4(2)	3(2)	1(2)
H(28)	43(3)	38(3)	43(3)	-13(2)	15(2)	-2(2)
H(29)	27(3)	27(2)	32(2)	-5(2)	0(2)	-1(2)
H(30)	55(3)	27(2)	38(2)	-8(2)	-1(2)	10(2)
H(31)	35(3)	41(3)	41(2)	-19(2)	0(2)	-3(2)
H(32)	43(3)	51(3)	52(3)	-14(3)	7(3)	-29(3)
H(33)	42(4)	64(4)	72(4)	-30(3)	26(3)	-26(3)
H(34)	49(3)	49(3)	36(3)	3(2)	-13(2)	-10(3)
H(35)	50(3)	41(3)	34(2)	7(2)	5(2)	19(2)
H(36)	32(3)	50(3)	42(3)	-6(2)	14(2)	-12(2)
H(37)	48(3)	35(3)	45(3)	0(2)	-9(2)	12(3)
H(38)	49(3)	42(3)	36(3)	4(2)	-19(2)	-4(2)
H(39)	42(3)	53(3)	45(3)	9(3)	-16(2)	-14(3)
H(40)	46(3)	31(2)	43(2)	-8(2)	19(2)	1(2)
H(41)	61(4)	45(3)	46(3)	-8(2)	31(3)	-12(3)
H(42)	53(4)	99(5)	50(3)	44(3)	-17(3)	-34(4)
H(43)	104(5)	51(3)	68(4)	34(3)	58(4)	37(4)
H(44)	48(4)	40(3)	60(3)	-8(3)	-18(3)	8(3)
H(45)	56(4)	41(3)	57(3)	-3(3)	13(3)	21(3)
H(46)	24(3)	56(3)	58(3)	-22(3)	4(2)	-9(2)
H(47)	68(5)	116(6)	56(4)	44(4)	-18(3)	-53(5)
H(48)	87(5)	55(4)	48(3)	-2(3)	-25(3)	33(4)
HY1	11(4)	36(4)	31(3)	6(3)	5(3)	-5(3)
HY2	40(7)	33(5)	28(4)	-14(3)	3(5)	8(5)
HYA	47(11)	33(8)	75(12)	-3(8)	-23(9)	6(7)
HYB	72(14)	69(12)	41(8)	-11(8)	6(9)	46(11)

Table C.5 Hydrogen coordinates (x 10^4) and isotropic

displacement parameters (A^2 x 10^3) for ir.

	x	y	z	U(eq)
H(1)	5852(4)	7201(6)	534(3)	48(1)
H(2)	7301(3)	8116(5)	-2017(2)	27(1)
H(3)	6055(4)	10676(6)	-723(3)	49(1)
H(4)	8624(3)	5076(5)	1940(3)	30(1)
H(5)	7910(3)	1615(5)	2075(3)	30(1)
H(6)	6406(3)	4837(5)	-1858(3)	36(1)
H(7)	8818(5)	3098(6)	-647(4)	59(2)
H(8)	5339(5)	7645(7)	-2220(4)	66(2)
H(9)	8064(3)	9285(6)	-777(3)	43(1)
H(10)	8978(4)	2668(6)	2728(3)	47(1)
H(12)	8507(3)	6563(5)	-2386(3)	36(1)
H(19)	7035(4)	411(6)	970(3)	48(1)
H(18)	7601(4)	4090(6)	2645(3)	44(1)
H(20)	6360(4)	974(6)	1693(3)	45(1)
H(21)	10045(3)	5689(6)	1588(3)	38(1)
H(22)	9358(4)	5643(6)	686(3)	47(1)
H(23)	10076(3)	4173(6)	918(3)	45(1)
H(24)	8624(4)	92(7)	1403(4)	59(2)
H(25)	4871(4)	5973(9)	-1069(5)	71(2)
H(26)	9818(3)	3933(5)	2768(3)	40(1)
H(27)	6954(3)	8744(5)	-57(3)	29(1)
H(28)	5574(3)	9077(6)	452(3)	40(1)
H(29)	7960(3)	1282(5)	85(3)	29(1)
H(30)	9096(4)	-479(5)	531(3)	40(1)

H(31)	7571(3)	5538(6)	-2431(3)	39(1)
H(32)	4900(4)	4428(7)	-1686(3)	48(1)
H(33)	9742(4)	2573(7)	-9(4)	58(2)
H(34)	5345(4)	6045(6)	-2833(3)	46(1)
H(35)	8345(4)	5303(6)	-1578(3)	42(1)
H(36)	8789(3)	8679(6)	-1459(3)	40(1)
H(37)	9824(4)	2392(6)	2120(3)	44(1)
H(38)	8645(4)	7630(6)	-567(3)	44(1)
H(39)	6394(4)	2029(7)	794(3)	48(1)
H(40)	9212(3)	1274(5)	-672(3)	39(1)
H(41)	6748(4)	2873(6)	2716(3)	49(1)
H(42)	6247(4)	7172(9)	-2719(4)	69(2)
H(43)	6606(5)	9866(7)	-1484(4)	71(2)
H(44)	9614(4)	841(6)	1172(4)	51(1)
H(45)	6694(4)	4276(7)	1951(4)	51(1)
H(46)	5095(4)	7800(7)	-254(4)	46(1)
H(47)	5483(5)	4451(10)	-717(4)	81(3)
H(48)	5539(5)	9413(7)	-1414(4)	65(2)
HY1	8279(4)	5321(8)	-222(4)	26(2)
HY2	7271(10)	3761(10)	-562(5)	34(2)
HY11	6393(9)	4235(19)	259(10)	36(3)
HY12	6421(10)	4970(20)	612(11)	35(4)
HYA	6862(13)	3815(16)	-240(13)	53(4)
HYB	7782(16)	4170(20)	-628(10)	61(5)
HY21	6271(14)	5000(30)	326(15)	22(5)
HY22	6507(15)	4280(30)	634(16)	30(5)

Table C.6 Torsion angles [deg] for ir.

C(6)-P(2)-C(1)-C(12)	46.1(2)
C(3)-P(2)-C(1)-C(12)	-62.7(2)
Ir(1)-P(2)-C(1)-C(12)	170.32(15)
C(6)-P(2)-C(1)-C(9)	176.36(17)
C(3)-P(2)-C(1)-C(9)	67.5(2)
Ir(1)-P(2)-C(1)-C(9)	-59.4(2)
C(4)-P(1)-C(2)-C(11)	-176.52(16)
C(5)-P(1)-C(2)-C(11)	-61.1(2)
Ir(1)-P(1)-C(2)-C(11)	61.04(19)
C(4)-P(1)-C(2)-C(7)	59.2(2)
C(5)-P(1)-C(2)-C(7)	174.64(16)
Ir(1)-P(1)-C(2)-C(7)	-63.22(19)
C(1)-P(2)-C(3)-C(13)	-71.9(2)
C(6)-P(2)-C(3)-C(13)	179.12(19)
Ir(1)-P(2)-C(3)-C(13)	55.0(2)
C(1)-P(2)-C(3)-C(19)	56.8(2)
C(6)-P(2)-C(3)-C(19)	-52.2(2)
Ir(1)-P(2)-C(3)-C(19)	-176.30(17)
C(2)-P(1)-C(4)-C(10)	178.44(17)
C(5)-P(1)-C(4)-C(10)	69.0(2)
Ir(1)-P(1)-C(4)-C(10)	-59.3(2)
C(2)-P(1)-C(4)-C(15)	47.6(3)
C(5)-P(1)-C(4)-C(15)	-61.8(2)
Ir(1)-P(1)-C(4)-C(15)	169.91(19)
C(2)-P(1)-C(5)-C(14)	-178.69(19)
C(4)-P(1)-C(5)-C(14)	-68.7(2)
Ir(1)-P(1)-C(5)-C(14)	59.4(2)
C(2)-P(1)-C(5)-C(8)	-49.9(2)
C(4)-P(1)-C(5)-C(8)	60.1(2)
Ir(1)-P(1)-C(5)-C(8)	-171.77(17)
C(1)-P(2)-C(6)-C(16)	61.5(2)

C(3)-P(2)-C(6)-C(16)	176.74(18)
Ir(1)-P(2)-C(6)-C(16)	-60.9(2)
C(1)-P(2)-C(6)-C(18)	-173.42(16)
C(3)-P(2)-C(6)-C(18)	-58.2(2)
Ir(1)-P(2)-C(6)-C(18)	64.1(2)

Least-squares planes (x,y,z in crystal coordinates) and deviations from them
(* indicates atom used to define plane)

5.8938 (0.0606) x - 5.8795 (0.0151) y + 10.1062 (0.0414) z = 1.5205 (0.0484)

* 0.0030 (0.0034) Ir1
* 0.0088 (0.0052) Cl1
* 0.0064 (0.0071) HY1
* -0.0207 (0.0129) HYB
* -0.0147 (0.0103) HY2
* 0.0381 (0.0134) HYA
* 0.0188 (0.0159) HY11
* -0.0396 (0.0165) HY12

Rms deviation of fitted atoms = 0.0228

15.7188 (0.0044) x - 0.5788 (0.0128) y - 2.2771 (0.0826) z = 11.3320 (0.0126)

Angle to previous plane (with approximate esd) = 67.683 (0.318)

* -0.0113 (0.0061) Ir1
* 0.0044 (0.0024) Cl1
* 0.0068 (0.0037) HY2

Rms deviation of fitted atoms = 0.0080

5.8225 (0.0853) x - 5.4518 (0.2473) y + 10.8756 (0.3908) z = 1.6948 (0.1450)

Angle to previous plane (with approximate esd) = 68.307 (0.422)

* 0.0000 (0.0000) Ir1
* 0.0000 (0.0000) HY11
* 0.0000 (0.0000) HY12

Rms deviation of fitted atoms = 0.0000

15.7188 (0.0044) x - 0.5788 (0.0128) y - 2.2771 (0.0826) z = 11.3320 (0.0126)

Angle to previous plane (with approximate esd) = 68.307 (0.422)

* -0.0113 (0.0061) Ir1
* 0.0044 (0.0024) Cl1
* 0.0068 (0.0037) HY2

Rms deviation of fitted atoms = 0.0080

APPENDIX D. Results for the Brief Exploration of the Reactivity of a Bulky Rh(I) Complex

D.1 Experimental

General Considerations. Any glove box manipulations were carried out under technical grade Ar (g) (Airgas USA) atmosphere. All other manipulations were carried out using standard Schlenk techniques. Where H_2 (g) was used, 100% H_2 (g) (Airgas USA). NMR Experiments conducted in Wilmad LPV NMR tubes (Aldrich). Where H_2 gas added to Wilmad LPV NMR tubes, less than 1 atm. Reagents AgOTf (99.9+ % Aldrich), AgF (99.9+ % Aldrich), $AgPh_4B$ (Aldrich), AgF_4B (98 % Aldrich), AgF_6P (98 % Acros), $AgSbF_6$ (Aldrich) and AgOTs (Aldrich) were used as received. The complex **AV1** was prepared according to literature by Professor Matthew Cain's Lab and used as received.[51] All other solvents and reagents were purified, dried and deoxygenated using conventional methods.

NMR Studies. Where deuterated solvents were used, benzene-d_6 D, 99.5% (Cambridge Isotopes). All NMR experiments were recorded on a Varian-INOVA 500 MHz NMR spectrometer except for ^{19}F experiments which were recorded on an Agilent DD2 300 MHz NMR spectrometer under ambient temperatures unless otherwise stated. ^{1}H, ^{13}C, ^{31}P, ^{19}F and ^{11}B at 500, 126, 121, 282 and 160 MHz. The ^{1}H NMR data are listed in ppm downfield from TMS at 0.00 ppm. The ^{13}C NMR data are listed in ppm relative to the solvent benzene-d_6.

Synthesis. **AV2**. A deep red solution of 1 mol of AV1 and benzene (20 mL) were reacted with 1.2 mol of AgOTf and left to stir under inert atmosphere overnight. After which an orange solution resulted. The solution was lyophilized, and NMR spectra were recorded. Single crystals for X-ray diffractometry data was attempted and could not be grown. $^{1}H\{^{13}C\}$ NMR **AV2** (500 MHz, 25 °C, C_6D_6) δ 8.01 (br, 3H, A), 7.73 (d, J = 2 Hz, 3H, B), 7.56 (br s, 3H, C), 7.34 (t, J = 5 Hz, 3H, D), 6.86 (t, J = 5 Hz, 3H, E), 6.73 (t, J = 5 Hz 3H, F), 6.31 (dd, J = 8, 14 Hz, 3H, G), 1.30 (s, 27H, H), 1.25 (s, 27H, I), 1.21 (s, 27H, J). $^{13}C\{^{1}H\}$ NMR **AV2** (126 MHz, 25 °C, C_6D_6) δ 156.40 (s, Ar), 155.43 (s, Ar), 152.81 (s, Ar), 143.42 (d, J = 10 Hz, P=C), 133.65 (s, Ar) , 133.19 (br, Ar), 132.87 (br, Ar), 129.08 (d, J = 11 Hz), 125.15 (s, Ar), 122.63 (s, Ar), 38.91 (s, CMe_3), 38.26 (s, CMe_3), 35.34 (s, CMe_3), 34.83 (s, *t*Bu), 34.54 (s, *t*Bu), 31.29 (s, *t*Bu). $^{31}P\{^{1}H\}$ NMR **AV2**

(121 MHz, 25 °C, C_6D_6) δ 227.7 (dd, *J* = 33, 174 Hz), 66.1 (dq, *J* = 33, 63 Hz). $^{19}F\{^{13}C\}$ NMR **AV2** (282 MHz, 25 °C, C_6D_6) δ -76.9 (s). See below for spectra.

AV3. A solution of AV2 was recrystallized by slow evaporation with MeCN. To which blood orange X-ray quality single crystals resulted for X-ray diffractometry results. See AVI. NMR spectra were recorded. $^{1}H\{^{13}C\}$ NMR **AV3** (500 MHz, 25 °C, C_6D_6) δ 8.38 (br, P=CH), 7.76 (d, mes*), 7.58 (m, mes*), 7.43 (br, Ar), 6.93 (m, Ar), 6.63 (m, Ar), 6.30 (dd, *J* = 15, 20 Hz, Ar), 1.45 (s, *t*Bu), 1.40 (s, *t*Bu), 1.35 (s, *t*Bu). $^{31}P\{^{1}H\}$ NMR **AV3** (202 MHz, 25 °C, C_6D_6) δ 229.4 (dd, *J* = 44, 162 Hz), 36.6 (dq, *J* = 42, 89 Hz). $^{19}F\{^{13}C\}$ NMR **AV3** (282 MHz, 25 °C, C_6D_6) δ -77.6 (s). See below for spectra.

AV4/AV5. A deep red solution of 1 mol of AV1 and benzene (20 mL) were reacted with 1.1 mol of AgF and left to stir under inert atmosphere overnight. After which a deep red colored solution remained. The solution was left to slowly evaporate from benzene layered with pentane, which resulted in solid of two colors, deep red and orange. NMR spectra were recorded. $^{1}H\{^{13}C\}$ NMR **AV4** and **AV5** (500 MHz, 25 °C, C_6D_6) δ 8.29 (br, P=CH), 7.78 (br, P=CH), 7.71 (d, mes*), 7.76 (d, mes*), 7.62 (d, mes*), 6.99 (t, *J* = 5 Hz, Ar), 6.93 (t, *J* = 5 Hz, Ar), 6.78 (t, *J* = 5 Hz, Ar), 6.69 (t, *J* = 5 Hz, Ar), 6.65 (overlapping signals, Ar), 6.48 (dd, *J* = 10, 15 Hz, Ar), 1.85 (s, *t*Bu), 1.67 (s, *t*Bu), 1.39 (s, *t*Bu), 1.38 (s, *t*Bu), 1.34 (s, *t*Bu), 1.33 (s, *t*Bu). $^{13}C\{^{1}H\}$ NMR **AV4** and **AV5** (126 MHz, 25 °C, C_6D_6) δ 156.36 (s, Ar), 152.45 (s, Ar), 149.89 (s, Ar), 144.68 (d, *J* = 13 Hz, P=C), 135.55 (s, Ar) , 130.82 (br, Ar), 130.59 (s, Ar), 128.19 (s), 127.12 (s, Ar), 126.16 (br, Ar), 123.13 (s, Ar), 122.85 (s, Ar), 40.26 (s, CMe_3), 39.35 (s, CMe_3), 38.92 (s, CMe_3), 38.74 (s, CMe_3), 35.44 (s, *t*Bu), 35.09 (s, *t*Bu), 34.63 (s, *t*Bu), 34.55 (s, *t*Bu), 33.66 (s, *t*Bu), 31.01 (s, *t*Bu). $^{31}P\{^{1}H\}$ NMR **AV4** and **AV5** (121 MHz, 25 °C, C_6D_6) δ 241.4 (ddd, *J* = 11, 27, 100 Hz), 231.9 (br, m), 42.2 (br, m), 38.2 (br, m). $^{19}F\{^{13}C\}$ NMR **AV4** and **AV5** (282 MHz, 25 °C, C_6D_6) δ -97.9 (s), (not in spectrum, AgF δ -336).[52] See below for spectra.

AV6. A deep red solution of 1 mol of AV1 and benzene (20 mL) were reacted with 1.2 mol of $AgPh_4B$ and left to stir under inert atmosphere overnight. After which a deep red colored solution remained. Visual inspection and NMR spectra confirmed the reagent had not dissolved and no reaction took place. However, a fresh reaction mixture was made in a J-Young tube using

C_6D_6 and after 4 hr of heat at 95 °C the reagent appeared to dissolve while the solution remained deep red in color. NMR spectra were recorded. $^{1}H\{^{13}C\}$ NMR **AV6** (500 MHz, 25 °C, C_6D_6) δ 8.29 (br, P=CH), 7.62 (br, Ar), 6.99 (t, *J* = 15, Ar), 6.78 (t, *J* = 10, Ar), 6.69 (t, *J* = 15, Ar), 6.57 (dd, *J* = 10, 20 Hz, Ar), 1.66 (s, *t*Bu), 1.38 (s, *t*Bu), 1.33 (s, *t*Bu). $^{31}P\{^{1}H\}$ NMR **AV6** (121 MHz, 25 °C, C_6D_6) δ 241.6 (dd, *J* = 45, 168 Hz), 38.4 (overlapping dq and 4-line pattern).

AV7. A deep red solution of 1 mol of AV1 and chloroform (20 mL) were reacted with 1.2 mol of AgF_4B. After 40 min a cranberry colored solution resulted and after 12 hr a blood orange solution resulted. A solid appeared in solution and was filtered off. The filtered solution was left to slowly evaporate from chloroform which resulted in a blood orange solid. NMR spectra were recorded. Partial spectrum $^{31}P\{^{1}H\}$ NMR **AV7** (121 MHz, 25 °C, C_6D_6) δ 227.7 (dd, *J* = 32, 91 Hz). Partial spectrum $^{19}F\{^{13}C\}$ NMR **AV7** (282 MHz, 25 °C, C_6D_6) δ -148.5 (br, counter ion), 150.4 (br, AgF_4B).[53] $^{11}B\{^{1}H\}$ NMR **AV7** (160 MHz, 25 °C, C_6D_6) δ 0.2 (s), (AgF_4B, δ -2.1).[54]

AV8. A deep red solution of 1 mol of AV1 and benzene (20 mL) were reacted with 1.2 mol of AgF_6P and left to stir under inert atmosphere overnight. After which an orange solution resulted. The solution was lyophilized, and NMR spectra were recorded. Publishable single crystals from X-ray diffractometry was not obtained. See AV(21). Of all the reactions attempted with AV1 this is the only one that resulted in the appearance of hydride shifts in ^{1}H NMR. Partial spectrum, hydride region, $^{1}H\{^{13}C\}$ NMR **AV8** (500 MHz, 25 °C, C_6D_6) δ -7.5 (m). Partial spectrum $^{31}P\{^{1}H\}$ NMR **AV8** (121 MHz, 25 °C, C_6D_6) δ 228.4 (dd, *J* = 32, 172 Hz). $^{19}F\{^{13}C\}$ NMR **AV8** (282 MHz, 25 °C, C_6D_6) δ -80.3 (br), -80.7 (s), -83.8 (br), -84.2 (s), {counter anion}; -146.3 (m), -150.0 (br), {unknown side product} (PF_5 δ -71, $^{-}PF_6$ δ -65).[55]

D.2 Results

Table D.1 Significant markers for reactivity of **AV1**.* Refer to spectrum.

Product	Reagent	^{1}H NMR (P=CH) (δ)	^{31}P NMR apical (1)P (δ), J_{small} and J_{large} (Hz)	^{31}P NMR equatorial (3)P (δ), J_{small} and J_{large} (Hz)	^{19}F NMR (δ)
AV1	x	8.16	241.1, 44, 169	39.2, 44, 99	x
AV2	AgOTf	8.01	227.7, 33, 174	66.1, 33, 63	-76.9
AV3	MeCN	8.38	229.4, 44, 162	36.6, 42, 89	-77.6
AV4/**AV5**	AgF	8.29/7.78	241.4, 231.9*	42.2, 38.2*	-97.9
AV6	$AgPh_4B$	8.29	241.6, 45, 168	38.4*	x
AV7	AgF_4B	8.68	227.7, 32, 91	x	-148.5
AV8	AgF_6P	Rh-H = -7.5	228.4, 32, 172	x	-80.3, -80.7, -83.8, -84.2, -146.3

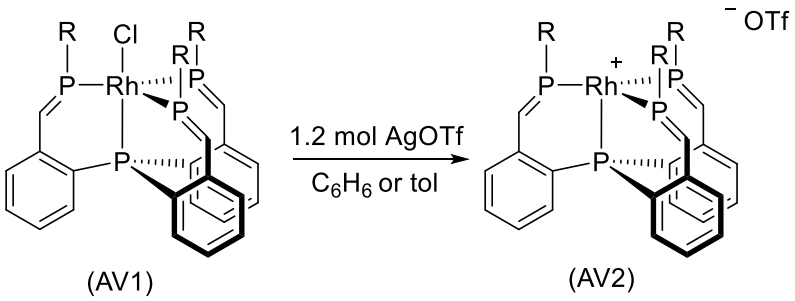

Scheme D.1 Reaction of **AV1** with AgOTf, (R = mes*).

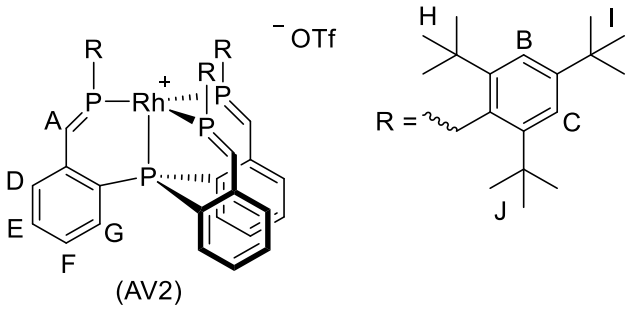

Figure D.1 AV2 labeled for ^{1}H NMR reference.

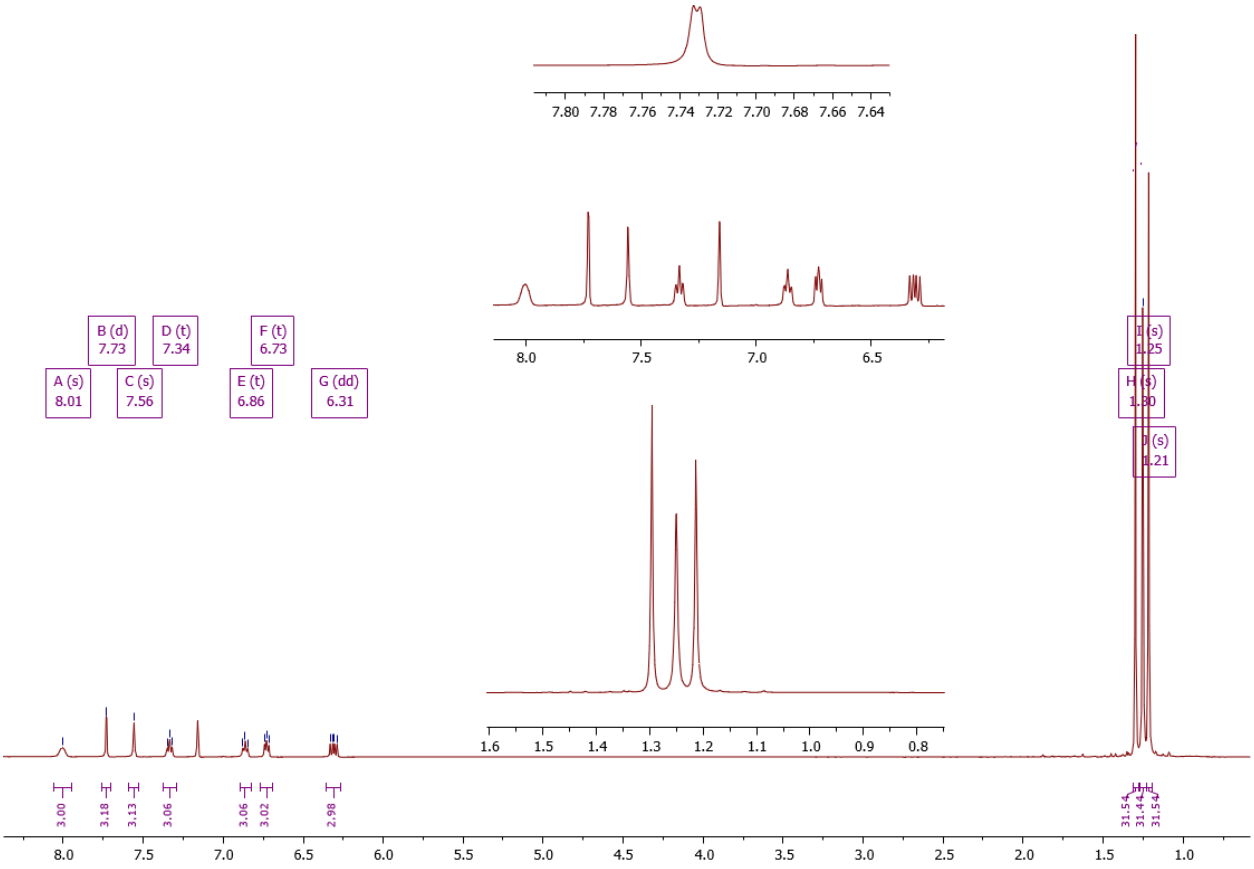

Figure D.2 ^{1}H{^{13}C} NMR **AV2** (500 MHz, 25 °C, C_6D_6) δ 8.01 (br, 3H, A), 7.73 (d, *J* = 2 Hz, 3H, B), 7.56 (br s, 3H, C), 7.34 (t, *J* = 5 Hz, 3H, D), 6.86 (t, *J* = 5 Hz, 3H, E), 6.73 (t, *J* = 5 Hz 3H, F), 6.31 (dd, *J* = 8, 14 Hz, 3H, G), 1.30 (s, 27H, H), 1.25 (s, 27H, I), 1.21 (s, 27H, J).

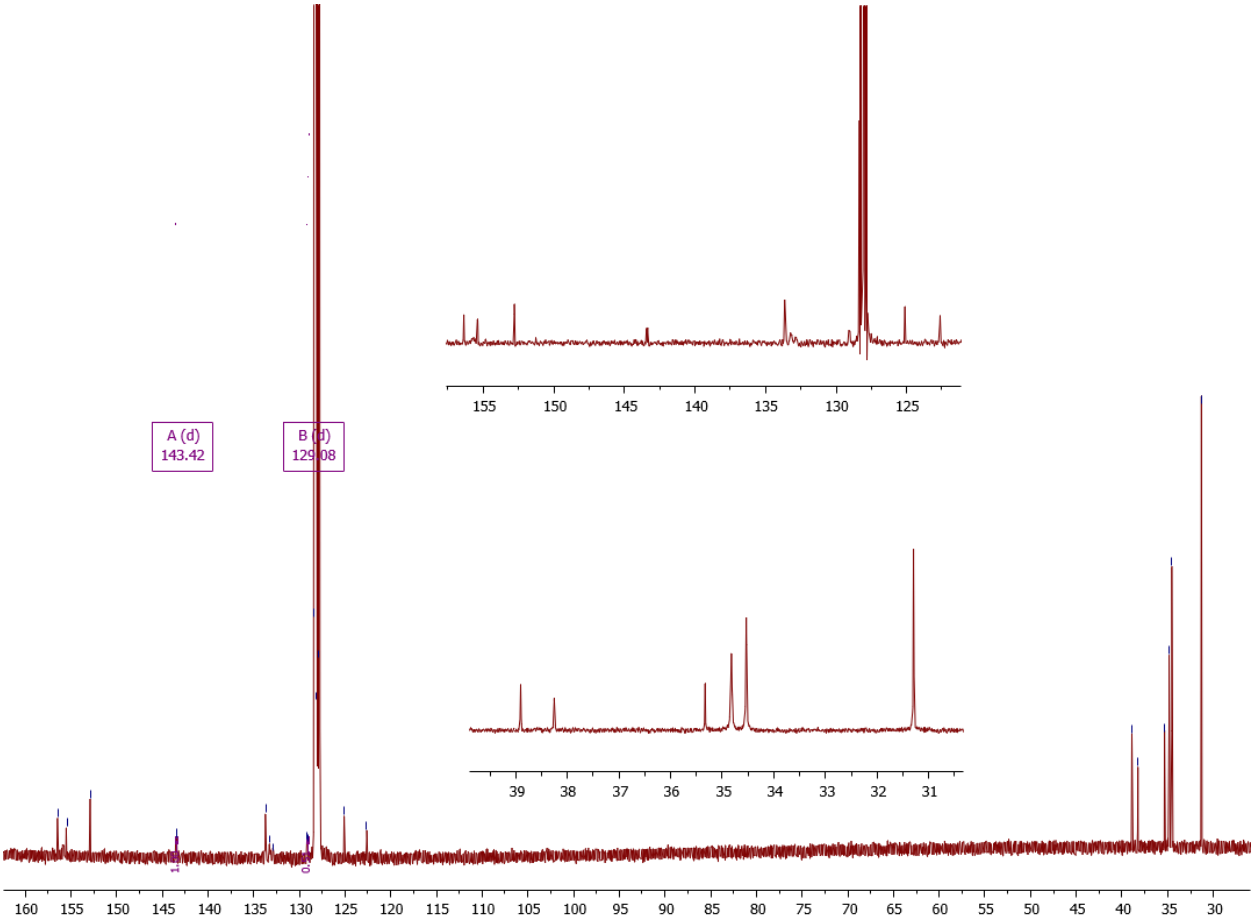

Figure D.3 $^{13}C\{^{1}H\}$ NMR **AV2** (126 MHz, 25 °C, C_6D_6) δ 156.40 (s, Ar), 155.43 (s, Ar), 152.81 (s, Ar), 143.42 (d, *J* = 10 Hz, P=C), 133.65 (s, Ar) , 133.19 (br, Ar), 132.87 (br, Ar), 129.08 (d, *J* = 11 Hz), 125.15 (s, Ar), 122.63 (s, Ar), 38.91 (s, CMe_3), 38.26 (s, CMe_3), 35.34 (s, CMe_3), 34.83 (s, *t*Bu), 34.54 (s, *t*Bu), 31.29 (s, *t*Bu).

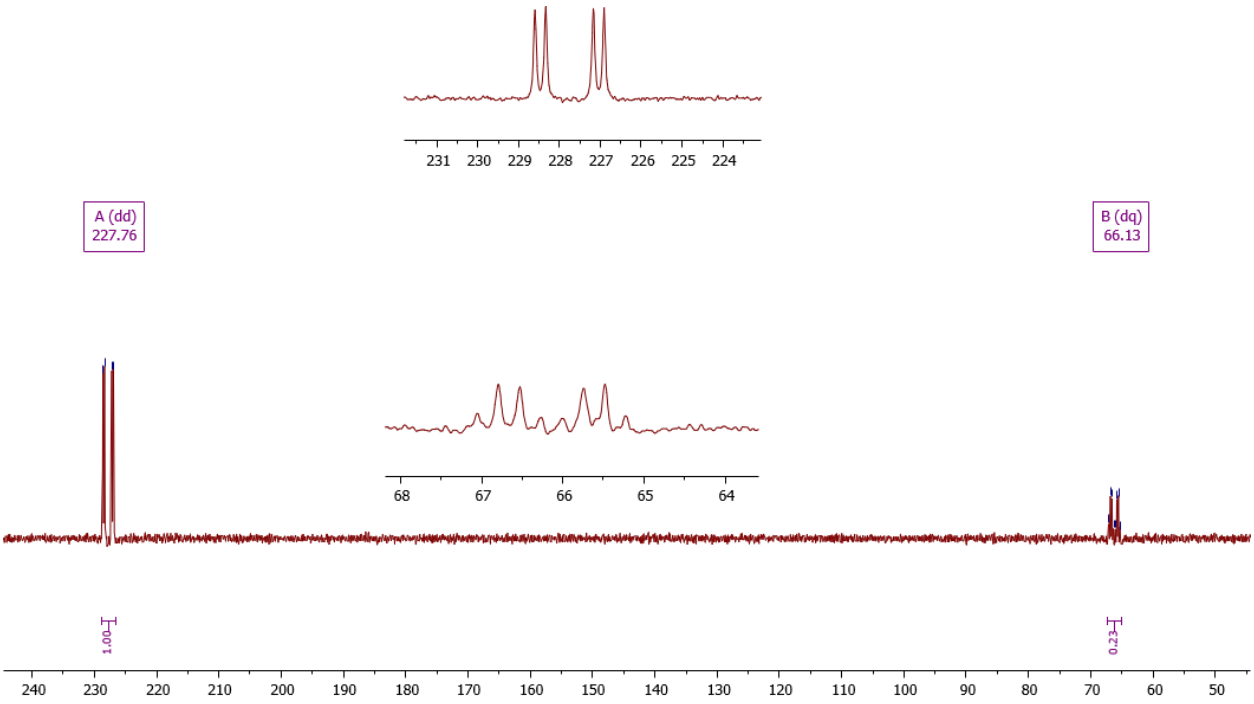

Figure D.4 $^{31}P\{^{1}H\}$ NMR **AV2** (121 MHz, 25 °C, C_6D_6) δ 227.7 (dd, *J* = 33, 174 Hz), 66.1 (dq, *J* = 33, 63 Hz).

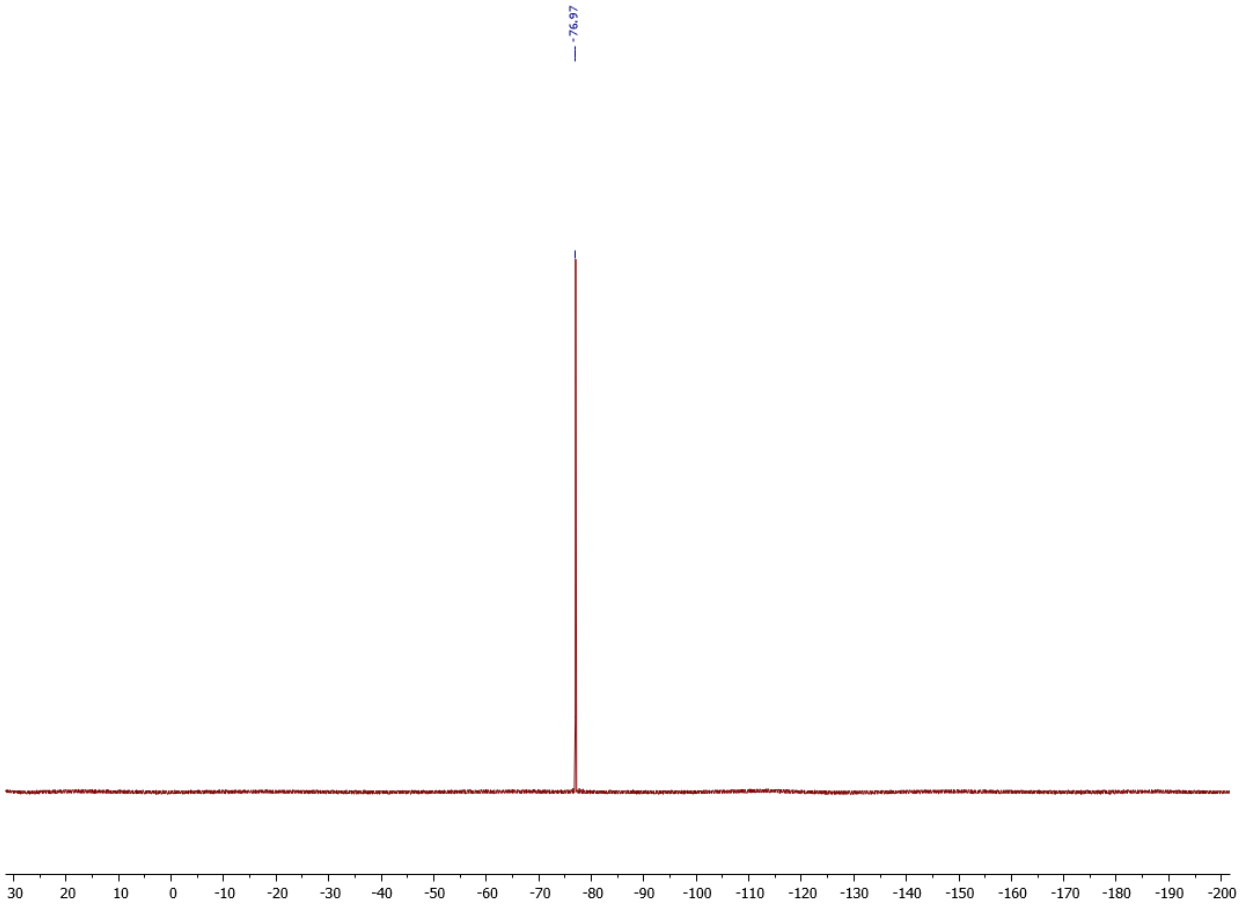

Figure D.5 $^{19}F\{^{13}C\}$ NMR **AV2** (282 MHz, 25 °C, C_6D_6) δ -76.9 (s).

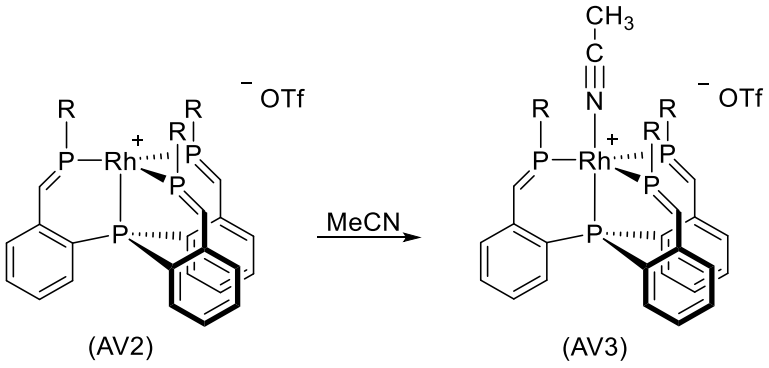

Scheme D.2 Recrystallization of **AV2** with MeCN, (R = mes*). *Single crystal XRD results for **AV3** in AVI.

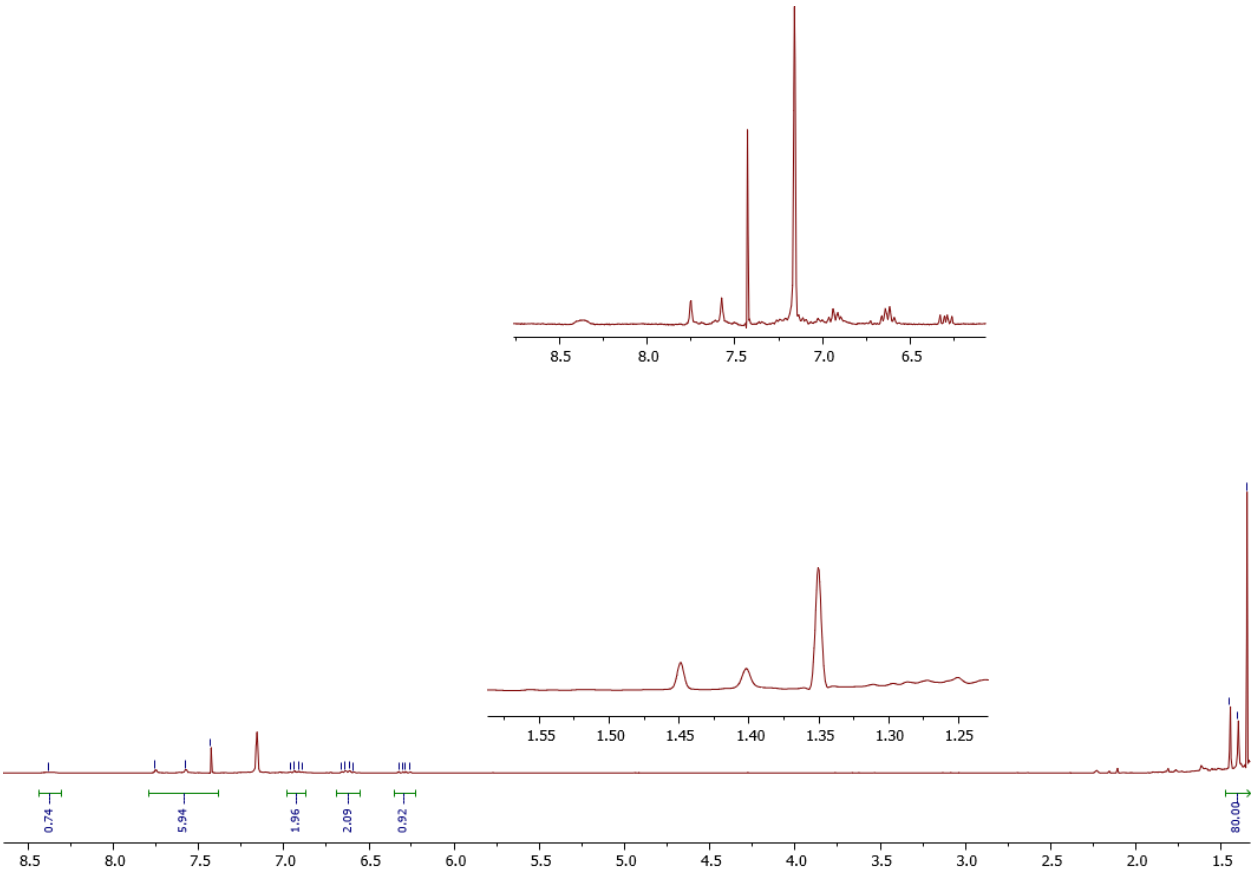

Figure D.6 $^{1}H\{^{13}C\}$ NMR **AV3** (500 MHz, 25 °C, C_6D_6) δ 8.38 (br, P=CH), 7.76 (d, mes*), 7.58 (m, mes*), 7.43 (br, Ar), 6.93 (m, Ar), 6.63 (m, Ar), 6.30 (dd, *J* = 15, 20 Hz, Ar), 1.45 (s, *t*Bu), 1.40 (s, *t*Bu), 1.35 (s, *t*Bu).

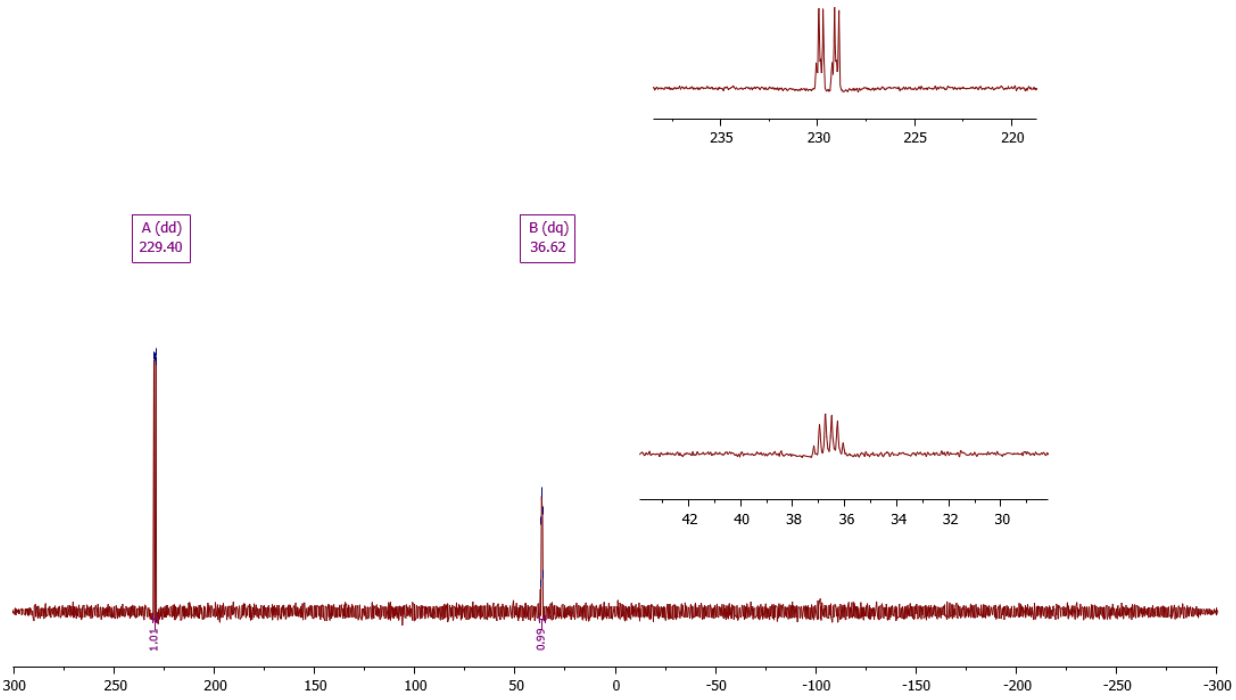

Figure D.7 $^{31}P\{^{1}H\}$ NMR **AV3** (202 MHz, 25 °C, C_6D_6) δ 229.4 (dd, *J* = 44, 162 Hz), 36.6 (dq, *J* = 42, 89 Hz).

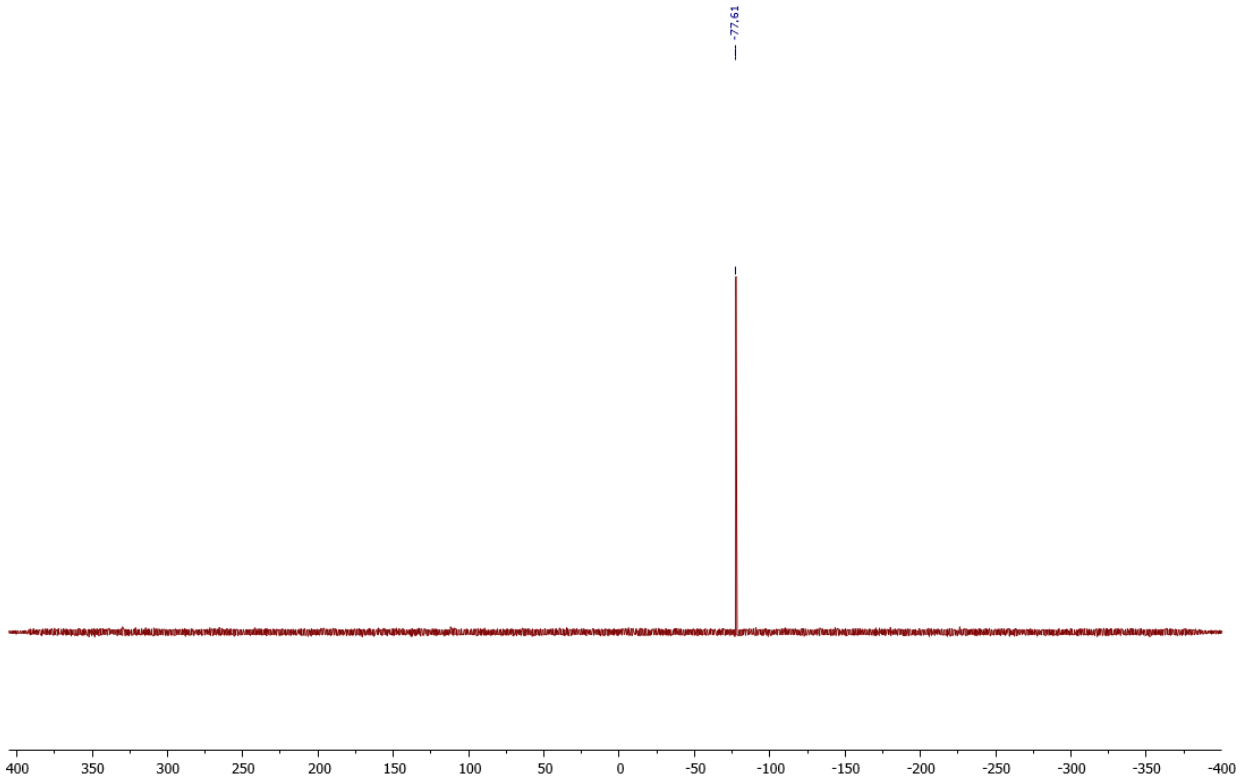

Figure D.8 $^{19}F\{^{13}C\}$ NMR **AV3** (282 MHz, 25 °C, C_6D_6) δ -77.6 (s).

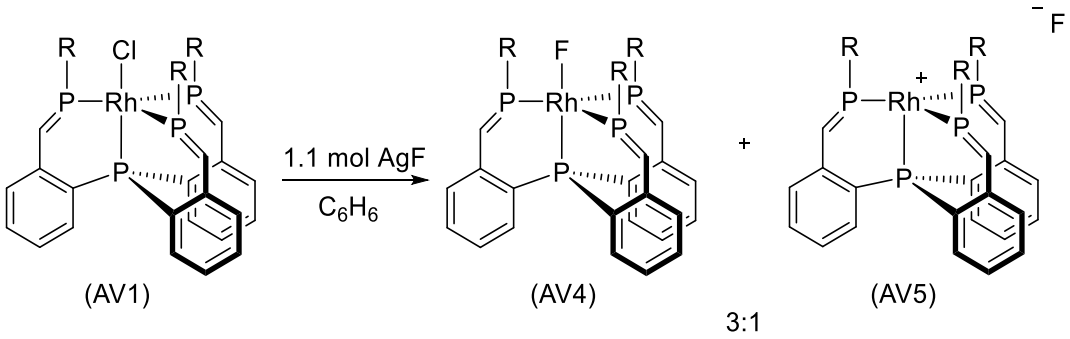

Scheme D.3 Reaction of **AV1** with AgF, (R = mes*).

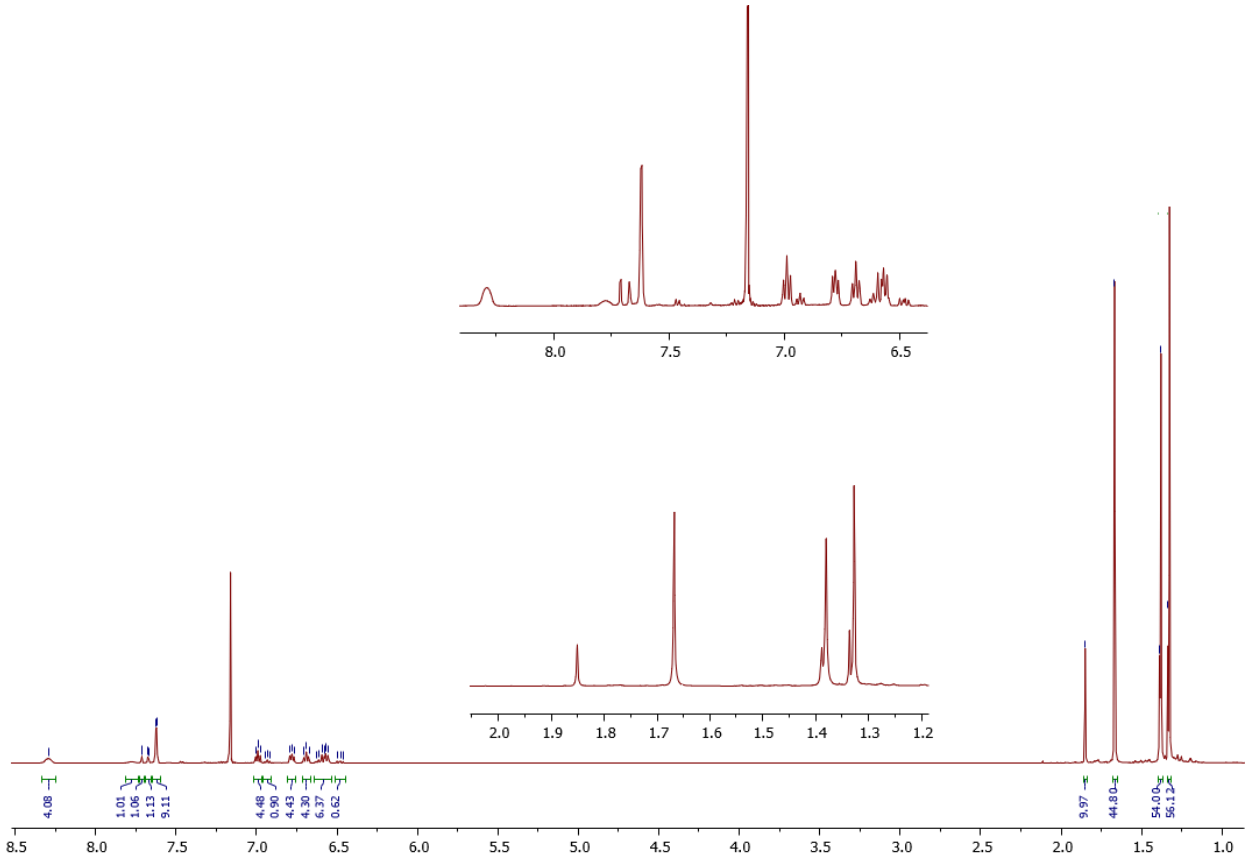

Figure D.9 $^{1}H\{^{13}C\}$ NMR **AV4** and **AV5** (500 MHz, 25 °C, C_6D_6) δ 8.29 (br, P=CH), 7.78 (br, P=CH), 7.71 (d, mes*), 7.76 (d, mes*), 7.62 (d, mes*), 6.99 (t, *J* = 5 Hz, Ar), 6.93 (t, *J* = 5 Hz, Ar), 6.78 (t, *J* = 5 Hz, Ar), 6.69 (t, *J* = 5 Hz, Ar), 6.65 (overlapping signals, Ar), 6.48 (dd, *J* = 10, 15 Hz, Ar), 1.85 (s, *t*Bu), 1.67 (s, *t*Bu), 1.39 (s, *t*Bu), 1.38 (s, *t*Bu), 1.34 (s, *t*Bu), 1.33 (s, *t*Bu).

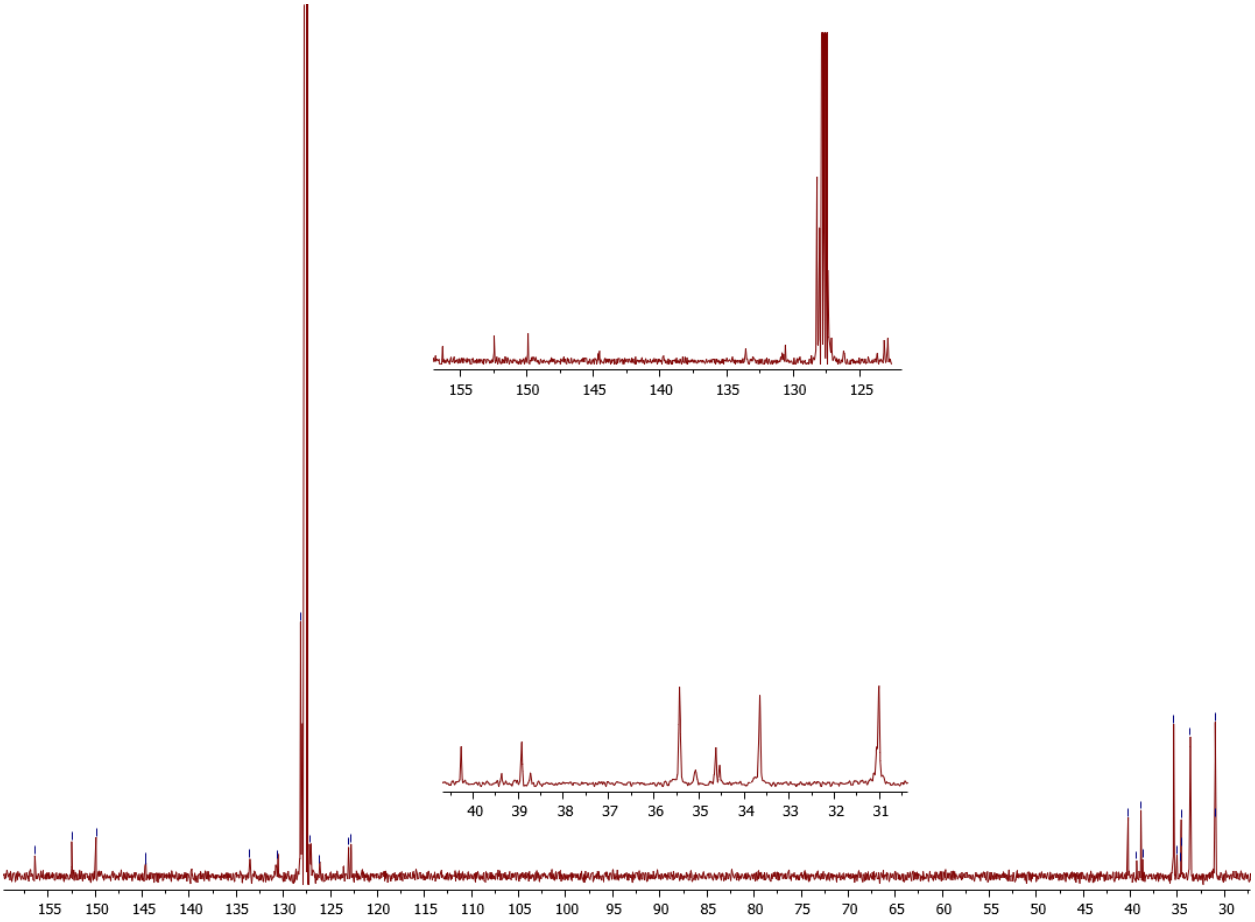

Figure D.10 $^{13}C\{^{1}H\}$ NMR **AV4** and **AV5** (126 MHz, 25 °C, C_6D_6) δ 156.36 (s, Ar), 152.45 (s, Ar), 149.89 (s, Ar), 144.68 (d, *J* = 13 Hz, P=C), 135.55 (s, Ar) , 130.82 (br, Ar), 130.59 (s, Ar), 128.19 (s), 127.12 (s, Ar), 126.16 (br, Ar), 123.13 (s, Ar), 122.85 (s, Ar), 40.26 (s, CMe_3), 39.35 (s, CMe_3), 38.92 (s, CMe_3), 38.74 (s, CMe_3), 35.44 (s, *t*Bu), 35.09 (s, *t*Bu), 34.63 (s, *t*Bu), 34.55 (s, *t*Bu), 33.66 (s, *t*Bu), 31.01 (s, *t*Bu).

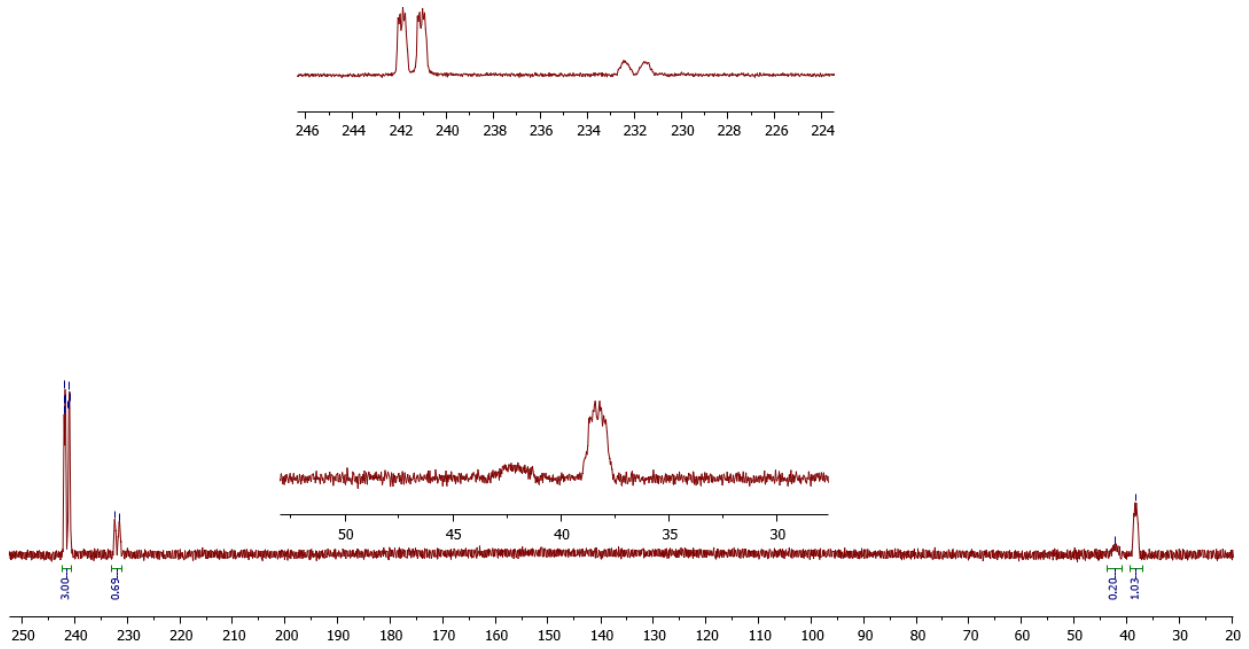

Figure D.11 $^{31}P\{^{1}H\}$ NMR **AV4** and **AV5** (121 MHz, 25 °C, C_6D_6) δ 241.4 (ddd, *J* = 11, 27, 100 Hz), 231.9 (br, m), 42.2 (br, m), 38.2 (br, m).

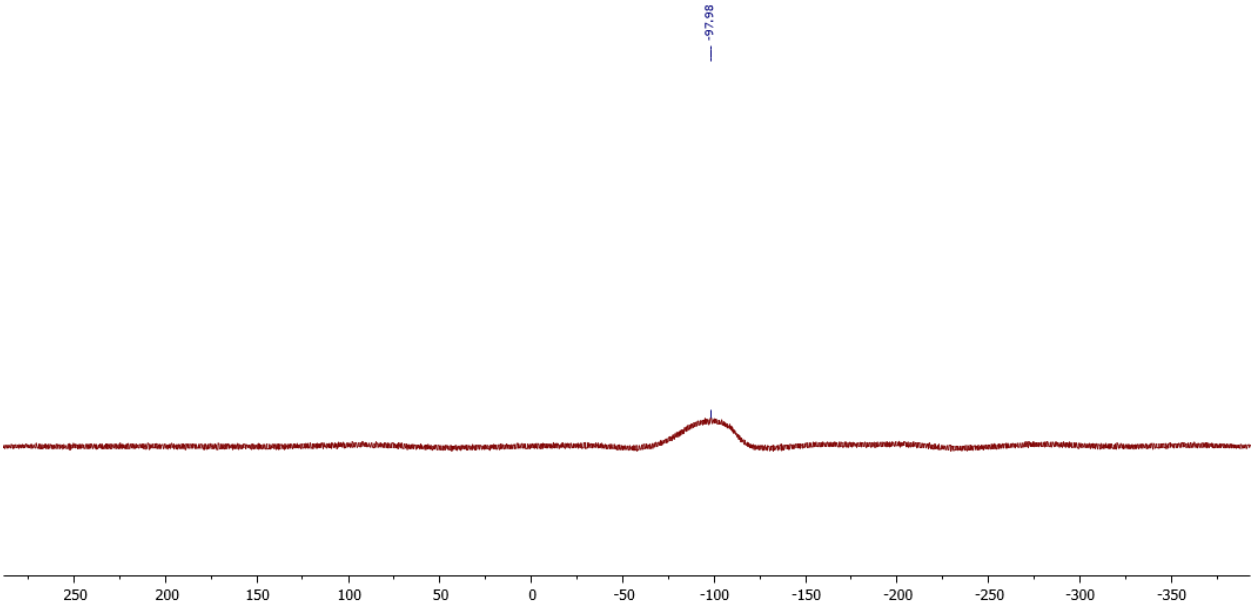

Figure D.12 $^{19}F\{^{13}C\}$ NMR **AV4** and **AV5** (282 MHz, 25 °C, C_6D_6) δ -97.9 (s), (not in spectrum, AgF δ -336).

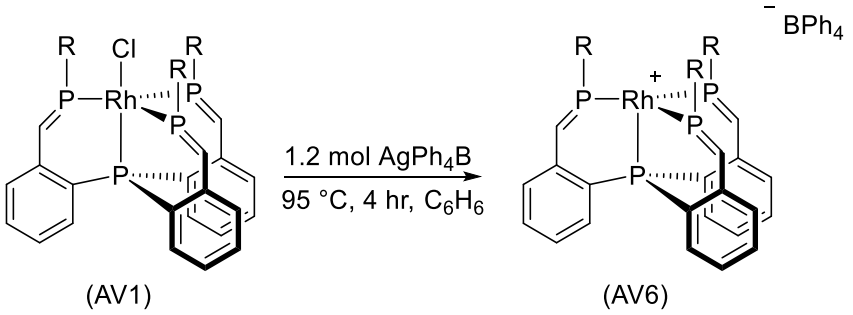

Scheme D.4 Reaction of **AV1** with $AgPh_4B$, (R = mes*).

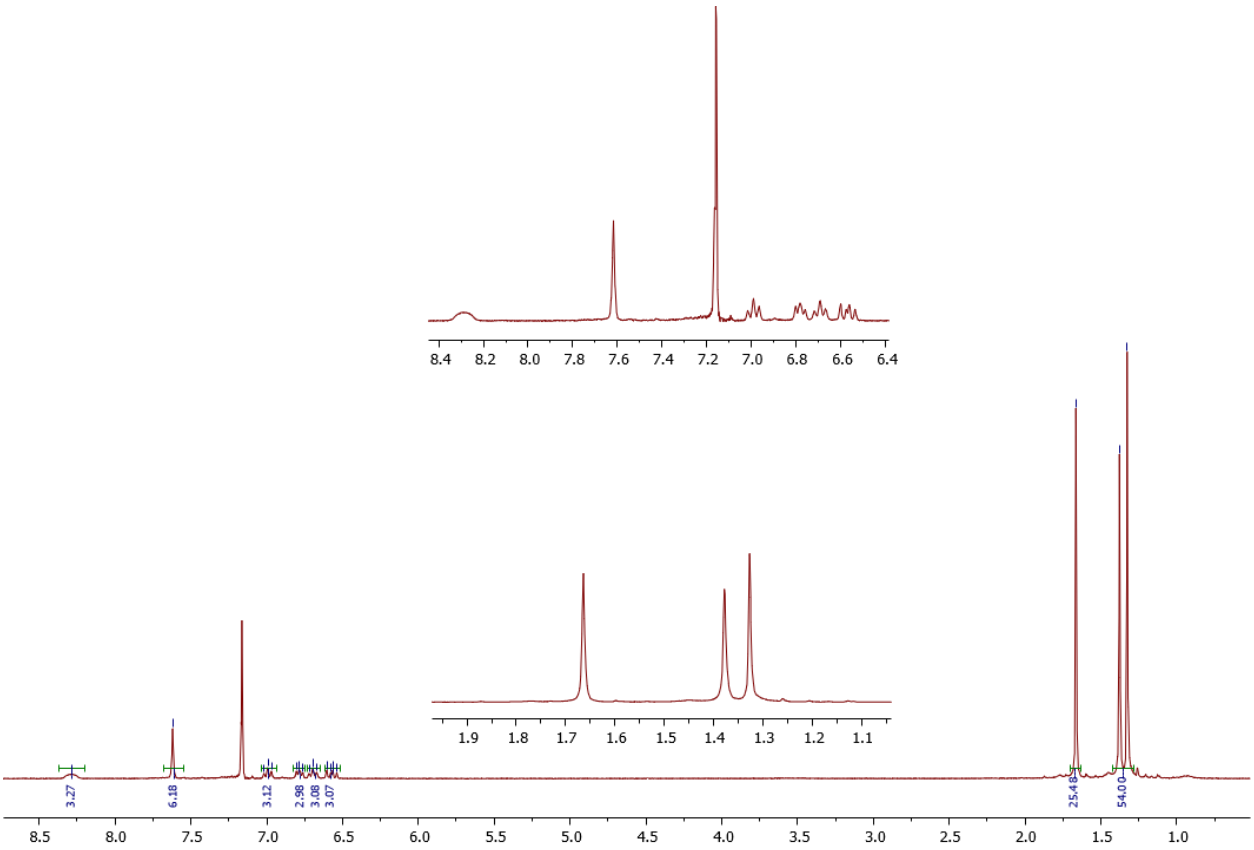

Figure D.13 $^{1}H\{^{13}C\}$ NMR **AV6** (500 MHz, 25 °C, C_6D_6) δ 8.29 (br, P=CH), 7.62 (br, Ar), 6.99 (t, *J* = 15, Ar), 6.78 (t, *J* = 10, Ar), 6.69 (t, *J* = 15, Ar), 6.57 (dd, *J* = 10, 20 Hz, Ar), 1.66 (s, *t*Bu), 1.38 (s, *t*Bu), 1.33 (s, *t*Bu).

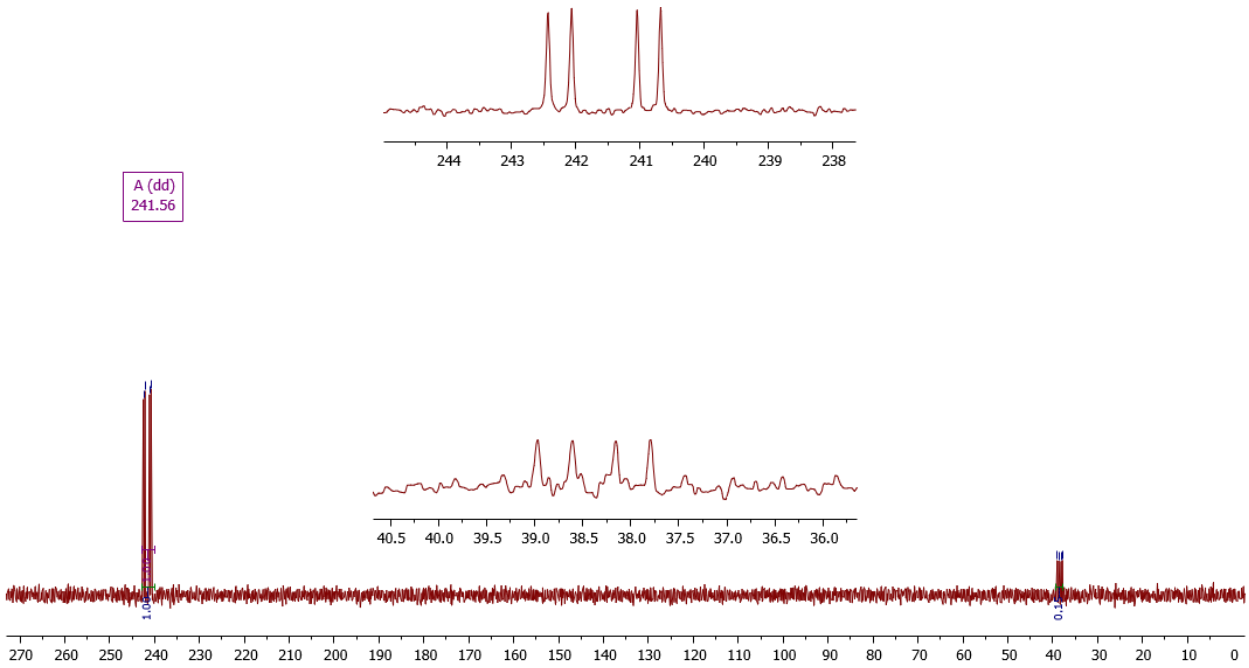

Figure D.14 $^{31}P\{^{1}H\}$ NMR **AV6** (121 MHz, 25 °C, C_6D_6) δ 241.6 (dd, *J* = 45, 168 Hz), 38.4 (overlapping dq and 4-line pattern).

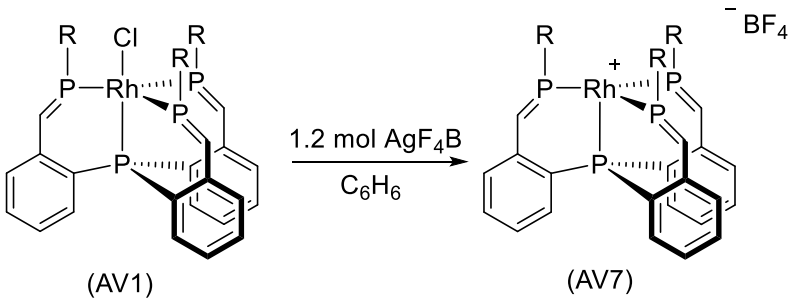

Scheme D.5 Reaction of **AV1** with AgF_4B. (R = mes*).

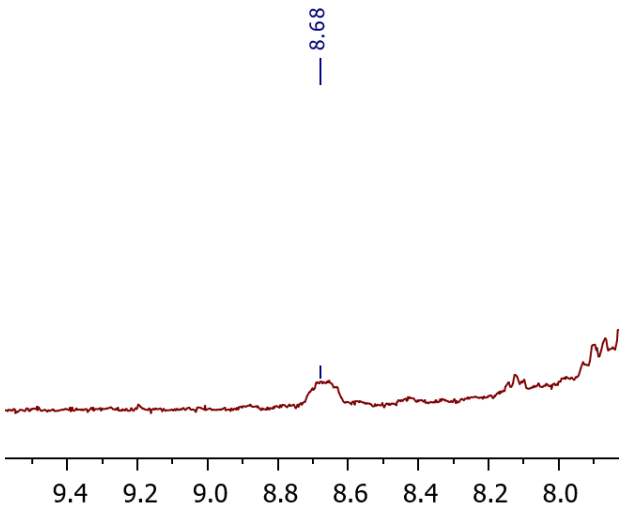

Figure D.15 Partial spectrum $^{1}H\{^{13}C\}$ NMR **AV7** (500 MHz, 25 °C, C_6D_6) δ 8.68 (br, P=CH).

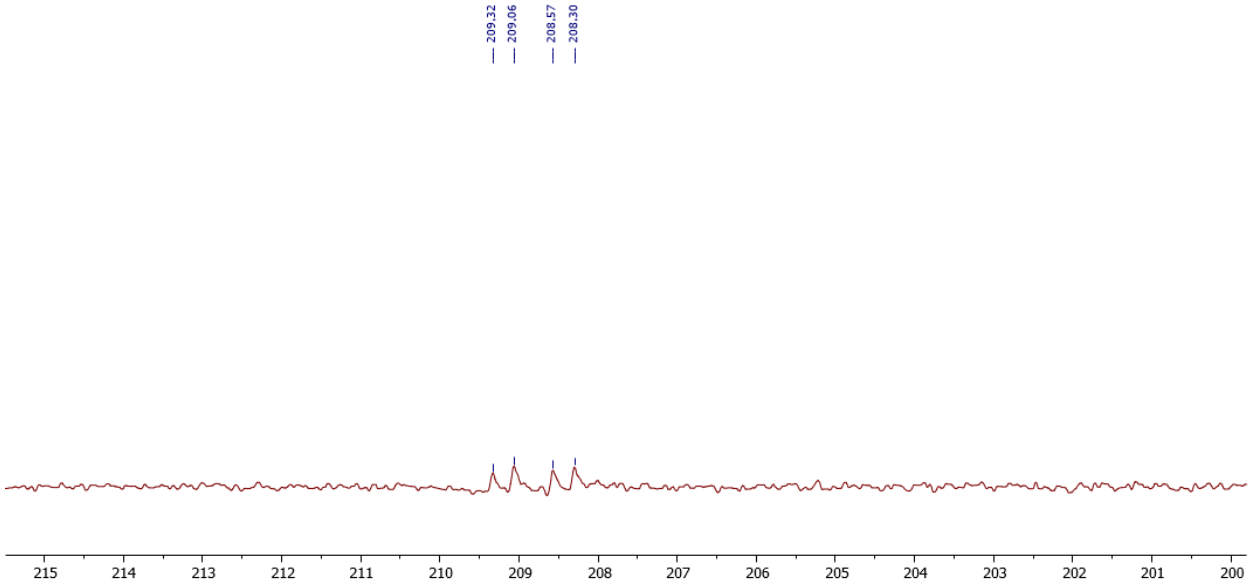

Figure D.16 Partial spectrum $^{31}P\{^{1}H\}$ NMR **AV7** (121 MHz, 25 °C, C_6D_6) δ 227.7 (dd, J = 32, 91 Hz).

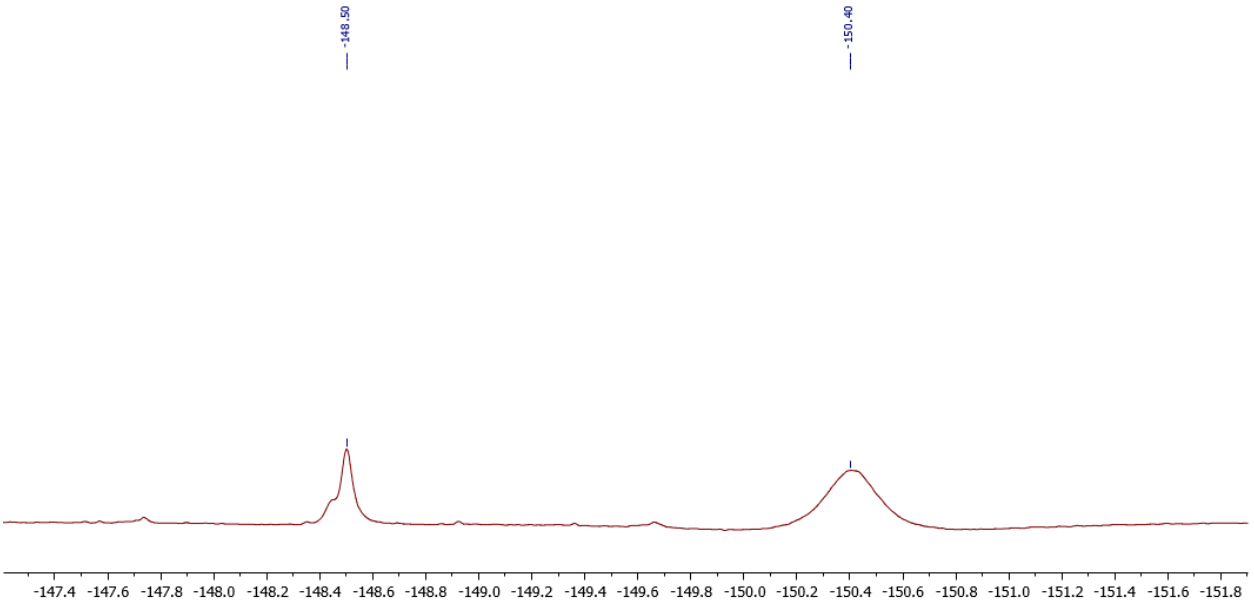

Figure D.17 Partial spectrum $^{19}F\{^{13}C\}$ NMR **AV7** (282 MHz, 25 °C, C_6D_6) δ -148.5 (br, counter ion), 150.4 (br, AgF_4B).

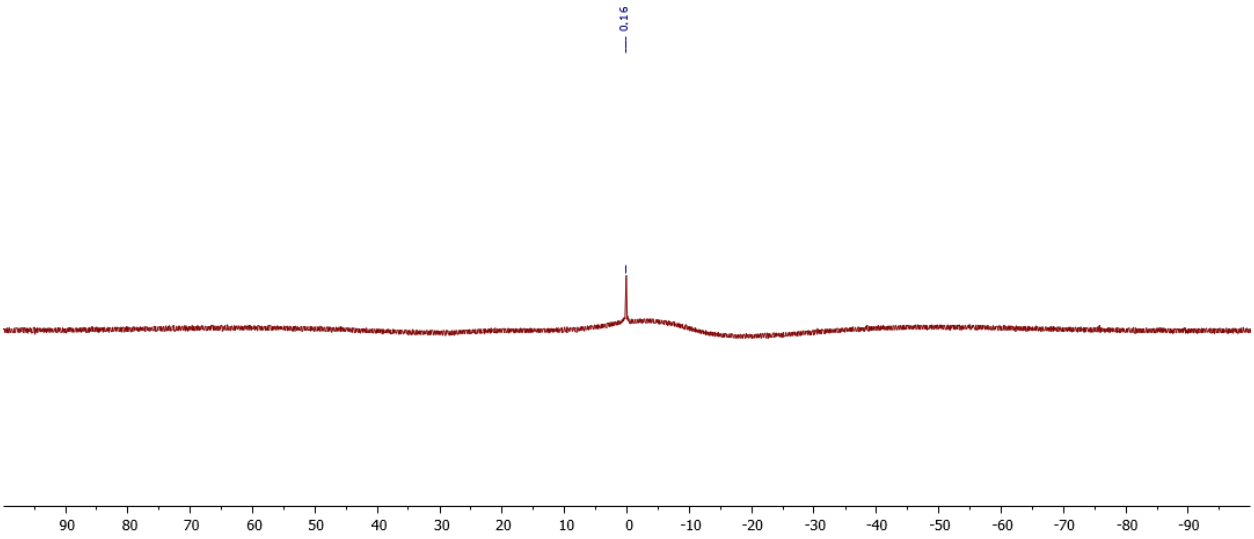

Figure D.18 $^{11}B\{^{1}H\}$ NMR **AV7** (160 MHz, 25 °C, C_6D_6) δ 0.2 (s), (AgF_4B, δ -1.875).

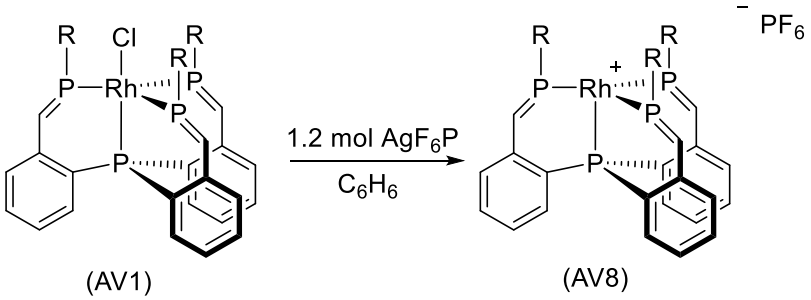

Scheme D.6 Expected product for the reaction of **AV1** and AgF_6P. (R = mes*).

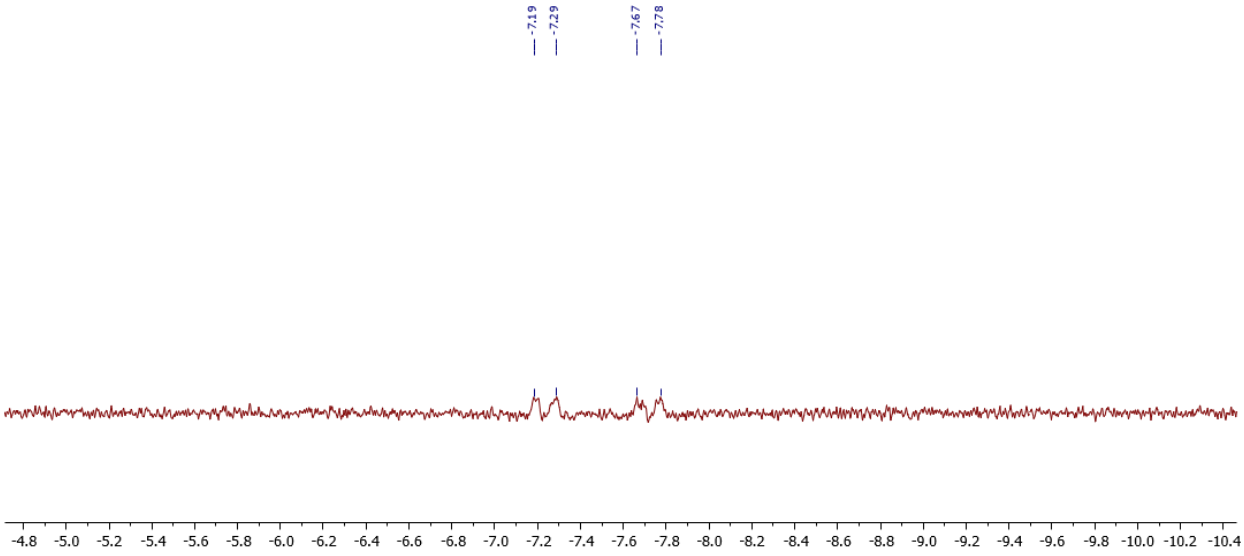

Figure D.19 Partial spectrum, hydride region, $^{1}H\{^{13}C\}$ NMR **AV8** (500 MHz, 25 °C, C_6D_6) δ -7.48 (m).

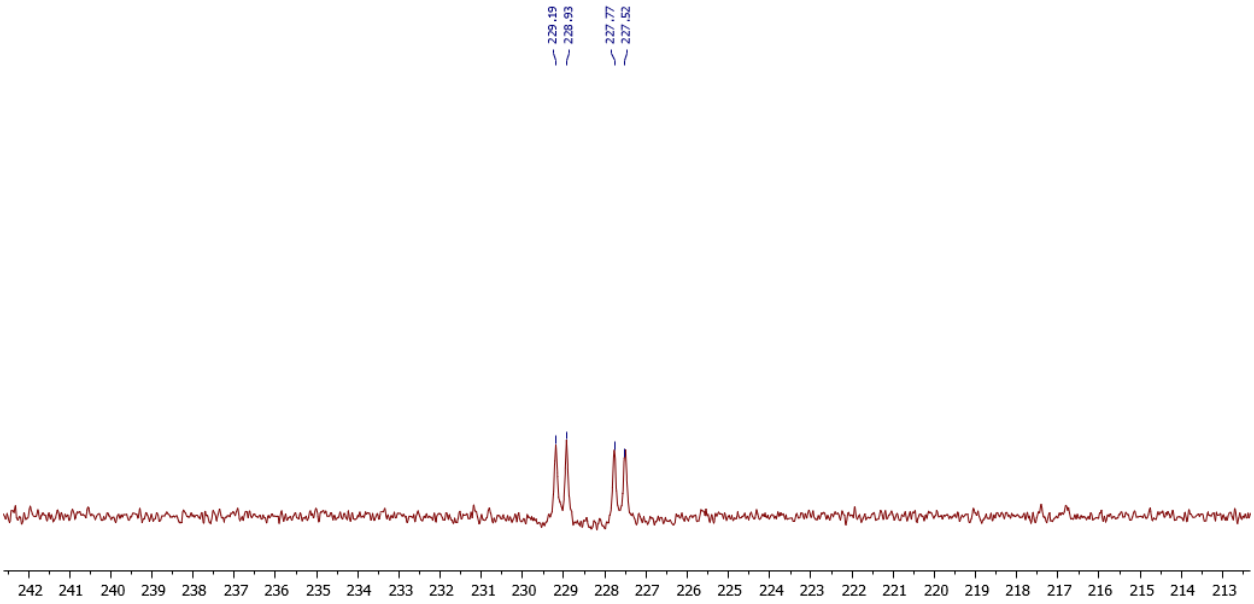

Figure D.20 Partial spectrum $^{31}P\{^{1}H\}$ NMR **AV8** (121 MHz, 25 °C, C_6D_6) δ 228.4 (dd, *J* = 32, 172 Hz).

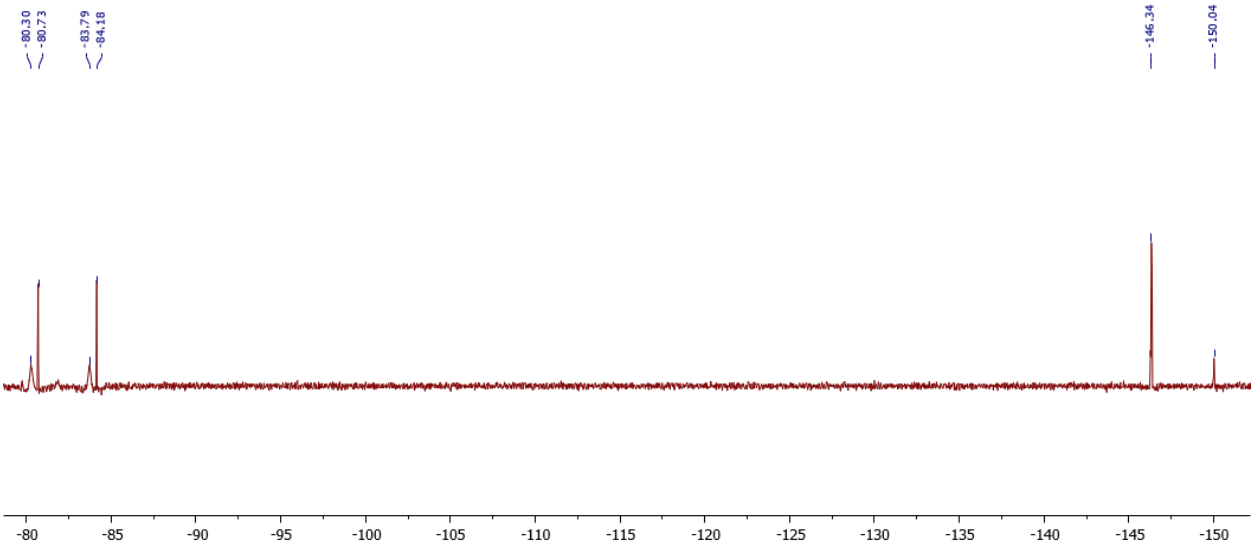

Figure D.21 $^{19}F\{^{13}C\}$ NMR **AV8** (282 MHz, 25 °C, C_6D_6) δ -80.3 (br), -80.7 (s), -83.8 (br), -84.2 (s), {counter anion}; -146.3 (m), -150.0 (br), {unknown side product} (PF_5 δ -71, $^{-}PF_6$ δ -65).

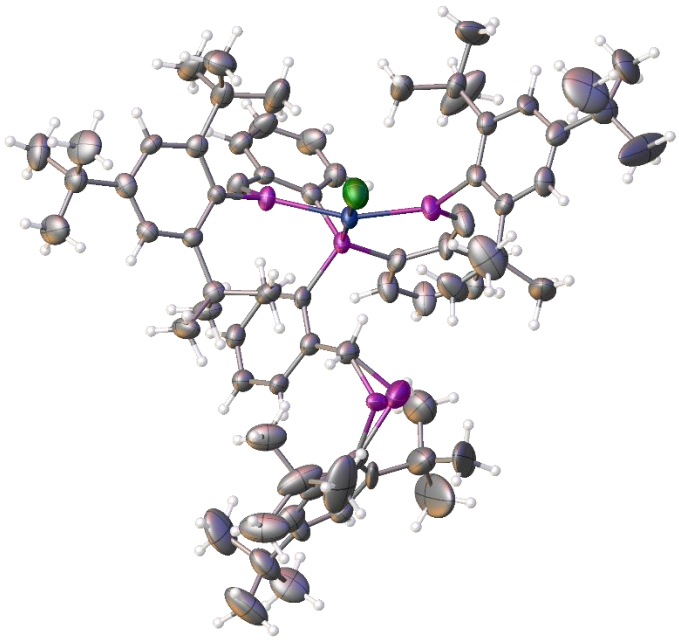

Figure D.22 Partially resolved single crystal XRD structure for **AV8**.

D.2.1 Failed Reactions

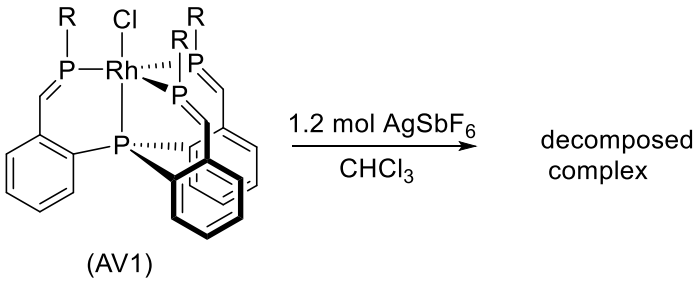

Scheme D.8 Reaction of **AV1** with $AgSbF_6$ results in decomposition.

Scheme D.9 Reaction of **AV1** with AgOTs results in incomplete reaction.

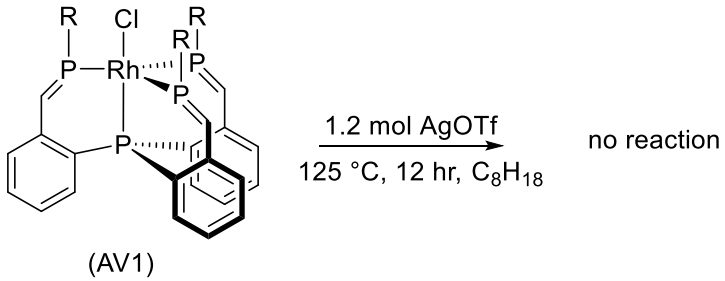

Scheme D.10 Reaction of **AV1** with AgOTf in octane results in no reaction.

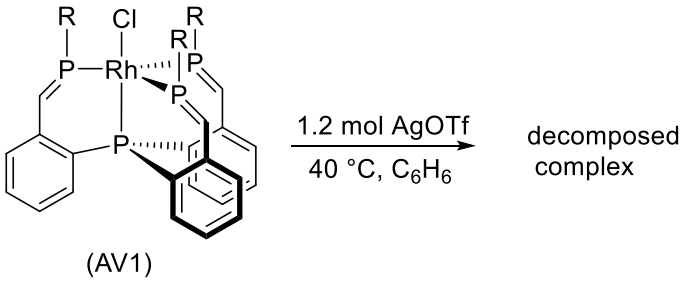

Scheme D.11 Reaction of **AV1** with AgOTf at 40 °C results in decomposition.

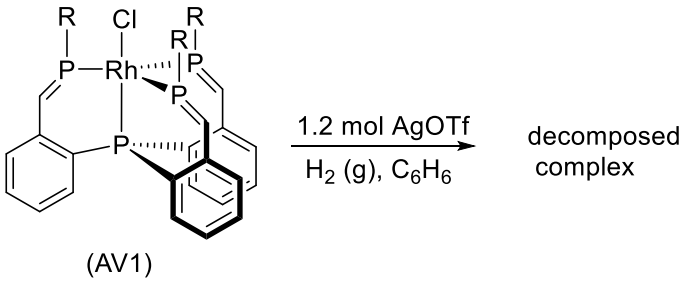

Scheme D.12 Reaction of **AV1** with AgOTf under 1 atm. of hydrogen pressure results in decomposition.

APPENDIX E. Supplemental Data, Single Crystal X-ray Diffractometry Data Set for AV3

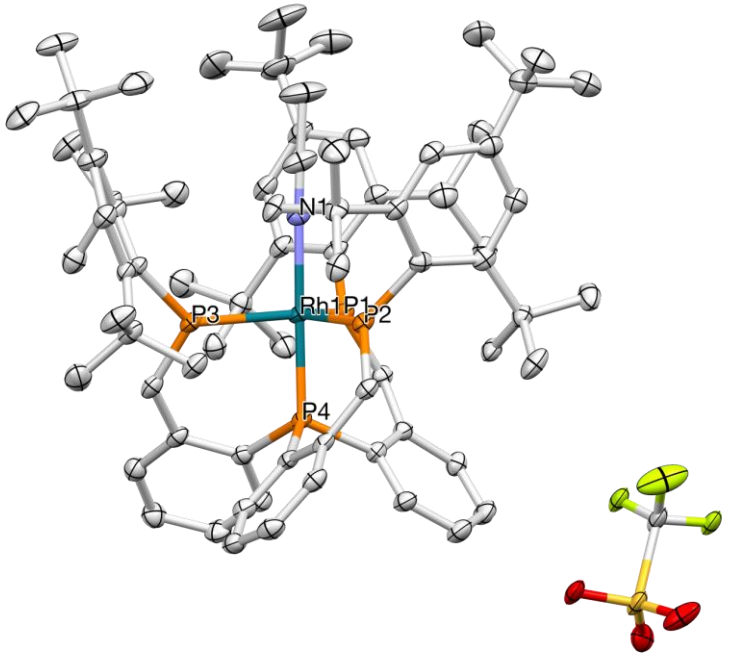

Figure E.1 ORTEP diagram of the structure determined for **AV3** at 100 K by single crystal X-ray diffraction analysis. Atoms in the rhodium coordination sphere have been labeled. Hydrogens have been omitted for clarity. Thermal ellipsoids at 50 % probability.

Table E.1 Crystal data and structure refinement for cain38_a_sq.

Identification code	Rh complex	
Empirical formula	C85 H110 F3 N O3 P4 Rh S	
Formula weight	1509.58	
Temperature	100.0 K	
Wavelength	0.71073 Å	
Crystal system	Triclinic	
Space group	P-1	
Unit cell dimensions	a = 15.3888(9) Å	α= 60.772(3)°.
	b = 18.1970(11) Å	β= 88.927(3)°.

	c = 18.5538(11) Å γ = 89.786(3)°.
Volume	4533.3(5) Å^3
Z	2
Density (calculated)	1.106 Mg/m^3
Absorption coefficient	0.330 mm^{-1}
F(000)	1598
Crystal size	0.27 x 0.12 x 0.08 mm^3
Theta range for data collection	1.258 to 26.156°.
Index ranges	-19<=h<=18, -22<=k<=22, -22<=l<=19
Reflections collected	96973
Independent reflections	18009 [R(int) = 0.1248]
Completeness to theta = 25.000°	100.0 %
Absorption correction	Semi-empirical from equivalents
Max. and min. transmission	0.188 and 0.100
Refinement method	Full-matrix least-squares on F^2
Data / restraints / parameters	18009 / 3 / 1053
Goodness-of-fit on F^2	1.078
Final R indices [I>2sigma(I)]	R1 = 0.0752, wR2 = 0.2190
R indices (all data)	R1 = 0.1008, wR2 = 0.2410
Extinction coefficient	n/a
Largest diff. peak and hole	2.792 and -1.281 e.Å^{-3}
SQUEEZE	119 e/uc: 2 toluene

Table E.2 Atomic coordinates (x 10^4) and equivalent isotropic displacement parameters (Å^{2}x 10^3)

for cain38_a_sq. U(eq) is defined as one third of the trace of the orthogonalized U^{ij} tensor.

	x	y	z	U(eq)

—

Rh(1)	4100(1)	8348(1)	3307(1)	19(1)
P(2)	4189(1)	8818(1)	1913(1)	20(1)
P(4)	5548(1)	8367(1)	3287(1)	18(1)
P(1)	4179(1)	6935(1)	4229(1)	19(1)
P(3)	4161(1)	9303(1)	3781(1)	21(1)
S(1)	8285(1)	2783(1)	1724(1)	18(1)
S(2)	8167(3)	6643(2)	552(3)	29(1)
F(3)	6830(3)	3615(3)	1223(3)	31(1)
N(1)	2748(3)	8328(2)	3308(2)	22(1)
F(2)	6687(3)	2271(3)	1896(3)	40(1)
F(1)	7162(3)	2866(4)	654(3)	39(1)
C(26)	6048(3)	7513(3)	3184(3)	20(1)
C(15)	2565(3)	10088(3)	878(3)	26(1)
C(3)	2593(3)	7619(3)	1059(3)	26(1)
C(25)	6047(3)	9321(3)	2450(3)	20(1)
C(27)	6713(3)	7697(3)	2601(3)	24(1)
C(30)	6296(3)	6038(3)	3676(3)	24(1)
C(31)	5808(3)	6668(3)	3725(3)	20(1)
C(38)	3305(3)	6261(3)	5802(3)	23(1)
C(2)	3376(3)	7882(3)	1235(3)	22(1)
C(33)	3345(3)	6285(3)	5018(3)	22(1)
C(20)	5795(3)	9626(3)	1624(3)	21(1)
C(37)	2509(3)	6046(3)	6235(3)	28(1)
O(3)	8722(3)	3508(3)	1052(4)	34(1)
C(63)	2548(3)	9108(3)	5089(3)	26(1)
C(4)	1820(3)	8058(3)	932(3)	29(1)
C(18)	3329(4)	10616(3)	304(3)	30(1)
C(24)	6694(3)	9728(3)	2632(3)	24(1)
C(60)	1822(3)	11101(3)	3161(3)	29(1)
C(6)	2612(3)	9162(3)	1047(3)	22(1)

C(61)	2587(3)	11377(3)	2695(3)	26(1)
C(75)	2017(4)	8304(4)	3303(4)	38(1)
C(32)	5072(3)	6380(3)	4310(3)	21(1)
C(21)	6267(3)	10322(3)	1008(3)	25(1)
C(57)	3351(3)	10112(3)	3644(3)	21(1)
C(16)	2544(4)	10163(3)	1666(3)	31(1)
C(58)	2603(3)	9865(3)	4190(3)	24(1)
C(34)	2621(3)	5974(3)	4769(3)	25(1)
C(51)	5035(3)	9383(3)	4254(3)	25(1)
C(65)	3313(4)	9095(4)	5607(3)	32(1)
C(1)	3372(3)	8634(3)	1298(3)	22(1)
O(1)	8544(3)	1977(3)	1828(4)	38(2)
C(29)	6952(3)	6232(3)	3087(3)	29(1)
C(19)	5077(3)	9312(3)	1345(3)	22(1)
C(22)	6906(3)	10723(3)	1192(3)	27(1)
C(36)	1770(3)	5848(3)	5948(4)	32(1)
C(35)	1855(3)	5778(3)	5254(3)	31(1)
C(28)	7157(3)	7069(3)	2535(3)	30(1)
C(67)	982(4)	11599(4)	2832(4)	43(2)
C(64)	2464(4)	8265(3)	5097(4)	34(1)
C(53)	6707(3)	7709(3)	4581(3)	24(1)
O(2)	8177(4)	2827(4)	2472(3)	40(2)
C(17)	1730(4)	10531(4)	410(4)	42(2)
C(39)	2618(3)	5778(3)	4044(3)	28(1)
C(5)	1866(3)	8835(3)	894(3)	28(1)
C(47)	4085(3)	6365(3)	6265(3)	25(1)
C(01L)	5763(3)	8798(3)	4548(3)	21(1)
C(54)	7124(3)	7644(3)	5265(3)	30(1)
C(23)	7122(3)	10438(3)	2011(3)	28(1)
C(52)	6040(3)	8272(3)	4215(3)	21(1)
C(59)	1867(3)	10369(3)	3909(3)	27(1)

C(62)	3356(3)	10924(3)	2906(3)	22(1)
C(7)	4193(3)	7353(3)	1291(3)	24(1)
C(40)	1820(4)	5248(4)	4085(4)	41(1)
C(71)	4172(3)	11387(3)	2369(3)	26(1)
C(66)	1745(4)	9159(4)	5565(4)	43(2)
C(11)	953(4)	7711(4)	821(4)	36(1)
C(41)	3410(4)	5240(3)	4080(3)	30(1)
C(42)	2584(4)	6572(4)	3197(3)	34(1)
C(55)	6872(3)	8161(3)	5589(3)	29(1)
C(73)	3945(4)	12238(4)	1609(4)	41(2)
C(50)	4619(4)	7175(3)	5766(3)	28(1)
C(8)	4673(3)	7004(3)	2105(3)	26(1)
C(10)	4814(4)	7874(4)	573(4)	36(1)
C(49)	4692(4)	5607(3)	6511(4)	33(1)
C(56)	6211(3)	8726(3)	5223(3)	26(1)
C(72)	4779(4)	11593(4)	2883(4)	38(1)
C(74)	4660(3)	10897(3)	2014(3)	30(1)
C(9)	3976(4)	6558(4)	1221(4)	36(1)
C(76)	1077(4)	8262(6)	3287(5)	68(2)
C(43)	886(4)	5687(5)	6409(5)	50(2)
C(78)	7190(4)	2894(4)	1347(4)	19(1)
C(48)	3806(4)	6359(4)	7065(3)	39(1)
F(4)	7141(6)	5387(5)	857(6)	29(1)
C(69)	1132(6)	12522(6)	2569(7)	46(3)
C(70)	234(5)	11264(7)	3431(6)	48(3)
C(68)	750(5)	11567(7)	2021(6)	45(3)
C(79)	3359(6)	4576(5)	1328(6)	67(2)
C(45)	587(9)	4761(9)	6677(10)	54(4)
F(6)	6791(6)	5955(5)	1519(6)	29(1)
C(81)	2714(17)	4183(8)	2576(7)	134(7)
C(12)	303(6)	7664(8)	1474(8)	58(3)

C(14)	1037(6)	6825(6)	919(7)	47(3)
O(4)	8684(8)	5983(8)	1205(7)	38(3)
C(80)	3388(9)	4188(6)	2151(8)	92(4)
C(83)	1852(9)	4831(11)	1511(17)	149(8)
C(13)	627(6)	8321(7)	-53(6)	47(3)
O(6)	8339(8)	6776(8)	-208(8)	45(3)
F(5)	6484(7)	6531(9)	285(6)	64(4)
C(84)	2595(9)	4933(6)	959(5)	91(4)
C(77)	7052(10)	6093(10)	843(11)	29(1)
O(5)	7979(7)	7319(6)	685(7)	29(1)
C(46)	832(8)	5904(11)	7036(9)	62(5)
C(44)	167(8)	6259(10)	5719(9)	74(5)
C(82)	1955(11)	4495(12)	2288(13)	119(6)
C(85)	4174(10)	4626(11)	820(15)	206(11)
C(69')	710(20)	11870(20)	3610(20)	89(14)
C(70')	250(20)	10950(20)	2990(30)	91(14)
C(68')	1000(20)	12330(20)	2120(20)	78(14)
C(14')	722(13)	6925(14)	1657(13)	47(6)
C(13')	1031(13)	7486(14)	166(12)	45(6)
C(12')	186(13)	8346(15)	636(18)	60(8)
C(45')	1104(11)	5206(16)	7426(11)	56(6)
C(46')	576(12)	6542(13)	6293(14)	61(8)
C(44')	304(15)	5210(20)	6270(20)	80(12)

Table E.3 Bond lengths [Å] and angles [°] for cain38_a_sq.

Rh(1)-P(2)	2.2952(13)
Rh(1)-P(4)	2.2288(12)
Rh(1)-P(1)	2.2942(12)
Rh(1)-P(3)	2.3009(13)
Rh(1)-N(1)	2.080(4)

P(2)-C(1)	1.851(5)
P(2)-C(19)	1.676(5)
P(4)-C(26)	1.821(5)
P(4)-C(25)	1.829(5)
P(4)-C(52)	1.823(5)
P(1)-C(33)	1.854(5)
P(1)-C(32)	1.669(5)
P(3)-C(57)	1.848(5)
P(3)-C(51)	1.666(5)
S(1)-O(3)	1.455(5)
S(1)-O(1)	1.439(5)
S(1)-O(2)	1.434(6)
S(1)-C(78)	1.810(7)
S(2)-O(4)	1.467(13)
S(2)-O(6)	1.329(14)
S(2)-C(77)	1.920(16)
S(2)-O(5)	1.398(10)
F(3)-C(78)	1.337(8)
N(1)-C(75)	1.128(7)
F(2)-C(78)	1.331(8)
F(1)-C(78)	1.311(8)
C(26)-C(27)	1.392(7)
C(26)-C(31)	1.412(7)
C(15)-C(18)	1.550(7)
C(15)-C(6)	1.559(7)
C(15)-C(16)	1.533(7)
C(15)-C(17)	1.551(7)
C(3)-H(3)	0.9500
C(3)-C(2)	1.400(7)
C(3)-C(4)	1.389(7)
C(25)-C(20)	1.414(7)

C(25)-C(24)	1.385(7)
C(27)-H(27)	0.9500
C(27)-C(28)	1.385(7)
C(30)-H(30)	0.9500
C(30)-C(31)	1.407(7)
C(30)-C(29)	1.387(7)
C(31)-C(32)	1.462(7)
C(38)-C(33)	1.433(7)
C(38)-C(37)	1.399(7)
C(38)-C(47)	1.554(7)
C(2)-C(1)	1.429(7)
C(2)-C(7)	1.555(7)
C(33)-C(34)	1.433(7)
C(20)-C(21)	1.414(7)
C(20)-C(19)	1.459(7)
C(37)-H(37)	0.9500
C(37)-C(36)	1.386(8)
C(63)-C(58)	1.561(7)
C(63)-C(65)	1.526(8)
C(63)-C(64)	1.533(7)
C(63)-C(66)	1.534(7)
C(4)-C(5)	1.383(8)
C(4)-C(11)	1.537(8)
C(18)-H(18A)	0.9800
C(18)-H(18B)	0.9800
C(18)-H(18C)	0.9800
C(24)-H(24)	0.9500
C(24)-C(23)	1.397(7)
C(60)-C(61)	1.389(7)
C(60)-C(67)	1.533(7)
C(60)-C(59)	1.379(7)

C(6)-C(1)	1.443(7)
C(6)-C(5)	1.390(7)
C(61)-H(61)	0.9500
C(61)-C(62)	1.389(7)
C(75)-C(76)	1.449(8)
C(21)-H(21)	0.9500
C(21)-C(22)	1.370(8)
C(57)-C(58)	1.438(7)
C(57)-C(62)	1.443(7)
C(16)-H(16A)	0.9800
C(16)-H(16B)	0.9800
C(16)-H(16C)	0.9800
C(58)-C(59)	1.395(7)
C(34)-C(35)	1.406(7)
C(34)-C(39)	1.552(7)
C(51)-C(01L)	1.461(7)
C(65)-H(65A)	0.9800
C(65)-H(65B)	0.9800
C(65)-H(65C)	0.9800
C(29)-H(29)	0.9500
C(29)-C(28)	1.390(7)
C(22)-H(22)	0.9500
C(22)-C(23)	1.391(8)
C(36)-C(35)	1.358(8)
C(36)-C(43)	1.544(7)
C(35)-H(35)	0.9500
C(28)-H(28)	0.9500
C(67)-C(69)	1.520(12)
C(67)-C(70)	1.492(10)
C(67)-C(68)	1.582(11)
C(67)-C(69')	1.78(4)

C(67)-C(70')	1.55(4)
C(67)-C(68')	1.33(3)
C(64)-H(64A)	0.9800
C(64)-H(64B)	0.9800
C(64)-H(64C)	0.9800
C(53)-H(53)	0.9500
C(53)-C(54)	1.386(7)
C(53)-C(52)	1.379(7)
C(17)-H(17A)	0.9800
C(17)-H(17B)	0.9800
C(17)-H(17C)	0.9800
C(39)-C(40)	1.543(8)
C(39)-C(41)	1.542(7)
C(39)-C(42)	1.531(7)
C(5)-H(5)	0.9500
C(47)-C(50)	1.533(7)
C(47)-C(49)	1.541(7)
C(47)-C(48)	1.533(7)
C(01L)-C(52)	1.429(7)
C(01L)-C(56)	1.391(7)
C(54)-H(54)	0.9500
C(54)-C(55)	1.392(8)
C(23)-H(23)	0.9500
C(59)-H(59)	0.9500
C(62)-C(71)	1.555(7)
C(7)-C(8)	1.527(7)
C(7)-C(10)	1.520(8)
C(7)-C(9)	1.552(7)
C(40)-H(40A)	0.9800
C(40)-H(40B)	0.9800
C(40)-H(40C)	0.9800

C(71)-C(73)	1.546(7)
C(71)-C(72)	1.519(8)
C(71)-C(74)	1.531(7)
C(66)-H(66A)	0.9800
C(66)-H(66B)	0.9800
C(66)-H(66C)	0.9800
C(11)-C(12)	1.526(12)
C(11)-C(14)	1.538(11)
C(11)-C(13)	1.543(11)
C(11)-C(14')	1.55(2)
C(11)-C(13')	1.46(2)
C(11)-C(12')	1.57(2)
C(41)-H(41A)	0.9800
C(41)-H(41B)	0.9800
C(41)-H(41C)	0.9800
C(42)-H(42A)	0.9800
C(42)-H(42B)	0.9800
C(42)-H(42C)	0.9800
C(55)-H(55)	0.9500
C(55)-C(56)	1.375(7)
C(73)-H(73A)	0.9800
C(73)-H(73B)	0.9800
C(73)-H(73C)	0.9800
C(50)-H(50A)	0.9800
C(50)-H(50B)	0.9800
C(50)-H(50C)	0.9800
C(8)-H(8A)	0.9800
C(8)-H(8B)	0.9800
C(8)-H(8C)	0.9800
C(10)-H(10A)	0.9800
C(10)-H(10B)	0.9800

C(10)-H(10C)	0.9800
C(49)-H(49A)	0.9800
C(49)-H(49B)	0.9800
C(49)-H(49C)	0.9800
C(56)-H(56)	0.9500
C(72)-H(72A)	0.9800
C(72)-H(72B)	0.9800
C(72)-H(72C)	0.9800
C(74)-H(74A)	0.9800
C(74)-H(74B)	0.9800
C(74)-H(74C)	0.9800
C(9)-H(9A)	0.9800
C(9)-H(9B)	0.9800
C(9)-H(9C)	0.9800
C(76)-H(76A)	0.9800
C(76)-H(76B)	0.9800
C(76)-H(76C)	0.9800
C(43)-C(45)	1.574(17)
C(43)-C(46)	1.401(14)
C(43)-C(44)	1.640(16)
C(43)-C(45')	1.69(2)
C(43)-C(46')	1.54(2)
C(43)-C(44')	1.36(2)
C(48)-H(48A)	0.9800
C(48)-H(48B)	0.9800
C(48)-H(48C)	0.9800
F(4)-C(77)	1.279(17)
C(69)-H(69A)	0.9800
C(69)-H(69B)	0.9800
C(69)-H(69C)	0.9800
C(70)-H(70A)	0.9800

C(70)-H(70B)	0.9800
C(70)-H(70C)	0.9800
C(68)-H(68A)	0.9800
C(68)-H(68B)	0.9800
C(68)-H(68C)	0.9800
C(79)-C(80)	1.335(15)
C(79)-C(84)	1.365(14)
C(79)-C(85)	1.531(15)
C(45)-H(45A)	0.9800
C(45)-H(45B)	0.9800
C(45)-H(45C)	0.9800
F(6)-C(77)	1.212(18)
C(81)-H(81)	0.9500
C(81)-C(80)	1.29(2)
C(81)-C(82)	1.30(2)
C(12)-H(12A)	0.9800
C(12)-H(12B)	0.9800
C(12)-H(12C)	0.9800
C(14)-H(14A)	0.9800
C(14)-H(14B)	0.9800
C(14)-H(14C)	0.9800
C(80)-H(80)	0.9500
C(83)-H(83)	0.9500
C(83)-C(84)	1.47(2)
C(83)-C(82)	1.28(2)
C(13)-H(13A)	0.9800
C(13)-H(13B)	0.9800
C(13)-H(13C)	0.9800
F(5)-C(77)	1.30(2)
C(84)-H(84)	0.9500
C(46)-H(46A)	0.9800

C(46)-H(46B)	0.9800
C(46)-H(46C)	0.9800
C(44)-H(44A)	0.9800
C(44)-H(44B)	0.9800
C(44)-H(44C)	0.9800
C(82)-H(82)	0.9500
C(85)-H(85A)	0.9800
C(85)-H(85B)	0.9800
C(85)-H(85C)	0.9800
C(69')-H(69D)	0.9800
C(69')-H(69E)	0.9800
C(69')-H(69F)	0.9800
C(70')-H(70D)	0.9800
C(70')-H(70E)	0.9800
C(70')-H(70F)	0.9800
C(68')-H(68D)	0.9800
C(68')-H(68E)	0.9800
C(68')-H(68F)	0.9800
C(14')-H(14D)	0.9800
C(14')-H(14E)	0.9800
C(14')-H(14F)	0.9800
C(13')-H(13D)	0.9800
C(13')-H(13E)	0.9800
C(13')-H(13F)	0.9800
C(12')-H(12D)	0.9800
C(12')-H(12E)	0.9800
C(12')-H(12F)	0.9800
C(45')-H(45D)	0.9800
C(45')-H(45E)	0.9800
C(45')-H(45F)	0.9800
C(46')-H(46D)	0.9800

C(46')-H(46E)	0.9800
C(46')-H(46F)	0.9800
C(44')-H(44D)	0.9800
C(44')-H(44E)	0.9800
C(44')-H(44F)	0.9800

P(2)-Rh(1)-P(3)	119.54(5)
P(4)-Rh(1)-P(2)	86.96(5)
P(4)-Rh(1)-P(1)	87.26(4)
P(4)-Rh(1)-P(3)	86.98(5)
P(1)-Rh(1)-P(2)	120.19(5)
P(1)-Rh(1)-P(3)	119.49(5)
N(1)-Rh(1)-P(2)	92.16(11)
N(1)-Rh(1)-P(4)	179.03(12)
N(1)-Rh(1)-P(1)	92.82(11)
N(1)-Rh(1)-P(3)	93.83(12)
C(1)-P(2)-Rh(1)	125.93(16)
C(19)-P(2)-Rh(1)	122.03(18)
C(19)-P(2)-C(1)	111.8(2)
C(26)-P(4)-Rh(1)	114.31(16)
C(26)-P(4)-C(25)	104.2(2)
C(26)-P(4)-C(52)	103.1(2)
C(25)-P(4)-Rh(1)	114.92(16)
C(52)-P(4)-Rh(1)	115.03(16)
C(52)-P(4)-C(25)	103.8(2)
C(33)-P(1)-Rh(1)	126.66(15)
C(32)-P(1)-Rh(1)	121.84(18)
C(32)-P(1)-C(33)	111.3(2)
C(57)-P(3)-Rh(1)	127.74(17)
C(51)-P(3)-Rh(1)	121.31(18)
C(51)-P(3)-C(57)	110.8(2)

O(3)-S(1)-C(78)	101.9(3)
O(1)-S(1)-O(3)	115.4(4)
O(1)-S(1)-C(78)	102.9(3)
O(2)-S(1)-O(3)	114.7(4)
O(2)-S(1)-O(1)	115.6(4)
O(2)-S(1)-C(78)	103.5(4)
O(4)-S(2)-C(77)	99.1(7)
O(6)-S(2)-O(4)	115.3(7)
O(6)-S(2)-C(77)	105.1(8)
O(6)-S(2)-O(5)	120.2(8)
O(5)-S(2)-O(4)	113.6(7)
O(5)-S(2)-C(77)	98.9(6)
C(75)-N(1)-Rh(1)	178.4(5)
C(27)-C(26)-P(4)	119.3(4)
C(27)-C(26)-C(31)	120.0(4)
C(31)-C(26)-P(4)	120.6(4)
C(18)-C(15)-C(6)	110.5(4)
C(18)-C(15)-C(17)	105.3(4)
C(16)-C(15)-C(18)	110.0(4)
C(16)-C(15)-C(6)	113.5(4)
C(16)-C(15)-C(17)	105.6(4)
C(17)-C(15)-C(6)	111.5(4)
C(2)-C(3)-H(3)	118.3
C(4)-C(3)-H(3)	118.3
C(4)-C(3)-C(2)	123.3(5)
C(20)-C(25)-P(4)	120.6(4)
C(24)-C(25)-P(4)	119.2(4)
C(24)-C(25)-C(20)	120.2(4)
C(26)-C(27)-H(27)	119.1
C(28)-C(27)-C(26)	121.7(5)
C(28)-C(27)-H(27)	119.1

C(31)-C(30)-H(30)	119.1
C(29)-C(30)-H(30)	119.1
C(29)-C(30)-C(31)	121.8(5)
C(26)-C(31)-C(32)	126.2(4)
C(30)-C(31)-C(26)	117.4(4)
C(30)-C(31)-C(32)	116.3(4)
C(33)-C(38)-C(47)	126.1(4)
C(37)-C(38)-C(33)	117.7(5)
C(37)-C(38)-C(47)	115.9(4)
C(3)-C(2)-C(1)	118.0(4)
C(3)-C(2)-C(7)	116.4(4)
C(1)-C(2)-C(7)	125.5(4)
C(38)-C(33)-P(1)	120.6(4)
C(38)-C(33)-C(34)	119.1(4)
C(34)-C(33)-P(1)	118.6(4)
C(25)-C(20)-C(19)	126.4(4)
C(21)-C(20)-C(25)	116.8(4)
C(21)-C(20)-C(19)	116.7(4)
C(38)-C(37)-H(37)	118.3
C(36)-C(37)-C(38)	123.3(5)
C(36)-C(37)-H(37)	118.3
C(65)-C(63)-C(58)	112.2(4)
C(65)-C(63)-C(64)	110.8(4)
C(65)-C(63)-C(66)	104.3(5)
C(64)-C(63)-C(58)	111.7(4)
C(64)-C(63)-C(66)	105.4(5)
C(66)-C(63)-C(58)	112.0(4)
C(3)-C(4)-C(11)	122.1(5)
C(5)-C(4)-C(3)	116.8(5)
C(5)-C(4)-C(11)	121.1(5)
C(15)-C(18)-H(18A)	109.5

C(15)-C(18)-H(18B)	109.5
C(15)-C(18)-H(18C)	109.5
H(18A)-C(18)-H(18B)	109.5
H(18A)-C(18)-H(18C)	109.5
H(18B)-C(18)-H(18C)	109.5
C(25)-C(24)-H(24)	119.3
C(25)-C(24)-C(23)	121.5(5)
C(23)-C(24)-H(24)	119.3
C(61)-C(60)-C(67)	119.9(5)
C(59)-C(60)-C(61)	116.8(5)
C(59)-C(60)-C(67)	123.3(5)
C(1)-C(6)-C(15)	125.9(4)
C(5)-C(6)-C(15)	116.6(4)
C(5)-C(6)-C(1)	117.4(4)
C(60)-C(61)-H(61)	118.1
C(60)-C(61)-C(62)	123.8(5)
C(62)-C(61)-H(61)	118.1
N(1)-C(75)-C(76)	178.7(8)
C(31)-C(32)-P(1)	125.4(4)
C(20)-C(21)-H(21)	118.7
C(22)-C(21)-C(20)	122.6(5)
C(22)-C(21)-H(21)	118.7
C(58)-C(57)-P(3)	118.7(4)
C(58)-C(57)-C(62)	119.0(4)
C(62)-C(57)-P(3)	121.0(3)
C(15)-C(16)-H(16A)	109.5
C(15)-C(16)-H(16B)	109.5
C(15)-C(16)-H(16C)	109.5
H(16A)-C(16)-H(16B)	109.5
H(16A)-C(16)-H(16C)	109.5
H(16B)-C(16)-H(16C)	109.5

C(57)-C(58)-C(63)	126.2(4)
C(59)-C(58)-C(63)	116.4(4)
C(59)-C(58)-C(57)	117.3(4)
C(33)-C(34)-C(39)	126.1(4)
C(35)-C(34)-C(33)	117.4(5)
C(35)-C(34)-C(39)	116.3(5)
C(01L)-C(51)-P(3)	126.3(4)
C(63)-C(65)-H(65A)	109.5
C(63)-C(65)-H(65B)	109.5
C(63)-C(65)-H(65C)	109.5
H(65A)-C(65)-H(65B)	109.5
H(65A)-C(65)-H(65C)	109.5
H(65B)-C(65)-H(65C)	109.5
C(2)-C(1)-P(2)	121.3(4)
C(2)-C(1)-C(6)	119.1(4)
C(6)-C(1)-P(2)	118.0(4)
C(30)-C(29)-H(29)	119.9
C(30)-C(29)-C(28)	120.1(5)
C(28)-C(29)-H(29)	119.9
C(20)-C(19)-P(2)	125.2(4)
C(21)-C(22)-H(22)	120.0
C(21)-C(22)-C(23)	119.9(5)
C(23)-C(22)-H(22)	120.0
C(37)-C(36)-C(43)	121.6(5)
C(35)-C(36)-C(37)	117.5(5)
C(35)-C(36)-C(43)	120.9(5)
C(34)-C(35)-H(35)	118.0
C(36)-C(35)-C(34)	124.0(5)
C(36)-C(35)-H(35)	118.0
C(27)-C(28)-C(29)	118.9(5)
C(27)-C(28)-H(28)	120.6

C(29)-C(28)-H(28)	120.6
C(60)-C(67)-C(68)	107.2(5)
C(60)-C(67)-C(69')	101.8(10)
C(60)-C(67)-C(70')	107.2(12)
C(69)-C(67)-C(60)	110.3(6)
C(69)-C(67)-C(68)	106.3(7)
C(70)-C(67)-C(60)	113.6(6)
C(70)-C(67)-C(69)	109.8(8)
C(70)-C(67)-C(68)	109.4(7)
C(70')-C(67)-C(69')	100(2)
C(68')-C(67)-C(60)	120.0(13)
C(68')-C(67)-C(69')	105(2)
C(68')-C(67)-C(70')	119(2)
C(63)-C(64)-H(64A)	109.5
C(63)-C(64)-H(64B)	109.5
C(63)-C(64)-H(64C)	109.5
H(64A)-C(64)-H(64B)	109.5
H(64A)-C(64)-H(64C)	109.5
H(64B)-C(64)-H(64C)	109.5
C(54)-C(53)-H(53)	119.3
C(52)-C(53)-H(53)	119.3
C(52)-C(53)-C(54)	121.4(5)
C(15)-C(17)-H(17A)	109.5
C(15)-C(17)-H(17B)	109.5
C(15)-C(17)-H(17C)	109.5
H(17A)-C(17)-H(17B)	109.5
H(17A)-C(17)-H(17C)	109.5
H(17B)-C(17)-H(17C)	109.5
C(40)-C(39)-C(34)	112.1(4)
C(41)-C(39)-C(34)	110.9(4)
C(41)-C(39)-C(40)	104.9(5)

C(42)-C(39)-C(34)	113.0(4)
C(42)-C(39)-C(40)	105.3(4)
C(42)-C(39)-C(41)	110.1(4)
C(4)-C(5)-C(6)	124.2(5)
C(4)-C(5)-H(5)	117.9
C(6)-C(5)-H(5)	117.9
C(50)-C(47)-C(38)	114.9(4)
C(50)-C(47)-C(49)	108.4(4)
C(49)-C(47)-C(38)	107.9(4)
C(48)-C(47)-C(38)	112.6(4)
C(48)-C(47)-C(50)	105.8(4)
C(48)-C(47)-C(49)	106.9(5)
C(52)-C(01L)-C(51)	125.5(4)
C(56)-C(01L)-C(51)	117.5(4)
C(56)-C(01L)-C(52)	117.0(4)
C(53)-C(54)-H(54)	120.2
C(53)-C(54)-C(55)	119.6(5)
C(55)-C(54)-H(54)	120.2
C(24)-C(23)-H(23)	120.5
C(22)-C(23)-C(24)	118.9(5)
C(22)-C(23)-H(23)	120.5
C(53)-C(52)-P(4)	119.6(4)
C(53)-C(52)-C(01L)	119.8(4)
C(01L)-C(52)-P(4)	120.6(4)
C(60)-C(59)-C(58)	124.4(5)
C(60)-C(59)-H(59)	117.8
C(58)-C(59)-H(59)	117.8
C(61)-C(62)-C(57)	117.8(4)
C(61)-C(62)-C(71)	116.1(4)
C(57)-C(62)-C(71)	125.8(4)
C(8)-C(7)-C(2)	114.5(4)

C(8)-C(7)-C(9)	103.8(4)
C(10)-C(7)-C(2)	109.7(4)
C(10)-C(7)-C(8)	109.8(4)
C(10)-C(7)-C(9)	105.7(4)
C(9)-C(7)-C(2)	112.8(4)
C(39)-C(40)-H(40A)	109.5
C(39)-C(40)-H(40B)	109.5
C(39)-C(40)-H(40C)	109.5
H(40A)-C(40)-H(40B)	109.5
H(40A)-C(40)-H(40C)	109.5
H(40B)-C(40)-H(40C)	109.5
C(73)-C(71)-C(62)	112.4(4)
C(72)-C(71)-C(62)	108.7(4)
C(72)-C(71)-C(73)	106.1(5)
C(72)-C(71)-C(74)	110.1(4)
C(74)-C(71)-C(62)	114.3(4)
C(74)-C(71)-C(73)	104.9(4)
C(63)-C(66)-H(66A)	109.5
C(63)-C(66)-H(66B)	109.5
C(63)-C(66)-H(66C)	109.5
H(66A)-C(66)-H(66B)	109.5
H(66A)-C(66)-H(66C)	109.5
H(66B)-C(66)-H(66C)	109.5
C(4)-C(11)-C(14)	112.8(5)
C(4)-C(11)-C(13)	107.9(6)
C(4)-C(11)-C(14')	107.0(9)
C(4)-C(11)-C(12')	112.3(9)
C(12)-C(11)-C(4)	108.7(6)
C(12)-C(11)-C(14)	108.0(7)
C(12)-C(11)-C(13)	110.3(7)
C(14)-C(11)-C(13)	109.0(7)

C(14')-C(11)-C(12')	106.3(14)
C(13')-C(11)-C(4)	110.7(9)
C(13')-C(11)-C(14')	110.4(13)
C(13')-C(11)-C(12')	110.1(13)
C(39)-C(41)-H(41A)	109.5
C(39)-C(41)-H(41B)	109.5
C(39)-C(41)-H(41C)	109.5
H(41A)-C(41)-H(41B)	109.5
H(41A)-C(41)-H(41C)	109.5
H(41B)-C(41)-H(41C)	109.5
C(39)-C(42)-H(42A)	109.5
C(39)-C(42)-H(42B)	109.5
C(39)-C(42)-H(42C)	109.5
H(42A)-C(42)-H(42B)	109.5
H(42A)-C(42)-H(42C)	109.5
H(42B)-C(42)-H(42C)	109.5
C(54)-C(55)-H(55)	120.4
C(56)-C(55)-C(54)	119.2(5)
C(56)-C(55)-H(55)	120.4
C(71)-C(73)-H(73A)	109.5
C(71)-C(73)-H(73B)	109.5
C(71)-C(73)-H(73C)	109.5
H(73A)-C(73)-H(73B)	109.5
H(73A)-C(73)-H(73C)	109.5
H(73B)-C(73)-H(73C)	109.5
C(47)-C(50)-H(50A)	109.5
C(47)-C(50)-H(50B)	109.5
C(47)-C(50)-H(50C)	109.5
H(50A)-C(50)-H(50B)	109.5
H(50A)-C(50)-H(50C)	109.5
H(50B)-C(50)-H(50C)	109.5

C(7)-C(8)-H(8A)	109.5
C(7)-C(8)-H(8B)	109.5
C(7)-C(8)-H(8C)	109.5
H(8A)-C(8)-H(8B)	109.5
H(8A)-C(8)-H(8C)	109.5
H(8B)-C(8)-H(8C)	109.5
C(7)-C(10)-H(10A)	109.5
C(7)-C(10)-H(10B)	109.5
C(7)-C(10)-H(10C)	109.5
H(10A)-C(10)-H(10B)	109.5
H(10A)-C(10)-H(10C)	109.5
H(10B)-C(10)-H(10C)	109.5
C(47)-C(49)-H(49A)	109.5
C(47)-C(49)-H(49B)	109.5
C(47)-C(49)-H(49C)	109.5
H(49A)-C(49)-H(49B)	109.5
H(49A)-C(49)-H(49C)	109.5
H(49B)-C(49)-H(49C)	109.5
C(01L)-C(56)-H(56)	118.5
C(55)-C(56)-C(01L)	123.0(5)
C(55)-C(56)-H(56)	118.5
C(71)-C(72)-H(72A)	109.5
C(71)-C(72)-H(72B)	109.5
C(71)-C(72)-H(72C)	109.5
H(72A)-C(72)-H(72B)	109.5
H(72A)-C(72)-H(72C)	109.5
H(72B)-C(72)-H(72C)	109.5
C(71)-C(74)-H(74A)	109.5
C(71)-C(74)-H(74B)	109.5
C(71)-C(74)-H(74C)	109.5
H(74A)-C(74)-H(74B)	109.5

H(74A)-C(74)-H(74C)	109.5
H(74B)-C(74)-H(74C)	109.5
C(7)-C(9)-H(9A)	109.5
C(7)-C(9)-H(9B)	109.5
C(7)-C(9)-H(9C)	109.5
H(9A)-C(9)-H(9B)	109.5
H(9A)-C(9)-H(9C)	109.5
H(9B)-C(9)-H(9C)	109.5
C(75)-C(76)-H(76A)	109.5
C(75)-C(76)-H(76B)	109.5
C(75)-C(76)-H(76C)	109.5
H(76A)-C(76)-H(76B)	109.5
H(76A)-C(76)-H(76C)	109.5
H(76B)-C(76)-H(76C)	109.5
C(36)-C(43)-C(45)	108.2(7)
C(36)-C(43)-C(44)	106.9(6)
C(36)-C(43)-C(45')	106.5(7)
C(45)-C(43)-C(44)	102.7(9)
C(46)-C(43)-C(36)	116.3(7)
C(46)-C(43)-C(45)	114.7(10)
C(46)-C(43)-C(44)	106.9(10)
C(46')-C(43)-C(36)	106.6(8)
C(46')-C(43)-C(45')	99.2(13)
C(44')-C(43)-C(36)	116.1(10)
C(44')-C(43)-C(45')	109.1(18)
C(44')-C(43)-C(46')	117.4(18)
F(3)-C(78)-S(1)	111.7(5)
F(2)-C(78)-S(1)	110.2(5)
F(2)-C(78)-F(3)	107.0(6)
F(1)-C(78)-S(1)	112.1(5)
F(1)-C(78)-F(3)	108.4(6)

F(1)-C(78)-F(2)	107.2(6)
C(47)-C(48)-H(48A)	109.5
C(47)-C(48)-H(48B)	109.5
C(47)-C(48)-H(48C)	109.5
H(48A)-C(48)-H(48B)	109.5
H(48A)-C(48)-H(48C)	109.5
H(48B)-C(48)-H(48C)	109.5
C(67)-C(69)-H(69A)	109.5
C(67)-C(69)-H(69B)	109.5
C(67)-C(69)-H(69C)	109.5
H(69A)-C(69)-H(69B)	109.5
H(69A)-C(69)-H(69C)	109.5
H(69B)-C(69)-H(69C)	109.5
C(67)-C(70)-H(70A)	109.5
C(67)-C(70)-H(70B)	109.5
C(67)-C(70)-H(70C)	109.5
H(70A)-C(70)-H(70B)	109.5
H(70A)-C(70)-H(70C)	109.5
H(70B)-C(70)-H(70C)	109.5
C(67)-C(68)-H(68A)	109.5
C(67)-C(68)-H(68B)	109.5
C(67)-C(68)-H(68C)	109.5
H(68A)-C(68)-H(68B)	109.5
H(68A)-C(68)-H(68C)	109.5
H(68B)-C(68)-H(68C)	109.5
C(80)-C(79)-C(84)	118.4(10)
C(80)-C(79)-C(85)	120.1(14)
C(84)-C(79)-C(85)	121.5(13)
C(43)-C(45)-H(45A)	109.5
C(43)-C(45)-H(45B)	109.5
C(43)-C(45)-H(45C)	109.5

H(45A)-C(45)-H(45B)	109.5
H(45A)-C(45)-H(45C)	109.5
H(45B)-C(45)-H(45C)	109.5
C(80)-C(81)-H(81)	116.8
C(80)-C(81)-C(82)	126.5(13)
C(82)-C(81)-H(81)	116.8
C(11)-C(12)-H(12A)	109.5
C(11)-C(12)-H(12B)	109.5
C(11)-C(12)-H(12C)	109.5
H(12A)-C(12)-H(12B)	109.5
H(12A)-C(12)-H(12C)	109.5
H(12B)-C(12)-H(12C)	109.5
C(11)-C(14)-H(14A)	109.5
C(11)-C(14)-H(14B)	109.5
C(11)-C(14)-H(14C)	109.5
H(14A)-C(14)-H(14B)	109.5
H(14A)-C(14)-H(14C)	109.5
H(14B)-C(14)-H(14C)	109.5
C(79)-C(80)-H(80)	120.0
C(81)-C(80)-C(79)	120.0(12)
C(81)-C(80)-H(80)	120.0
C(84)-C(83)-H(83)	119.8
C(82)-C(83)-H(83)	119.8
C(82)-C(83)-C(84)	120.3(11)
C(11)-C(13)-H(13A)	109.5
C(11)-C(13)-H(13B)	109.5
C(11)-C(13)-H(13C)	109.5
H(13A)-C(13)-H(13B)	109.5
H(13A)-C(13)-H(13C)	109.5
H(13B)-C(13)-H(13C)	109.5
C(79)-C(84)-C(83)	116.6(10)

C(79)-C(84)-H(84)	121.7
C(83)-C(84)-H(84)	121.7
F(4)-C(77)-S(2)	107.1(10)
F(4)-C(77)-F(5)	107.8(15)
F(6)-C(77)-S(2)	112.7(12)
F(6)-C(77)-F(4)	108.2(13)
F(6)-C(77)-F(5)	110.3(13)
F(5)-C(77)-S(2)	110.6(11)
C(43)-C(46)-H(46A)	109.5
C(43)-C(46)-H(46B)	109.5
C(43)-C(46)-H(46C)	109.5
H(46A)-C(46)-H(46B)	109.5
H(46A)-C(46)-H(46C)	109.5
H(46B)-C(46)-H(46C)	109.5
C(43)-C(44)-H(44A)	109.5
C(43)-C(44)-H(44B)	109.5
C(43)-C(44)-H(44C)	109.5
H(44A)-C(44)-H(44B)	109.5
H(44A)-C(44)-H(44C)	109.5
H(44B)-C(44)-H(44C)	109.5
C(81)-C(82)-H(82)	121.1
C(83)-C(82)-C(81)	117.8(14)
C(83)-C(82)-H(82)	121.1
C(79)-C(85)-H(85A)	109.5
C(79)-C(85)-H(85B)	109.5
C(79)-C(85)-H(85C)	109.5
H(85A)-C(85)-H(85B)	109.5
H(85A)-C(85)-H(85C)	109.5
H(85B)-C(85)-H(85C)	109.5
C(67)-C(69')-H(69D)	109.5
C(67)-C(69')-H(69E)	109.5

C(67)-C(69')-H(69F)	109.5
H(69D)-C(69')-H(69E)	109.5
H(69D)-C(69')-H(69F)	109.5
H(69E)-C(69')-H(69F)	109.5
C(67)-C(70')-H(70D)	109.5
C(67)-C(70')-H(70E)	109.5
C(67)-C(70')-H(70F)	109.5
H(70D)-C(70')-H(70E)	109.5
H(70D)-C(70')-H(70F)	109.5
H(70E)-C(70')-H(70F)	109.5
C(67)-C(68')-H(68D)	109.5
C(67)-C(68')-H(68E)	109.5
C(67)-C(68')-H(68F)	109.5
H(68D)-C(68')-H(68E)	109.5
H(68D)-C(68')-H(68F)	109.5
H(68E)-C(68')-H(68F)	109.5
C(11)-C(14')-H(14D)	109.5
C(11)-C(14')-H(14E)	109.5
C(11)-C(14')-H(14F)	109.5
H(14D)-C(14')-H(14E)	109.5
H(14D)-C(14')-H(14F)	109.5
H(14E)-C(14')-H(14F)	109.5
C(11)-C(13')-H(13D)	109.5
C(11)-C(13')-H(13E)	109.5
C(11)-C(13')-H(13F)	109.5
H(13D)-C(13')-H(13E)	109.5
H(13D)-C(13')-H(13F)	109.5
H(13E)-C(13')-H(13F)	109.5
C(11)-C(12')-H(12D)	109.5
C(11)-C(12')-H(12E)	109.5
C(11)-C(12')-H(12F)	109.5

H(12D)-C(12')-H(12E)	109.5
H(12D)-C(12')-H(12F)	109.5
H(12E)-C(12')-H(12F)	109.5
C(43)-C(45')-H(45D)	109.5
C(43)-C(45')-H(45E)	109.5
C(43)-C(45')-H(45F)	109.5
H(45D)-C(45')-H(45E)	109.5
H(45D)-C(45')-H(45F)	109.5
H(45E)-C(45')-H(45F)	109.5
C(43)-C(46')-H(46D)	109.5
C(43)-C(46')-H(46E)	109.5
C(43)-C(46')-H(46F)	109.5
H(46D)-C(46')-H(46E)	109.5
H(46D)-C(46')-H(46F)	109.5
H(46E)-C(46')-H(46F)	109.5
C(43)-C(44')-H(44D)	109.5
C(43)-C(44')-H(44E)	109.5
C(43)-C(44')-H(44F)	109.5
H(44D)-C(44')-H(44E)	109.5
H(44D)-C(44')-H(44F)	109.5
H(44E)-C(44')-H(44F)	109.5

Symmetry transformations used to generate equivalent atoms:

Table E.4 Anisotropic displacement parameters ($Å^2 x\ 10^3$) for cain38_a_sq. The anisotropic displacement factor exponent takes the form: $-2\pi^2[\ h^2\ a^{*2}U^{11} + ...\ + 2\ h\ k\ a^*\ b^*\ U^{12}\ ]$

	U^{11}	U^{22}	U^{33}	U^{23}	U^{13}	U^{12}
Rh(1)	16(1)	19(1)	19(1)	-8(1)	2(1)	3(1)
P(2)	19(1)	20(1)	20(1)	-8(1)	2(1)	4(1)

P(4)	16(1)	17(1)	20(1)	-9(1)	2(1)	2(1)
P(1)	18(1)	18(1)	19(1)	-7(1)	2(1)	2(1)
P(3)	20(1)	21(1)	21(1)	-10(1)	3(1)	4(1)
S(1)	12(1)	16(1)	23(1)	-7(1)	-7(1)	-3(1)
S(2)	29(2)	23(2)	40(2)	-20(1)	17(1)	-3(1)
F(3)	34(2)	25(2)	34(3)	-15(2)	-5(2)	19(2)
N(1)	21(2)	21(2)	19(2)	-7(2)	0(2)	3(2)
F(2)	13(2)	36(3)	69(4)	-23(3)	16(2)	-9(2)
F(1)	32(3)	69(4)	36(3)	-41(3)	-17(2)	10(2)
C(26)	19(2)	21(2)	22(2)	-12(2)	1(2)	2(2)
C(15)	26(3)	22(2)	26(3)	-9(2)	-6(2)	9(2)
C(3)	29(3)	26(3)	25(3)	-13(2)	0(2)	2(2)
C(25)	19(2)	16(2)	23(2)	-8(2)	6(2)	3(2)
C(27)	19(2)	23(2)	30(3)	-12(2)	4(2)	2(2)
C(30)	26(3)	21(2)	26(3)	-12(2)	-1(2)	4(2)
C(31)	17(2)	25(2)	21(2)	-13(2)	-1(2)	3(2)
C(38)	25(3)	17(2)	23(3)	-7(2)	6(2)	3(2)
C(2)	25(3)	22(2)	15(2)	-5(2)	1(2)	2(2)
C(33)	20(2)	17(2)	22(2)	-5(2)	2(2)	4(2)
C(20)	20(2)	19(2)	24(3)	-10(2)	4(2)	5(2)
C(37)	29(3)	26(3)	29(3)	-13(2)	8(2)	4(2)
O(3)	24(3)	26(3)	43(3)	-10(3)	11(2)	-17(2)
C(63)	29(3)	23(2)	23(3)	-8(2)	9(2)	5(2)
C(4)	27(3)	33(3)	26(3)	-13(2)	3(2)	0(2)
C(18)	38(3)	24(3)	25(3)	-10(2)	0(2)	5(2)
C(24)	20(2)	25(3)	26(3)	-12(2)	2(2)	2(2)
C(60)	23(3)	31(3)	30(3)	-12(2)	1(2)	5(2)
C(6)	23(2)	22(2)	19(2)	-8(2)	2(2)	4(2)
C(61)	27(3)	24(3)	26(3)	-12(2)	2(2)	4(2)
C(75)	24(3)	44(3)	37(3)	-13(3)	5(2)	8(2)
C(32)	21(2)	22(2)	20(2)	-10(2)	0(2)	1(2)

C(21)	27(3)	24(2)	20(3)	-7(2)	5(2)	5(2)
C(57)	19(2)	21(2)	25(3)	-12(2)	2(2)	5(2)
C(16)	34(3)	29(3)	32(3)	-17(2)	0(2)	13(2)
C(58)	25(3)	23(2)	24(3)	-11(2)	4(2)	2(2)
C(34)	22(2)	22(2)	26(3)	-9(2)	2(2)	1(2)
C(51)	25(3)	26(3)	22(3)	-12(2)	6(2)	3(2)
C(65)	38(3)	30(3)	25(3)	-12(2)	5(2)	2(2)
C(1)	20(2)	26(2)	17(2)	-9(2)	1(2)	0(2)
O(1)	12(3)	22(3)	81(5)	-27(3)	-12(3)	7(2)
C(29)	28(3)	24(3)	36(3)	-17(2)	3(2)	6(2)
C(19)	22(2)	20(2)	23(3)	-9(2)	2(2)	5(2)
C(22)	24(3)	22(2)	29(3)	-7(2)	7(2)	-1(2)
C(36)	27(3)	28(3)	39(3)	-16(2)	11(2)	2(2)
C(35)	21(3)	29(3)	38(3)	-14(2)	0(2)	1(2)
C(28)	25(3)	30(3)	35(3)	-16(2)	8(2)	3(2)
C(67)	20(3)	50(4)	48(4)	-17(3)	-1(3)	13(3)
C(64)	36(3)	28(3)	33(3)	-11(2)	8(2)	-2(2)
C(53)	22(2)	25(3)	26(3)	-15(2)	0(2)	4(2)
O(2)	56(4)	44(4)	22(3)	-17(3)	-17(3)	0(3)
C(17)	35(3)	34(3)	56(4)	-20(3)	-18(3)	14(3)
C(39)	24(3)	29(3)	28(3)	-12(2)	1(2)	-2(2)
C(5)	24(3)	31(3)	29(3)	-14(2)	-1(2)	8(2)
C(47)	29(3)	24(3)	22(3)	-10(2)	3(2)	0(2)
C(01L)	20(2)	20(2)	21(2)	-8(2)	6(2)	0(2)
C(54)	24(3)	28(3)	34(3)	-13(2)	-4(2)	6(2)
C(23)	20(2)	27(3)	36(3)	-16(2)	4(2)	0(2)
C(52)	18(2)	22(2)	23(2)	-10(2)	3(2)	-1(2)
C(59)	21(2)	30(3)	29(3)	-14(2)	6(2)	3(2)
C(62)	22(2)	25(2)	24(3)	-15(2)	1(2)	4(2)
C(7)	24(2)	23(2)	25(3)	-13(2)	-1(2)	4(2)
C(40)	38(3)	48(4)	42(3)	-26(3)	5(3)	-11(3)

C(71)	26(3)	22(2)	28(3)	-9(2)	7(2)	2(2)
C(66)	43(3)	38(3)	34(3)	-8(3)	15(3)	14(3)
C(11)	26(3)	41(3)	47(4)	-25(3)	-2(2)	0(2)
C(41)	33(3)	25(3)	30(3)	-13(2)	-2(2)	3(2)
C(42)	33(3)	33(3)	32(3)	-13(3)	-3(2)	3(2)
C(55)	30(3)	34(3)	25(3)	-15(2)	-3(2)	0(2)
C(73)	38(3)	27(3)	38(3)	-2(3)	15(3)	7(2)
C(50)	33(3)	27(3)	25(3)	-13(2)	1(2)	-2(2)
C(8)	26(3)	27(3)	30(3)	-17(2)	-1(2)	8(2)
C(10)	42(3)	32(3)	32(3)	-14(3)	6(2)	15(2)
C(49)	35(3)	28(3)	36(3)	-15(2)	-11(2)	5(2)
C(56)	28(3)	25(3)	28(3)	-14(2)	4(2)	-2(2)
C(72)	37(3)	43(3)	37(3)	-23(3)	14(3)	-12(3)
C(74)	30(3)	24(3)	30(3)	-11(2)	9(2)	4(2)
C(9)	36(3)	34(3)	47(4)	-27(3)	-14(3)	12(2)
C(76)	20(3)	96(6)	78(6)	-34(5)	3(3)	7(3)
C(43)	29(3)	61(4)	64(5)	-33(4)	23(3)	-5(3)
C(78)	15(3)	20(3)	25(4)	-13(3)	-5(3)	5(3)
C(48)	40(3)	52(4)	26(3)	-20(3)	6(2)	-8(3)
F(4)	29(2)	23(2)	40(2)	-20(1)	17(1)	-3(1)
C(69)	39(5)	40(5)	54(7)	-19(5)	0(4)	22(4)
C(70)	22(4)	68(7)	36(5)	-11(5)	3(4)	13(4)
C(68)	25(4)	64(6)	45(5)	-26(5)	-7(4)	14(4)
C(79)	70(5)	57(5)	92(7)	-51(5)	15(5)	-13(4)
C(45)	30(7)	61(9)	53(8)	-14(7)	13(5)	-10(6)
F(6)	29(2)	23(2)	40(2)	-20(1)	17(1)	-3(1)
C(81)	290(20)	67(7)	44(6)	-24(5)	37(11)	-43(11)
C(12)	34(5)	75(8)	86(9)	-57(7)	21(5)	-16(5)
C(14)	32(5)	53(6)	61(7)	-33(5)	-1(4)	-8(4)
O(4)	37(7)	59(8)	32(6)	-34(6)	6(5)	-6(6)
C(80)	131(10)	63(6)	100(9)	-52(6)	-65(8)	21(6)

C(83)	73(8)	164(14)	310(20)	-188(18)	-90(12)	56(9)
C(13)	33(5)	59(6)	53(6)	-29(5)	-14(4)	-1(4)
O(6)	37(7)	34(7)	43(5)	-5(5)	15(5)	14(5)
F(5)	39(6)	92(10)	22(5)	3(6)	0(4)	26(6)
C(84)	162(12)	73(6)	39(5)	-27(4)	-40(6)	10(7)
C(77)	29(2)	23(2)	40(2)	-20(1)	17(1)	-3(1)
O(5)	29(2)	23(2)	40(2)	-20(1)	17(1)	-3(1)
C(46)	43(7)	99(13)	66(10)	-57(10)	29(7)	-18(8)
C(44)	31(6)	93(11)	86(11)	-34(9)	20(6)	15(6)
C(82)	103(10)	143(14)	161(16)	-115(14)	66(10)	-62(10)
C(85)	150(14)	159(14)	390(30)	-204(19)	152(17)	-74(11)
C(69')	43(17)	90(30)	110(30)	-40(20)	-10(17)	50(18)
C(70')	70(20)	90(30)	90(30)	-20(20)	-40(20)	50(20)
C(68')	53(18)	100(30)	60(20)	-20(20)	8(15)	46(19)
C(14')	32(10)	52(12)	55(13)	-23(10)	1(9)	-5(9)
C(13')	46(12)	55(13)	39(12)	-26(10)	-10(9)	-4(9)
C(12')	30(11)	53(14)	110(20)	-50(15)	-35(12)	13(9)
C(45')	32(9)	82(16)	34(10)	-14(10)	23(7)	-7(9)
C(46')	36(10)	56(12)	70(16)	-16(11)	27(10)	17(8)
C(44')	35(13)	150(30)	110(30)	-120(30)	55(15)	-55(17)

Table E.5 Hydrogen coordinates (x 10^4) and isotropic displacement parameters ($Å^2$x 10^3) for cain38_a_sq.

	x	y	z	U(eq)
H(3)	2590	7116	1023	31

H(27)	6867	8269	2240	29
H(30)	6173	5463	4058	29
H(37)	2473	6036	6751	34
H(18A)	3878	10411	593	45
H(18B)	3253	11209	153	45
H(18C)	3339	10563	-197	45
H(24)	6851	9520	3191	29
H(61)	2584	11906	2203	32
H(21)	6136	10519	445	30
H(16A)	3065	9900	1986	46
H(16B)	2025	9877	1997	46
H(16C)	2531	10759	1517	46
H(65A)	3857	9039	5354	48
H(65B)	3248	8617	6167	48
H(65C)	3326	9620	5632	48
H(29)	7262	5794	3060	35
H(22)	7201	11195	761	33
H(35)	1367	5585	5085	37
H(28)	7594	7206	2119	36
H(64A)	1944	8272	4797	51
H(64B)	2414	7808	5669	51
H(64C)	2979	8178	4830	51
H(53)	6883	7357	4359	28
H(17A)	1744	11124	272	64
H(17B)	1218	10254	760	64
H(17C)	1700	10496	-99	64
H(5)	1355	9167	754	34
H(54)	7580	7250	5510	36
H(23)	7553	10721	2146	33
H(59)	1362	10197	4256	33
H(40A)	1814	4718	4609	61

H(40B)	1850	5127	3625	61
H(40C)	1288	5562	4047	61
H(66A)	1763	9687	5585	64
H(66B)	1742	8682	6128	64
H(66C)	1219	9142	5285	64
H(41A)	3946	5547	4040	44
H(41B)	3392	5122	3618	44
H(41C)	3394	4708	4603	44
H(42A)	2046	6878	3159	51
H(42B)	2598	6412	2763	51
H(42C)	3085	6933	3125	51
H(55)	7154	8123	6057	35
H(73A)	3520	12145	1275	61
H(73B)	4473	12493	1277	61
H(73C)	3698	12617	1794	61
H(50A)	4897	7167	5290	43
H(50B)	5066	7211	6117	43
H(50C)	4235	7663	5572	43
H(8A)	4892	7471	2173	40
H(8B)	5162	6659	2100	40
H(8C)	4274	6657	2565	40
H(10A)	4511	8073	51	54
H(10B)	5309	7526	588	54
H(10C)	5024	8358	618	54
H(49A)	4368	5084	6856	50
H(49B)	5180	5648	6821	50
H(49C)	4913	5607	6012	50
H(56)	6054	9085	5442	32
H(72A)	4462	11912	3102	57
H(72B)	5270	11930	2537	57
H(72C)	4995	11069	3343	57

H(74A)	4868	10365	2467	44
H(74B)	5156	11232	1676	44
H(74C)	4267	10780	1671	44
H(9A)	3591	6185	1682	54
H(9B)	4514	6261	1238	54
H(9C)	3685	6727	698	54
H(76A)	905	8247	2788	102
H(76B)	826	8758	3285	102
H(76C)	866	7752	3776	102
H(48A)	3389	6813	6939	58
H(48B)	4317	6444	7324	58
H(48C)	3533	5816	7445	58
H(69A)	1257	12578	3056	69
H(69B)	610	12844	2304	69
H(69C)	1625	12739	2178	69
H(70A)	153	10665	3613	73
H(70B)	-294	11572	3164	73
H(70C)	353	11337	3910	73
H(68A)	1215	11840	1605	67
H(68B)	202	11861	1804	67
H(68C)	691	10978	2150	67
H(45A)	666	4654	6211	82
H(45B)	-28	4691	6846	82
H(45C)	936	4363	7141	82
H(81)	2778	3927	3157	161
H(12A)	502	7253	2024	86
H(12B)	-267	7491	1380	86
H(12C)	255	8219	1437	86
H(14A)	1401	6852	467	70
H(14B)	459	6610	902	70
H(14C)	1304	6448	1449	70

H(80)	3905	3916	2424	111
H(83)	1292	5017	1287	179
H(13A)	652	8900	-148	71
H(13B)	26	8177	-101	71
H(13C)	996	8273	-464	71
H(84)	2546	5232	375	110
H(46A)	1267	5588	7454	93
H(46B)	251	5766	7293	93
H(46C)	942	6509	6801	93
H(44A)	320	6856	5477	112
H(44B)	-410	6160	5984	112
H(44C)	160	6102	5283	112
H(82)	1494	4472	2646	143
H(85A)	4040	4929	231	308
H(85B)	4635	4925	931	308
H(85C)	4368	4055	973	308
H(69D)	543	11361	4122	133
H(69E)	229	12269	3427	133
H(69F)	1219	12130	3713	133
H(70D)	326	10724	2611	136
H(70E)	-318	11233	2894	136
H(70F)	268	10494	3561	136
H(68D)	1427	12706	2154	117
H(68E)	422	12586	2029	117
H(68F)	1154	12222	1667	117
H(14D)	1145	6480	1768	71
H(14E)	139	6725	1633	71
H(14F)	737	7072	2099	71
H(13D)	1027	7999	-373	68
H(13E)	542	7123	209	68
H(13F)	1578	7186	224	68

H(12D)	188	8552	1036	90
H(12E)	-367	8061	682	90
H(12F)	259	8822	76	90
H(45D)	1396	4670	7585	84
H(45E)	559	5100	7746	84
H(45F)	1482	5569	7539	84
H(46D)	995	6756	6538	91
H(46E)	6	6473	6564	91
H(46F)	530	6943	5702	91
H(44D)	-4	5572	5757	120
H(44E)	-115	4959	6731	120
H(44F)	611	4769	6216	120

—

LITERATURE CITED

(1) Crabtree, R. H. *The Organometallic Chemistry of the Transition Metals*, 5th ed.; John Wiley and Sons LTD: Hoboken, 2009.

(2) Collman, James P.; Hegedus, Louis S.; Norton, Jack R.; Finke, R. G. *Principles and Applications of Organotransition Metal Chemistry*; University Science Books: Mill Valley, 1987.

(3) Hieber, W.; Leutert, F. Zur Kenntnis Des Koordinativ Gebundenen Kohlenoxyds: Bildung von Eisencarbonylwasserstoff. *Naturwissenschaften* **1931**, *19* (17), 360–361.

(4) Vancea, L.; Graham, W. A. G. Stereochemically Non-Rigid Six-Coordinate Metal Carbonyl Complexes. *J. Organomet. Chem.* **1977**, *134*, 219–227.

(5) Ewens, R. V. G.; Lister, M. W. The Structure of Iron Pentacarbonyl, and of Iron and Cobalt Carbonyl Hydrides. *Trans. Faraday Soc.* **1939**, *35*, 681–691.

(6) Krumholz, P.; Stettiner, H. M. A. The Acid Properties of Iron Tetracarbonyl Hydride. *J. Am. Chem. Soc.* **1949**, *71* (9), 3035–3039.

(7) McNeill, E. A.; Scholer, F. R. Molecular Structure of the Gaseous Metal Carbonyl Hydrides of Manganese, Iron, and Cobalt. *J. Am. Chem. Soc.* **1977**, *99* (19), 6243–6249.

(8) Drouin, B. J.; Kukolich, S. G. Molecular Structure of Tetracarbonyldihydroiron: Microwave Measurements and Density Functional Theory Calculations. *J. Am. Chem. Soc.* **1998**, *120* (27), 6774–6780.

(9) Halpern, J. Mechanistic Aspects of Homogeneous Catalytic Hydrogenation and Related Processes. *Inorganica Chim. Acta* **1981**, *50* (C), 11–19.

(10) Cotton, Albert F, Wilkinson, Geoffrey, Murillo, Carlos A., Bockman, M. *Advanced Inorganic Chemistry*, 6th ed.; John Wiley and Sons LTD: New York.

(11) Vaska, L. Hydrido Complexes of Iridium. *J. Am. Chem. Soc.* **1961**, *83* (3), 756.

(12) Vaska, L.; DiLuzio, J. W. Carbonyl and Hydrido-Carbonyl Complexes of Iridium by Reaction with Alcohols. Hydrido Complexes by Reaction with Acid. *J. Am. Chem. Soc.*

1961, *83* (12), 2784–2785.

(13) Dedieu, A.; Strich, A. A Molecular Orbital Analysis of the Oxidative Addition of Hydrogen to the Chlorotris(Triphenylphosphine)Rhodium(I) Complex. *Inorg. Chem.* **1979**, *18* (10), 2940–2943.

(14) Crabtree, R. H.; Quirk, J. M. Oxidative versus Reductive Additions: A 13C NMR Study of H2, HX (X = Cl, Br, OR I), and Cl2 Additions to Some Iridium(I) Complexes. *J. Organomet. Chem.* **1980**, *199* (1), 99–106.

(15) Saillard, J. Y.; Hoffmann, R. C-H and H-H Activation in Transition Metal Complexes and on Surfaces. *J. Am. Chem. Soc.* **1984**, *106* (7), 2006–2026.

(16) Kubas, G. J. *Metal Dihydrogen and Sigma-Bond Complexes: Structure, Theory, and Reactivity*, 1st ed.; Fackler, J. P., Ed.; Springer Science+Business Media: New York, 2001.

(17) Albright, T. A.; Burdett, Jeremy K.; Whangbo, M.-H. *Orbital Interactions in Chemistry*, 2nd ed.; John Wiley and Sons LTD: Hoboken, 2013.

(18) Theor, I. P.; Osborn, B. J. A.; Jardine, F. H.; Young, J. F.; Wilkinson, G. Inorg. Phys. Theor. **1965**, No. 1.

(19) Vaska, L.; Werneke, M. F. Activation of Molecular Hydrogen by Metal Complexes: Mechanism and Some Controlling Factors. *Trans. N. Y. Acad. Sci.* **1971**, *172* (13), 546–562.

(20) Johnson, T. J.; Albinati, A.; Koetzle, T. F.; Ricci, J.; Eisenstein, O.; Huffman, J. C.; Caulton, K. G. OsH5(PMe2Ph)3+: Structure, Reactivity, and Its Use as a Catalyst Precursor for Olefin Hydrogenation and Hydroformylation. *Inorg. Chem.* **1994**, *33* (22), 4966–4976.

(21) Desrosiers, P. J.; Cai, L.; Lin, Z.; Richards, R.; Halpern, J. Assessment of the “T1 Criterion” for Distinguishing between Classical and Nonclassical Transition-Metal Hydrides: Hydride Relaxation Rates in Tris(Triarylphosphine)Osmium Tetrahydrides and Related Polyhydrides. *J. Am. Chem. Soc.* **1991**, *113* (11), 4173–4184.

(22) Gilboa, Haggai; Chapman, Bogdan E.; Kuchel, P. W. Spin – Lattice Relaxation Times of H 2 and D 2 in Aqueous Solutions. *J. Magn. Reson.* **1996**, *119*, 1–5.

(23) Kubas, G. J.; Nelson, J. E.; Bryan, J. C.; Eckert, J.; Wisniewski, L.; Zilm, K. Isolation of an Extremely Labile Dihydrogen Complex, Cr(CO)3(PPri3)2(H2), Containing the Shortest Ligated H-H Bond. *Inorg. Chem.* **1994**, *33* (13), 2954–2960.

(24) Van Der Stays, L. S.; Huffman, J. C.; Caulton, K. G.; Eckert, J.; Hall, J. H.; Kubas, G. J.; Vergamini, P. J.; Eisenstein, O.; Jackson, S. A.; Koetzle, T. F. An Attractive #x201C;Cis-Effect#x201D; of Hydride on Neighbor Ligands: Experimental and Theoretical Studies on the Structure and Intramolecular Rearrangements of Fe(H)2(H2-H2)(PEtPh2)3. *J. Am. Chem. Soc.* **1990**, *112* (12), 4831–4841.

(25) Došlić, N.; Gomzi, V.; Mališ, M.; Matanović, I.; Eckert, J. Fluxionality of Hydrogen Ligands in Fe(H)2(H2) (PEtPh2)3. *Inorg. Chem.* **2011**, *50* (21), 10740–10747.

(26) Grellier, M.; Vendier, L.; Chaudret, B.; Albinati, A.; Rizzato, S.; Mason, S.; Sabo-Etienne, S. Synthesis, Neutron Structure, and Reactivity of the Bis(Dihydrogen) Complex RuH2(H2-H2)2(PCyp 3)2 Stabilized by Two Tricyclopentylphosphines. *J. Am. Chem. Soc.* **2005**, *127* (50), 17592–17593.

(27) Yousufuddin, M.; Wen, T. Bin; Mason, S. A.; McIntyre, G. J.; Jia, G.; Bau, R. A Neutron Diffraction Study of [OsClH 3 (PPh 3) 3]: A Complex Containing a Highly “Stretched” Dihydrogen Ligand. *Angew. Chemie - Int. Ed.* **2005**, *44* (44), 7227–7230.

(28) Werner, H.; Wolf, J.;Hoehn, A. Basic Metals. LI. New Hydridorhodium(III) and -Iridium(III) Complexes with Triisoprpylphosphine Ligands. Dihydrido Compounds C5H5MH2(PR’3) as Metal Bases. *J. Organomet. Chem.* **1985**, *287(3)*, 395–407.

(29) Mediati, Mario; Tachibana, Glen N.; Jensen, C. M. Isolation and Characterization of IrH2Cl(H2)[P(i-Pr)3]2: A Neutral Dihydrogen Complex of Iridium. *Inorg. Chem.* **1990**, *29*, 3–5.

(30) Mediati, M.; Tachibana, G. N.; Jensen, C. M. Solid-State and Solution Dynamics of the Reversible Loss of Hydrogen from the Iridium Nonclassical Polyhydride Complexes IrClH2(PR3)2(H2) (R = Pri, Cy, But). *Inorg. Chem* **1992**, *31*, 1827–1832.

(31) Eckert, J.; Jensen, C. M.; Koetzle, T. F.; Husebo, T. Le; Nicol, J.; Wu, P. Inelastic Neutron Scattering Studies of IrIH2(H2)(PPri3)2 and Neutron Diffraction Structure Determination of IrIH2(H2)(PPri3)2·C10H8: Implications on the Mechanism of the Interconversion of Dihydrogen and Hydride Ligands. *J. Am. Chem. Soc.* **1995**, *117* (27), 7271–7272.

(32) Le-Husebo, T.; Jensen, C. M. Influence of Halide Ligands on the Energetics of Reversible Loss of Hydrogen from the Iridium Nonclassical Polyhydride Complexes IrXH2(H2)(PPri3)2 (X= Cl, Br, I). *Inorg. Chem* **1993**, *32*, 3797–3798.

(33) Li, S.; Hall, M. B.; Eckert, J.; Jensen, C. M.; Albinati, A. Transition Metal Polyhydride Complexes. 10. Intramolecular Hydrogen Exchange in the Octahedral Iridium(III) Dihydrogen Dihydride Complexes IrXH2(H2-H2)(PR3)2(X = Cl, Br, I). *J. Am. Chem. Soc.* **2000**, *122* (12), 2903–2910.

(34) Clot, E.; Eisenstein, O. Influence of Ancillary Ligands on the Kinetics and the Thermodynamics of H2 Addition to IrXH2(PR3)2 (X) Cl, Br, I and R) H, Me): Comparison between Density Functional Theory and Perturbation Theory. *J. Phys. Chem. A* **1998**, *102* (98), 3592–3598.

(35) Herde, L. Cyclooctene and 1, 5 Cyclooctadiene Complexes of Iridium. *Inorg. Synth.* **1974**, *15*, 18–20.

(36) Garlaschelli, L.; Khan, S. I.; Bau, R. X-Ray and Neutron Diffraction Study of H5Ir[P(i-Pr)3]2. *J.* **1985**, No. 107, 7212–7213.

(37) Albinati, A.; Bakhmutov, V. I.; Caulton, K. G.; Clot, E.; Eckert, J.; Eisenstein, O.; Gusev, D. G.; Grushin, V. V; Hauger, B. E. Reaction of Molecular Hydrogen (H2) with Chlorohydridoiridium Phosphines IrHCl2P2 (P = PPr-Iso3 or PBu-Tert2Ph): Stereoelectronic Control of the Stability of Molecular H2 Transition Metal Complexes. *J. Am. Chem. Soc.* **1993**, *115* (16), 7300–7312.

(38) Ozin, G. A.; Garcia-Prieto, J. Pd(N1-H2). *J. Am. Chem. Soc.* **1986**, *108*, 3099–3100.

(39) Cotton, F. A.; Luck, R. L. Solution and Solid-State Conformational Isomers of the Molecular Dihydrogen Complex ReCl(H2)(PMePh2)4: Does It Contain an Asymmetric

Molecular Dihydrogen Ligand? *Inorg. Chem.* **1991**, *30* (4), 767–774.

(40) van Beek, J. A. M.; van Koten, G.; Smeets, W. J. J.; Spek, A. L. I2 1986. *J. Am. Chem. Soc.* **1986**, *108*, 5010–5011.

(41) Jensen, Craig, M. No Title. *Chem. Commun.* **1999**, 2443–2449.

(42) Gottker-Schnetmann, Inigo; White, Peter S.; Brookhart, M. No Title. *Organometallics* **2004**, *23*, 1766–1776.

(43) Brayton, D. F.; Beaumont, P. R.; Fukushima, E. Y.; Sartain, H. T.; Morales-Morales, D.; Jensen, C. M. Synthesis, Characterization, and Dehydrogenation Activity of an Iridium Arsenic Based Pincer Catalyst. *Organometallics* **2014**, *33* (19).

(44) Jensen, C. M. Unpublished XRD Data.

(45) Uhrı, B.; Barlow, P. N. Gradient-Enhanced One-Dimensional Proton Chemical-Shift Correlation with Full Sensitivity. **1997**, *255* (126), 248–255.

(46) Hamilton, D. G.; Crabtree, R. H. An NMR Method for Distinguishing Classical from Nonclassical Structures in Transition-Metal Polyhydrides. *J. Am. Chem. Soc.* **1988**, *110* (13), 4126–4133.

(47) Luo, Xiao Liang; Kubas, Gregory J, Bryan, Jeffrey C.; Burns, Carol J.; Unkefer, C. J. Eta2 Coordination of Si-H Sigma Bonds to Transition -Metal Fragments That Also Bind. *JACS* **1994**, *116*, 10312–10313.

(48) Butts, Matthew D.; Bryan, Jeffrey C.; Luo, Xiao-Liang, Kubas, G. J. Comparison of H-H versus Si-H Sigma-Bond Coordination and Activation on 16e Metal Fragments. *Inorg. Chem* **1997**, *36*, 3341–3353.

(49) Park, Sehoon; Brookhart, M. Development and Mechanistic Investigation of a Highly. *JACS* **2012**, *134*, 640–653.

(50) Calimano, Elisa; Tilley, T. D. Synthesis and Reactivity of Rhodium and Iridium Alkene. *Dalt. Trans.* **2010**, *39*, 9250–9263.

(51) Miura-Akagi, P. M.; Nakashige, M. L.; Maile, C. K.; Oshiro, S. M.; Gurr, J. R.; Yoshida, W. Y.; Royappa, A. T.; Krause, C. E.; Rheingold, A. L.; Hughes, R. P.; et al. Synthesis of

a Tris(Phosphaalkene)Phosphine Ligand and Fundamental Organometallic Reactions on Its Sterically Shielded Metal Complexes. *Organometallics* **2016**, *35* (13), 2224–2231.

(52) Gabuda, S. P.; Zemskov, S. V. NMR and Structural Features of Noble-Metal Flourides. *J. Struct. Chem.* **1987**, *28* (3), 379–393.

(53) Baum, K.; Nelson, H. M. Reactions of Alkyldifluoramines with Acids. *J. Am. Chem. Soc.* **1966**, *88* (19), 4459–4463.

(54) Phillips, W. D.; Miller, H. C.; Mutterties, E. L. No. *J. Am. Chem. Soc.* **1959**, *81*, 4496.

(55) Reich, H. J. Flourine NMR Data https://www.chem.wisc.edu/areas/reich/nmr/11-f-data.htm.